

# **Development of Simple Method for Preparation of Mesoporous Alumina Based Adsorbents and Their Application in Removal of Fluoride Ion from Water**

**THESIS**

Submitted in partial fulfillment  
of the requirements for the degree of  
**DOCTOR OF PHILOSOPHY**

**by**

**DAYANANDA D**

**ID. No. 2011PHXF001G**

Under the Supervision of  
**Dr. Narendra Nath Ghosh**



**BITS Pilani**  
Pilani | Dubai | Goa | Hyderabad

**BIRLA INSTITUTE OF TECHNOLOGY AND SCIENCE, PILANI**

**2015**

**BIRLA INSTITUTE OF TECHNOLOGY AND SCIENCE, PILANI**

**CERTIFICATE**

This is to certify that the thesis entitled “**Development of Simple Method for Preparation of Mesoporous Alumina Based Adsorbents and Their Application in Removal of Fluoride Ion from Water**” and submitted by **Dayananda D**, ID No. 2011PHXF001G for award of Ph.D. of the Institute embodies original work done by him under my supervision.

Signature of the Supervisor : Narendranath Ghosh  
Name in capital letters : **Dr. NARENDRA NATH GHOSH**  
Designation : Associate Professor

Date: 27.11.2015

## Acknowledgements

I wish to express my sincere gratitude to my supervisor, Dr. N. N. Ghosh for his continuous support, motivation and encouragement throughout the duration of my research work. I am deeply indebted to him for his thoughtful guidance, patience, expertise and his invaluable suggestions.

I gratefully acknowledge the financial support of a Junior Research Fellow (JRF) and Senior Research Fellow (SRF) from Board of Research in Nuclear Science (BRNS) and BITS Pilani towards my Ph.D programme.

I am extremely grateful to Prof. V. S. Rao (Acting Vice Chancellor, BITS, Pilani), Prof. Sasikumar Punnekkat (Director, BITS, Pilani - K. K. Birla Goa Campus), Prof. R. N. Saha (Deputy Director, Research & Educational Development and Administration, BITS, Pilani), Prof. S. K. Verma, (Dean, Academic Research (Ph. D. Programme), BITS, Pilani), Prof. P. K. Das (Associate Dean, Academic Research, BITS, Pilani - K. K. Birla Goa Campus) and Prof. Sunil Bhand (Dean, Sponsored Research and Consulting, BITS, Pilani) for providing me with the facilities to conduct my research work at BITS, Pilani - K. K. Birla Goa Campus.

I am also thankful to Prof. R.N. Behera, Head of the Department, Department of Chemistry for the facilities and the help provided as well as his continuous encouragement during my work. I extend my sincere thanks to Prof. A. P. Koley (Associate Dean: Instruction, BITS, Pilani - K. K. Birla Goa Campus) for his encouragement at various phases of my Ph.D programme.

I extend my sincere thanks to my Doctoral Advisory Committee members Prof. Sunil Bhand (Professor, Department of Chemistry) and Prof. Halan Prakash (Associate Professor, Department of Chemistry) for their valuable advice, motivation and their support at various phases of my work and. I want to thank Dr. P. Bhavana, Dr. H.

Prakash, Dr. M. Banerjee and Dr. A. Chattopadhyay (Doctoral Research Committee, Department of Chemistry) for their support at various phases of my work.

I am very thankful to Dr. Arunachalam and Dr. S.V.Rao (NCCCM, BARC Hyderabad) for helping me in fluoride analysis.

I am indebted to Dr. V. S. Prasad, Scientist, Chemical Technology division, NIIST, Thiruvananthapuram, Kerala, for helping me in HRTEM analysis.

I am grateful to my ex- research colleague Dr. Bhanudas Naik, Dr. Amit Rajput and Dr. Subhenjit Hazra for their help, motivation and valuable suggestions. I am thankful to them for guiding me in instrumental analysis. I am also thank my research colleagues Mr. Barun Kumar Ghosh and Mr. Debabrato Moitra for helping me in various ways.

I am thankful to Mr. Tharun Kanna and Mr. Swapnil Gupta, undergraduate students, BITS- Pilani, K. K. Birla, Goa Campus, for their help during my research work.

I am extremely thankful to my fellow research scholars from BITS-Pilani, K. K. Birla Goa Campus. I will always be grateful to them for their support throughout my research work.

I am thankful to Mr. Digambar Waingankar and Mrs. Princy Johnson (Lab Technician, Department of Chemistry) for their help and co-operation.

I also thank the non-teaching staff of BITS-Pilani, K. K. Birla Goa Campus for their kind help.

Finally, I owe my warmest gratitude to my parents and all my family members for their love and moral support.

## Abstract

Though it is a well known fact that a significant portion of human population all around the world is suffering from consumption of fluoride contaminated ground water, but to date defluoridation of drinking water is a major challenge. Several techniques have been invented for this purpose which are capable of removing  $F^-$  from water at various contamination levels. Amongst these techniques, adsorption based methods are found to be more convenient and cost effective. Most commonly used adsorbent for defluoridation of water is either activated  $Al_2O_3$  or  $Al_2O_3$  based materials. Activated alumina is extensively used adsorbent for defluoridation of drinking water because of its high affinity and selectivity for  $F^-$  ions.

In this research work, an aqueous solution based cost effective chemical method has been developed for preparation of mesoporous  $Al_2O_3$ , and  $ZrO_2$ ,  $MgO$  and  $CaO$  nanoparticle loaded mesoporous  $Al_2O_3$ . The synthesized adsorbents were characterized using powder X-ray diffractometer (XRD),  $N_2$  adsorption-desorption surface area and pore size analyzer and High Resolution Transmission Electron Microscope (HRTEM). The synthesized adsorbents have been thoroughly investigated for the adsorption of  $F^-$  by batch adsorption method. Investigations on the effect of various processing parameters (such as composition of adsorbents, contact time, initial pH of the solution, adsorbent dose and initial  $F^-$  concentration of the solution) on  $F^-$  adsorption property of synthesized materials were performed.

Synthesized mesoporous  $Al_2O_3$  showed more  $F^-$  adsorption capacity than commercial  $Al_2O_3$ . Incorporation of metal oxide nanoparticle ( $ZrO_2$ ,  $MgO$  and  $CaO$ ) enhanced the  $F^-$  adsorption capacity of mesoporous  $Al_2O_3$ .  $CaO$  nanoparticle loaded mesoporous  $Al_2O_3$  showed faster kinetics as well as higher  $F^-$  adsorption capacity. The maximum  $F^-$  adsorption capacity of  $CaO$  nanoparticle loaded mesoporous  $Al_2O_3$  was  $137\text{ mg g}^{-1}$  and exhibited good  $F^-$  removal efficiency over a wide range of pH. Kinetic data revealed that, fluoride sorption on 20 wt.%  $CaO$  loaded mesoporous  $Al_2O_3$  was rapid, and  $\sim 90\%$  fluoride removal was achieved within 15 min. Generally, the fluoride concentration in contaminated ground water is  $\sim 5\text{-}10\text{ mg L}^{-1}$ . When the solutions having  $F^-$  concentration of  $5\text{ mg L}^{-1}$  and  $10\text{ mg L}^{-1}$  was treated with  $CaO$  nanoparticle loaded mesoporous  $Al_2O_3$ , the  $F^-$  concentration of treated water were reduced to below  $1\text{ mg L}^{-1}$ , which is well below the recommendation of WHO.

# TABLE OF CONTENTS

	Page No.
Acknowledgements	iii
Abstract	v
List of Tables	xi
List of Figures	xii
List of Abbreviations	xvi
List of Symbols	xvii
<b>1. Introduction</b>	<b>1</b>
1.1. Scope of research work	1
1.2. Fluoride in drinking water	1
1.3. Methods of defluoridation from aqueous solutions	2
1.3.1. Precipitation-Coagulation	2
1.3.2. Membrane Based Processes	3
1.3.3. Ion-Exchange Method	5
1.3.4. Adsorption	6
1.4. F <sup>-</sup> adsorption mechanisms on adsorbents	6
1.4.1. Factors influencing F <sup>-</sup> adsorption	11
1.4.1.1. pH	11
1.4.1.2. Co-existing anions	11
1.4.1.3. Temperature	13
1.4.2. Adsorption kinetics	13
1.4.3. Adsorption isotherms	14
1.5. Different adsorbents used for defluoridation of water	15
1.5.1. Al <sub>2</sub> O <sub>3</sub> based adsorbents	16
1.5.1.1. Activated Alumina (AA)	16
1.5.1.2. Mesoporous Al <sub>2</sub> O <sub>3</sub>	20
1.5.1.3. Modified Activated Alumina	22
1.5.2. Mechanism of F <sup>-</sup> adsorption on Al <sub>2</sub> O <sub>3</sub> based adsorbents	32
1.5.3. Nano particle based adsorbents	33
1.6. Gap in existing research	40

1.7. Objectives	40
1.8. Characterization details	41
1.9. Fluoride adsorption experiments	42
1.10. Fluoride analysis	43
1.11. Outlay of thesis	44
<b>2. Preparation of mesoporous Al<sub>2</sub>O<sub>3</sub> and their fluoride removal performance from water</b>	<b>45</b>
2.1. Experimental procedure for materials synthesis	45
2.1.1. Materials used	45
2.1.2. Synthesis of mesoporous Al <sub>2</sub> O <sub>3</sub>	45
2.2. Results and discussions	46
2.2.1. Characterization of adsorbents	46
2.2.1.1. X-ray diffraction analysis	46
2.2.1.2. N <sub>2</sub> adsorption-desorption analysis	47
2.2.1.3. HRTEM analysis	47
2.2.1.4. Analysis of pH <sub>PZC</sub> of the adsorbents	48
2.2.2. Fluoride adsorption studies	49
2.2.2.1. Determination of unknown F <sup>-</sup> concentration	49
2.2.2.2. Effect of contact time	50
2.2.2.3. Effect of adsorbent dose	50
2.2.2.4. Adsorption kinetics	51
2.2.2.5. Effect of initial fluoride concentration	53
2.2.2.6. Adsorption isotherm study	53
2.2.2.7. Effect of initial pH	55
2.2.2.8. Effect of co-existing anions	56
2.3. Summary of results	57
<b>3. Preparation of ZrO<sub>2</sub> nanoparticle loaded mesoporous Al<sub>2</sub>O<sub>3</sub> based adsorbents and their fluoride removal performance from water</b>	<b>58</b>
3.1. Experimental procedure for materials synthesis	58
3.1.1. Materials used	58
3.1.2. Synthesis of mesoporous Al <sub>2</sub> O <sub>3</sub>	58

3.1.3. Preparation of ZrO <sub>2</sub> nanoparticle loaded mesoporous Al <sub>2</sub> O <sub>3</sub>	58
3.2. Results and discussion	59
3.2.1. Characterization of adsorbents	59
3.2.1.1. X-ray diffraction analysis	59
3.2.1.2. N <sub>2</sub> adsorption-desorption analysis	60
3.2.1.3. HRTEM analysis	62
3.2.1.4. Analysis of pH <sub>PZC</sub> of the adsorbents	63
3.2.2. Fluoride adsorption studies	63
3.2.2.1. Optimization of adsorbent composition	63
3.2.2.2. Effect of adsorbent dose	64
3.2.2.3. Effect of contact time	65
3.2.2.4. Adsorption kinetics	66
3.2.2.5. Effect of initial fluoride concentration	69
3.2.2.6. Adsorption Isotherms	70
3.2.2.7. Effect of initial pH	71
3.2.2.8. Effect of competing anions	72
3.3. Summary of results	73

<b>4. Preparation of MgO nanoparticle loaded mesoporous Al<sub>2</sub>O<sub>3</sub> based adsorbents and their fluoride removal performance from water</b>	74
4.1. Experimental procedure for materials synthesis	74
4.1.1. Materials used	74
4.1.2. Synthesis of mesoporous Al <sub>2</sub> O <sub>3</sub>	74
4.1.3. Preparation of MgO nanoparticle loaded mesoporous Al <sub>2</sub> O <sub>3</sub>	74
4.2. Results and discussion	75
4.2.1. Characterization of adsorbents	75
4.2.1.1. X-ray diffraction analysis	75
4.2.1.2. N <sub>2</sub> adsorption-desorption analysis	76
4.2.1.3. HRTEM analysis	76
4.2.1.4. Analysis of pH <sub>PZC</sub> of the adsorbents	78
4.2.2. Fluoride adsorption studies	79
4.2.2.1. Optimization of adsorbent composition	79
4.2.2.2. Effect of adsorbent dose	79



4.2.2.3. Effect of contact time	80
4.2.2.4. Adsorption kinetics	81
4.2.2.5. Effect of initial fluoride concentration	83
4.2.2.6. Adsorption Isotherms	85
4.2.2.7. Effect of initial pH	87
4.2.2.8. Effect of competing anions	88
4.3. Summary of results	88
<b>5. Preparation of CaO nanoparticle loaded mesoporous Al<sub>2</sub>O<sub>3</sub> based adsorbents and their fluoride removal performance from water</b>	<b>89</b>
5.1. Experimental procedure for materials synthesis	89
5.1.1. Materials used	89
5.1.2. Synthesis of mesoporous Al <sub>2</sub> O <sub>3</sub>	89
5.1.3. Preparation of CaO nanoparticle loaded mesoporous Al <sub>2</sub> O <sub>3</sub>	89
5.2. Results and discussion	90
5.2.1. Characterization of adsorbents	90
5.2.1.1. X-ray diffraction analysis	90
5.2.1.2. N <sub>2</sub> adsorption-desorption analysis	91
5.2.1.3. HRTEM analysis	92
5.2.1.4. Analysis of pH <sub>PZC</sub> of the adsorbents	92
5.2.2. Fluoride adsorption studies	94
5.2.2.1. Optimization of adsorbent composition	94
5.2.2.2. Effect of adsorbent dose	95
5.2.2.3. Effect of contact time	96
5.2.2.4. Adsorption kinetics	96
5.2.2.5. Effect of initial fluoride concentration	100
5.2.2.6. Adsorption Isotherms	100
5.2.2.7. Effect of initial pH	102
5.2.2.8. Effect of competing anions	102
5.3. Summary of results	104
<b>6. Conclusions and future scope of work</b>	<b>105</b>
6.1. Conclusions	105

6.2. Future scope of work	106
<b>References</b>	107
<b>List of Publications</b>	Appendix I
<b>Bio-data of candidate</b>	Appendix II
<b>Bio-data of supervisor</b>	Appendix III

## List of Tables

Table	Page No.
1.1. Various alumina based adsorbents used for defluoridation of water.	26
1.2. Various nano particle based adsorbents used for defluoridation of water.	37
2.1. Comparison of pseudo-first order and pseudo-second order kinetic models parameters, and calculated $q_{e(cal)}$ and experimental $q_{e(exp)}$ values for different initial $F^-$ concentrations of synthesized $Al_2O_3$ .	53
2.2. Freundlich and Langmuir isotherm constants for $F^-$ adsorption on synthesized $Al_2O_3$ and commercial $Al_2O_3$ at pH of $6.8 \pm 0.2$ .	55
3.1. Surface area and pore size parameters obtained by means of $N_2$ adsorption-desorption study.	60
3.2. Comparison of pseudo-first order and pseudo-second order kinetic models parameters, and calculated $q_{e(cal)}$ and experimental $q_{e(exp)}$ values for different initial $F^-$ concentrations of $Al_2O_3$ and $15ZrO_2@Al_2O_3$ .	68
3.3. Langmuir and Freundlich isotherm parameters for $F^-$ adsorption on $Al_2O_3$ and $15ZrO_2@Al_2O_3$ at pH of $6.8 \pm 0.2$ .	71
4.1. Surface area and pore size parameters of the synthesized adsorbents obtained by means of $N_2$ adsorption-desorption study.	77
4.2. Comparison of pseudo-first order and pseudo-second order kinetic models parameters, and calculated $q_{e(cal)}$ and experimental $q_{e(exp)}$ values for different initial $F^-$ concentrations of $Al_2O_3$ and $40MgO@Al_2O_3$ .	84
4.3. Langmuir and Freundlich isotherm parameters for $F^-$ adsorption on $Al_2O_3$ and $40MgO@Al_2O_3$ at pH of $6.8 \pm 0.2$ .	87
5.1. Surface area and pore size parameters of the synthesized adsorbents obtained by means of $N_2$ adsorption-desorption study.	92
5.2. Comparison of pseudo-first order and pseudo-second order kinetic models parameters, and calculated $q_{e(cal)}$ and experimental $q_{e(exp)}$ values for different initial $F^-$ concentrations of $Al_2O_3$ and $20CaO@Al_2O_3$ .	99
5.3. Langmuir and Freundlich isotherm parameters for $F^-$ adsorption on $Al_2O_3$ and $20CaO@Al_2O_3$ at pH of $6.8 \pm 0.2$ .	101
6.1. Comparison of $F^-$ adsorption performance of synthesized adsorbents.	106

## List of Figures

Figure	Page no
1.1. Adsorption of F <sup>-</sup> on the surface of ion exchange resin.	7
1.2. Adsorption of F <sup>-</sup> ion on the surface of adsorbent by H-bonding.	8
1.3. Ligand exchange mechanism of F <sup>-</sup> adsorption.	9
1.4. Adsorption of F <sup>-</sup> on the chemically modified adsorbent surface.	10
2.1. Room temperature powder XRD pattern of synthesized Al <sub>2</sub> O <sub>3</sub> and commercial Al <sub>2</sub> O <sub>3</sub> .	46
2.2. (A) N <sub>2</sub> adsorption- desorption isotherms and (B) pore size distribution of (a) synthesized Al <sub>2</sub> O <sub>3</sub> and (b) commercial Al <sub>2</sub> O <sub>3</sub> .	47
2.3. HRTEM image of synthesized Al <sub>2</sub> O <sub>3</sub> .	48
2.4. Plot for determination of pHPZC of commercial Al <sub>2</sub> O <sub>3</sub> and synthesized Al <sub>2</sub> O <sub>3</sub> .	49
2.5. Calibration curve for determining the unknown F <sup>-</sup> concentrations ( $\lambda_{\max} = 550 \text{ nm}$ ).	49
2.6. Effect of contact time on F <sup>-</sup> removal of synthesized Al <sub>2</sub> O <sub>3</sub> and commercial Al <sub>2</sub> O <sub>3</sub> . ( $C_0 = 5 \text{ mg L}^{-1}$ , adsorbent dose = $5 \text{ g L}^{-1}$ , pH = $6.8 \pm 0.2$ ).	50
2.7. Effect of adsorbent dose on F <sup>-</sup> removal of synthesized Al <sub>2</sub> O <sub>3</sub> . ( $C_0 = 10 \text{ mg L}^{-1}$ , contact time = 8 h, pH = $6.8 \pm 0.2$ ).	51
2.8. Adsorption kinetic curves of F <sup>-</sup> at different initial F <sup>-</sup> concentrations (adsorbent dose = $3 \text{ g L}^{-1}$ ; $C_0 = 5, 10, 20, 30 \text{ mg L}^{-1}$ , pH = $6.8 \pm 0.2$ ).	52
2.9. (i) Pseudo first order kinetic and (ii) Pseudo second order kinetic fit for F <sup>-</sup> adsorption on synthesized Al <sub>2</sub> O <sub>3</sub> at $C_0 = 5, 10, 20, 30 \text{ mg L}^{-1}$ , pH = $6.8 \pm 0.2$ .	52
2.10. Effect of initial F <sup>-</sup> concentration on F <sup>-</sup> adsorption capacity of synthesized Al <sub>2</sub> O <sub>3</sub> and commercial Al <sub>2</sub> O <sub>3</sub> (initial F <sup>-</sup> concentration = 5- 100 mg L <sup>-1</sup> , adsorbent dose = $3 \text{ g L}^{-1}$ , contact time = 10 h, pH = $6.8 \pm 0.2$ ).	54
2.11. (i) Freundlich adsorption isotherm and (ii) Langmuir adsorption isotherm fits for adsorption of F <sup>-</sup> on synthesized Al <sub>2</sub> O <sub>3</sub> and commercial Al <sub>2</sub> O <sub>3</sub> . (adsorbent dose = $3 \text{ g L}^{-1}$ , $C_0 = 5- 100 \text{ mg L}^{-1}$ , pH = $6.8 \pm 0.2$ ).	54
2.12. Effect of initial pH on F <sup>-</sup> adsorption capacity of synthesized Al <sub>2</sub> O <sub>3</sub> (adsorbent dose = $3 \text{ g L}^{-1}$ , $C_0 = 30 \text{ mg L}^{-1}$ , contact time = 8 h).	56
2.13. Effect of co-existing anions on F <sup>-</sup> adsorption capacity of Al <sub>2</sub> O <sub>3</sub> (adsorbent dose = $3 \text{ g L}^{-1}$ , $C_0 = 10 \text{ mg L}^{-1}$ , contact time = 8 h).	57

3.1. XRD pattern of (a) Al <sub>2</sub> O <sub>3</sub> , (b) 5ZrO <sub>2</sub> @Al <sub>2</sub> O <sub>3</sub> , (c) 10 ZrO <sub>2</sub> @Al <sub>2</sub> O <sub>3</sub> , (d) 15ZrO <sub>2</sub> @Al <sub>2</sub> O <sub>3</sub> and (e) 20ZrO <sub>2</sub> @Al <sub>2</sub> O <sub>3</sub> .	59
3.2. (a) N <sub>2</sub> -adsorption desorption isotherms and (b) Pore size distributions (inset) of pure Al <sub>2</sub> O <sub>3</sub> and ZrO <sub>2</sub> loaded aluminas	61
3.3. HRTEM images of (a) Al <sub>2</sub> O <sub>3</sub> , (b) 15ZrO <sub>2</sub> @Al <sub>2</sub> O <sub>3</sub> and (c) shows 15ZrO <sub>2</sub> @Al <sub>2</sub> O <sub>3</sub> with higher magnification, showing the fringes of ZrO <sub>2</sub> nanoparticle.	62
3.4. Plot for determination of pH <sub>PZC</sub> of Al <sub>2</sub> O <sub>3</sub> and 15ZrO <sub>2</sub> @Al <sub>2</sub> O <sub>3</sub> .	63
3.5. Effect of ZrO <sub>2</sub> loading on mesoporous Al <sub>2</sub> O <sub>3</sub> for removal of F <sup>-</sup> . (C <sub>0</sub> = 30 mg L <sup>-1</sup> , adsorbent dose = 3 g L <sup>-1</sup> , contact time = 8 h, pH = 6.8 ± 0.2).	64
3.6. Effect of adsorbent dose on F <sup>-</sup> adsorption capacity of adsorbents. (C <sub>0</sub> = 10 mg L <sup>-1</sup> , contact time = 8 h, pH = 6.8 ± 0.2).	65
3.7. Effect of contact time on F <sup>-</sup> adsorption capacity of adsorbents (C <sub>0</sub> = 30 mg L <sup>-1</sup> , adsorbent dose = 3 g L <sup>-1</sup> , pH = 6.8 ± 0.2).	66
3.8. Adsorption kinetic curves of F <sup>-</sup> adsorption on 15ZrO <sub>2</sub> @Al <sub>2</sub> O <sub>3</sub> at different initial F <sup>-</sup> concentrations (C <sub>0</sub> = 5, 10, 20 and 30 mg L <sup>-1</sup> , adsorbent dose = 3 g L <sup>-1</sup> , pH = 6.8 ± 0.2).	67
3.9. (i) Pseudo first order and (ii) Pseudo second order adsorption kinetic model for F <sup>-</sup> adsorption on 15ZrO <sub>2</sub> @Al <sub>2</sub> O <sub>3</sub> . (C <sub>0</sub> = 5, 10, 20 and 30 mg L <sup>-1</sup> , adsorbent dose = 3 g L <sup>-1</sup> , pH = 6.8 ± 0.2).	67
3.10. Effect of initial F <sup>-</sup> concentration on F <sup>-</sup> adsorption capacity of Al <sub>2</sub> O <sub>3</sub> and 15ZrO <sub>2</sub> @Al <sub>2</sub> O <sub>3</sub> (adsorbent dose= 3 g L <sup>-1</sup> , contact time= 8 h, pH= 6.8± 0.2).	69
3.11. (i) Freundlich adsorption isotherm and (ii) Langmuir adsorption isotherm fits for adsorption of F <sup>-</sup> on Al <sub>2</sub> O <sub>3</sub> and 15ZrO <sub>2</sub> @Al <sub>2</sub> O <sub>3</sub> . (C <sub>0</sub> =5 to 100 mg L <sup>-1</sup> , adsorbent dose = 3 g L <sup>-1</sup> , contact time = 8 h, pH = 6.8 ± 0.2).	70
3.12. Effect of initial pH on F <sup>-</sup> adsorption capacity of Al <sub>2</sub> O <sub>3</sub> and 15ZrO <sub>2</sub> @Al <sub>2</sub> O <sub>3</sub> (adsorbent dose = 3 g L <sup>-1</sup> , C <sub>0</sub> = 30 mg L <sup>-1</sup> , contact time = 8 h).	72
3.13. Effect of co-existing anions on F <sup>-</sup> adsorption capacity of Al <sub>2</sub> O <sub>3</sub> and 15ZrO <sub>2</sub> @Al <sub>2</sub> O <sub>3</sub> (adsorbent dose =3 g L <sup>-1</sup> , C <sub>0</sub> =10 mg L <sup>-1</sup> , contact time=8h)	73
4.1. XRD pattern of (a) Al <sub>2</sub> O <sub>3</sub> , (b) 10MgO@Al <sub>2</sub> O <sub>3</sub> , (c) 20MgO@Al <sub>2</sub> O <sub>3</sub> , (d) 30MgO @Al <sub>2</sub> O <sub>3</sub> , (e) 40MgO@Al <sub>2</sub> O <sub>3</sub> and (f) 50MgO@Al <sub>2</sub> O <sub>3</sub> .	75

4.2. (i) N <sub>2</sub> -adsorption desorption isotherms and (ii) Pore size distributions of (a) Al <sub>2</sub> O <sub>3</sub> , (b) 10MgO@Al <sub>2</sub> O <sub>3</sub> , (c) 20MgO@Al <sub>2</sub> O <sub>3</sub> , (d) 30MgO@Al <sub>2</sub> O <sub>3</sub> , (e) 40MgO@Al <sub>2</sub> O <sub>3</sub> and (f) 50MgO@Al <sub>2</sub> O <sub>3</sub> .	77
4.3. HRTEM images of (a) Al <sub>2</sub> O <sub>3</sub> , (b) 40MgO@Al <sub>2</sub> O <sub>3</sub> (MgO nanoparticles are shown within the circle).	78
4.4. Plot for determination of pH <sub>PZC</sub> of Al <sub>2</sub> O <sub>3</sub> and 40MgO@Al <sub>2</sub> O <sub>3</sub> .	78
4.5. Effect of MgO loading on mesoporous Al <sub>2</sub> O <sub>3</sub> for removal of F <sup>-</sup> . (C <sub>0</sub> = 30 mg L <sup>-1</sup> , adsorbent dose = 3 g L <sup>-1</sup> , contact time = 8 h, pH = 6.8 ± 0.2).	79
4.6. Effect of adsorbent dose on F <sup>-</sup> adsorption capacity of adsorbents. (C <sub>0</sub> = 10 mg L <sup>-1</sup> , contact time = 8 h, pH = 6.8 ± 0.2).	80
4.7. Effect of contact time on F <sup>-</sup> adsorption capacity of adsorbents (C <sub>0</sub> = 30 mg L <sup>-1</sup> , adsorbent dose = 3 g L <sup>-1</sup> , pH = 6.8 ± 0.2).	81
4.8. Adsorption kinetic curves of F <sup>-</sup> adsorption on 40MgO@Al <sub>2</sub> O <sub>3</sub> at different initial F <sup>-</sup> concentrations (C <sub>0</sub> = 5, 10, 20 and 30 mg L <sup>-1</sup> , adsorbent dose = 3 g L <sup>-1</sup> , pH = 6.8 ± 0.2).	82
4.9. (i) Pseudo first order and (ii) Pseudo second order adsorption kinetic model for F <sup>-</sup> adsorption on 40MgO@Al <sub>2</sub> O <sub>3</sub> . (C <sub>0</sub> = 5, 10, 20 and 30 mg L <sup>-1</sup> , adsorbent dose = 3 g L <sup>-1</sup> , pH = 6.8 ± 0.2).	83
4.10. Effect of initial F <sup>-</sup> concentration on F <sup>-</sup> adsorption capacity of Al <sub>2</sub> O <sub>3</sub> and 40MgO@Al <sub>2</sub> O <sub>3</sub> (C <sub>0</sub> = 5 to 1000 mg L <sup>-1</sup> , adsorbent dose = 3 g L <sup>-1</sup> , contact time = 8 h, pH = 6.8 ± 0.2).	85
4.11. (i) Freundlich adsorption isotherm models and (ii) Langmuir adsorption isotherm models for adsorption of F <sup>-</sup> on mesoporous Al <sub>2</sub> O <sub>3</sub> and 40MgO@Al <sub>2</sub> O <sub>3</sub> . (C <sub>0</sub> = 5 to 1000 mg L <sup>-1</sup> , adsorbent dose = 3 g L <sup>-1</sup> , contact time = 8 h, pH = 6.8 ± 0.2) (The inset is isotherm models at low F <sup>-</sup> concentration ranging from 5 to 100 mg L <sup>-1</sup> )	86
4.12. Effect of initial pH on F <sup>-</sup> adsorption capacity of Al <sub>2</sub> O <sub>3</sub> and 40MgO@Al <sub>2</sub> O <sub>3</sub> (adsorbent dose= 3 g L <sup>-1</sup> , C <sub>0</sub> = 30 mg L <sup>-1</sup> , contact time=8 h).	87
4.13. Effect of co-existing anions on F <sup>-</sup> adsorption capacity of Al <sub>2</sub> O <sub>3</sub> and 40MgO@Al <sub>2</sub> O <sub>3</sub> (adsorbent dose= 3 g L <sup>-1</sup> , C <sub>0</sub> =10 mg L <sup>-1</sup> , contact time=8h).	88
5.1. XRD pattern of (a) mesoporous Al <sub>2</sub> O <sub>3</sub> , (b) 5CaO@Al <sub>2</sub> O <sub>3</sub> , (c) 10CaO@Al <sub>2</sub> O <sub>3</sub> , (d) 15CaO@Al <sub>2</sub> O <sub>3</sub> , (e) 20CaO@Al <sub>2</sub> O <sub>3</sub> and (f) 30CaO@Al <sub>2</sub> O <sub>3</sub> .	90

5.2. (i) N <sub>2</sub> -adsorption desorption isotherms and (ii) Pore size distributions of (a) mesoporous Al <sub>2</sub> O <sub>3</sub> , (b) 5CaO@Al <sub>2</sub> O <sub>3</sub> , (c) 10CaO@Al <sub>2</sub> O <sub>3</sub> , (d) 15CaO@Al <sub>2</sub> O <sub>3</sub> , (e) 20CaO@Al <sub>2</sub> O <sub>3</sub> and (f) 30CaO@Al <sub>2</sub> O <sub>3</sub> .	91
5.3. HRTEM images of (a) Al <sub>2</sub> O <sub>3</sub> and (b) 20CaO@Al <sub>2</sub> O <sub>3</sub> . CaO nanoparticles are shown within the circle.	93
5.4. Plot for determination of pH <sub>PZC</sub> of Al <sub>2</sub> O <sub>3</sub> and 20CaO@Al <sub>2</sub> O <sub>3</sub> adsorbent.	93
5.5. Effect of CaO loading on mesoporous Al <sub>2</sub> O <sub>3</sub> for removal of F <sup>-</sup> (C <sub>0</sub> = 30 mg L <sup>-1</sup> , adsorbent dose = 3 g L <sup>-1</sup> , contact time = 8 h, pH = 6.8 ± 0.2).	95
5.6. Effect of adsorbent dose on F <sup>-</sup> adsorption capacity of adsorbents. (C <sub>0</sub> = 10 mg L <sup>-1</sup> , contact time = 8 h, pH = 6.8 ± 0.2).	96
5.7. Effect of contact time on F <sup>-</sup> adsorption capacity of adsorbents. (C <sub>0</sub> = 30 mg L <sup>-1</sup> , adsorbent dose = 3 g L <sup>-1</sup> , pH = 6.8 ± 0.2).	97
5.8. Adsorption kinetic curves of F <sup>-</sup> adsorption on 20CaO@Al <sub>2</sub> O <sub>3</sub> at different initial F <sup>-</sup> concentrations (C <sub>0</sub> = 5, 10, 20 and 30 mg L <sup>-1</sup> , adsorbent dose = 3 g L <sup>-1</sup> , pH = 6.8 ± 0.2).	97
5.9. (i) Pseudo first order adsorption kinetic model and (ii) Pseudo second order adsorption kinetic model for F <sup>-</sup> adsorption on 20CaO@Al <sub>2</sub> O <sub>3</sub> (C <sub>0</sub> = 5, 10, 20 and 30 mg L <sup>-1</sup> , adsorbent dose = 3 g L <sup>-1</sup> , pH = 6.8 ± 0.2).	98
5.10. Effect of initial F <sup>-</sup> concentration on F <sup>-</sup> adsorption capacity of Al <sub>2</sub> O <sub>3</sub> and 20CaO@Al <sub>2</sub> O <sub>3</sub> (adsorbent dose = 3 g L <sup>-1</sup> , contact time = 8 h, pH = 6.8 ± 0.2).	100
5.11. (i) Freundlich adsorption isotherm and (ii) Langmuir adsorption isotherm for adsorption of F <sup>-</sup> on Al <sub>2</sub> O <sub>3</sub> and 20CaO@Al <sub>2</sub> O <sub>3</sub> . (C <sub>0</sub> = 5 to 1000 mg L <sup>-1</sup> , adsorbent dose = 3 g L <sup>-1</sup> , contact time = 8 h).	102
5.12. Effect of initial pH on F <sup>-</sup> adsorption capacity of Al <sub>2</sub> O <sub>3</sub> and 20CaO@Al <sub>2</sub> O <sub>3</sub> (adsorbent dose = 3 g L <sup>-1</sup> , C <sub>0</sub> = 30 mg L <sup>-1</sup> , contact time = 8 h).	103
5.13. Effect of co-existing anions on F <sup>-</sup> adsorption capacity of Al <sub>2</sub> O <sub>3</sub> and 20CaO@Al <sub>2</sub> O <sub>3</sub> (adsorbent dose = 3 g L <sup>-1</sup> , C <sub>0</sub> = 10 mg L <sup>-1</sup> , contact time = 8 h).	103

## List of Abbreviations

<b>Abbreviations</b>	<b>Description</b>
AA	Activated alumina
AC	Activated carbon
ACNT	Aligned carbon nanotubes
AOMO	Aluminum oxide- manganese oxide
BET	Brunauer-Emmett-Teller
BJH	Barrett-Joyner-Halenda
CNT	Carbon nanotubes
FTIR	Fourier-transformed infra-red
HMOCA	Hydrous manganese oxide coated alumina
HRTEM	High resolution transmission electron micrograph
ICDD	International centre for diffraction data
IUPAC	International union of pure and applied chemistry
LDH	Layered double hydroxides
MAAA	Magnesia-amended activated alumina
MAS NMR	Magic-angle spinning nuclear magnetic resonance
MGA	Metallurgical grade alumina
MOCA	Manganese oxide coated alumina
NEERI	National Environmental Engineering Research Institute
NF	Nanofiltration
nHAp	Nano-hydroxyapatite
PZC	Point of zero charge
RO	Reverse osmosis
SEM	Scanning electron micrograph
THA	Treated hydrated alumina
TEA	Triethanol amine
UHA	Untreated hydrated alumina
WHO	World Health Organization
wt. %	weight percentage
XRD	X- ray diffraction
XPS	X-ray photoelectron spectroscopy



## List of Symbols

<b>Symbols</b>	<b>Description</b>
L	Liter
g	Grams
°C	Degree Celsius
t	Time
$q_t$	Amount of $F^-$ adsorbed on adsorbent at time t
$q_e$	Amount of $F^-$ adsorbed on adsorbent at equilibrium
$k_1$	Rate constant for pseudo first order kinetics
$k_2$	Rate constant for pseudo second order kinetics
$K_f$	Freundlich constant related to adsorbent capacity
1/n	Freundlich constant related to adsorption intensity
$C_0$	Initial fluoride concentration
$C_e$	Equilibrium fluoride concentration
b	Langmuir constant related to sorption energy
$Q_0$	Maximum fluoride adsorption capacity
nm	Nanometer
h	Hour
J	Joule
$\gamma$	Gamma
kV	Kilo Volts
M	Molarity
$\lambda_{max}$	Wavelength of maximum absorption
$R^2$	Correlation coefficient
r	Separation factor or equilibrium parameter
a.u	Arbitrary units

# Chapter 1

## Introduction

### 1.1. Scope of research work

The focus of this research work is (i) Development of simple and cost-effective method for the preparation of mesoporous  $\text{Al}_2\text{O}_3$  and metal oxide ( $\text{ZrO}_2$ ,  $\text{MgO}$ ,  $\text{CaO}$ ) nanoparticle loaded mesoporous  $\text{Al}_2\text{O}_3$  based adsorbents for removal of fluoride from water (ii) Investigations on effect of compositions of the adsorbents and various processing parameters on fluoride adsorption property of synthesized adsorbents.

In this chapter, various types of methodologies employed for defluoridation of water is described. As adsorption is the most important and widely employed technique, here we discuss this method in detail. In depth discussions about (i) different proposed mechanisms for adsorption, (ii) factors which influence the adsorption process, (iii) various adsorption isotherm models, (iv) different types of adsorbents (particularly  $\text{Al}_2\text{O}_3$  based adsorbents), and (v) recently developed nanoparticle based adsorbents and performance of various adsorbents are described here.<sup>1</sup>

### 1.2. Fluoride in drinking water

The presence of trace amount of  $\text{F}^-$  in drinking water is essential to prevent dental caries, but its presence in high concentration poses threat to human life.<sup>2</sup> Excess intake of  $\text{F}^-$  through drinking water leads to dental fluorosis (yellowish, brownish stains or mottling of the enamel), skeletal fluorosis (pain and stiffness in the back bone and joints), etc.<sup>3-5</sup> Accumulation of  $\text{F}^-$  over a long period of time can lead to cancer, osteosclerosis (brittle bones and calcified ligaments), gastrointestinal discomfort, deformities in red blood cells and sometimes neurological impairment.<sup>2-7</sup>

$\text{F}^-$  pollution in the environment occurs through natural and anthropogenic sources.<sup>8-10</sup>  $\text{F}^-$  in ground water derives mainly from dissolution of rock minerals and soils with which water interacts. When water percolates through rocks containing  $\text{F}^-$ , it leaches out  $\text{F}^-$  from these rocks.<sup>11</sup> Some  $\text{F}^-$  rich rocks are fluorospar (sedimentary rocks, limestones and sandstones), cryolite (igneous and granite) and fluorapatite.<sup>12</sup> Besides these natural sources,  $\text{F}^-$  can also be found in effluents from semiconductor,

electroplating, metal processing, fertilizers, aluminum, steel, glass manufacturing industries etc.<sup>13-15</sup> Discharge of  $F^-$  compound containing waste water from these industries into surface water also leads to an increase of  $F^-$  levels in ground and surface water.<sup>16</sup>

The World Health Organization (WHO) has classified  $F^-$  as one of the major contaminants in drinking water.<sup>3, 17</sup> As per WHO recommendation, the desirable limit and permissible limit of  $F^-$  in drinking water are  $1.0 \text{ mg L}^{-1}$  and  $1.5 \text{ mg L}^{-1}$  respectively. The problem of excessive  $F^-$  in drinking water has engulfed many parts of the world mainly in India and China, and today millions of people rely knowingly or unknowingly on groundwater with  $F^-$  concentrations above WHO permissible limit.<sup>18, 19</sup> There are more than 25 countries in which endemic fluorosis has been reported.<sup>19-22</sup> High  $F^-$  concentrations in ground water are found in many parts of South Asia, Africa, the Middle East, North, Central and South America, Europe.<sup>18, 23</sup> Severe problems associated with high  $F^-$  concentration of ground water are observed in India, China, Sri Lanka, and Rift valley countries in Africa.<sup>24-26</sup> It has been estimated that, at present residents of 17 states of India severely suffer from various diseases caused by the presence of high level  $F^-$  concentration in water and throughout India ~ 56.2 million people are affected by fluorosis.<sup>19, 27, 28</sup> Clean water (in this context, water with  $F^-$  ion within permissible limit) is one of the basic needs of a vast population of human race.

### **1.3. Methods of defluoridation from aqueous solutions**

Since 1930s there has been a continuous effort to remove  $F^-$  from water and for this purpose various methods have been invented.<sup>2, 19, 29-32</sup> The prominent methods for defluoridation of water are precipitation-coagulation, membrane separation, ion-exchange, adsorption etc.

#### **1.3.1. Precipitation-Coagulation**

Precipitation-coagulation method is a widely used technique for defluoridation of drinking water. Precipitation processes involve addition of the chemicals which can remove  $F^-$  as precipitate.  $F^-$  ions form precipitates with aluminum sulfate and lime or

with calcium and phosphate compounds.<sup>33, 34</sup> Two steps are involved in this precipitation-coagulation process: (i) lime dosing for precipitation and (ii) addition of alum for coagulation. Here, addition of alum triggers two reactions in water: formation of insoluble  $\text{Al}(\text{OH})_3$  by reacting with some of the alkalinity of water and reaction with  $\text{F}^-$  ions present in water. pH range of 5.5 to 7.5 has been reported as optimum pH for this process.<sup>35</sup> Most commonly used coagulants are lime and alum.<sup>29</sup> For defluoridation of water in India, Nalgonda Technique (developed by National Environmental Engineering Research Institute (NEERI), India) is one of the widely used methods, particularly at community levels.<sup>31, 36-38</sup> In this technique prescribed amounts of lime, alum and bleaching powder are added to the  $\text{F}^-$  containing water and then rapid mixing, flocculation, sedimentation, filtration and disinfection steps are performed for removing  $\text{F}^-$  from water.<sup>19</sup> Based on Nalgonda technique, bucket defluoridation system has also been developed for domestic use. By using this process it is possible to get ~ 20 L of purified water per day with residual  $\text{F}^-$  concentration of ~1- 1.5  $\text{mg L}^{-1}$ .<sup>29</sup> Based on this technique “Fill and draw” type systems have also been developed.<sup>29</sup>

Though, the co-precipitation technique based on aluminum salts is a well established method, some of the limitations associated with this method are low treatment efficiency, requirement of large dosage of aluminum sulfate and requirement of skilled manpower for operation. It also converts a greater portion of  $\text{F}^-$  into soluble aluminum fluoride complexes, which itself is toxic.<sup>39</sup>

### 1.3.2. Membrane Based Processes

Reverse osmosis (RO), nanofiltration (NF), dialysis and electrodialysis methods are membrane based processes which have been used for defluoridation of water.<sup>29, 40-44</sup> The driving force for  $\text{F}^-$  removal through RO process is the difference in chemical potential, created due to pressure gradient across the membrane.<sup>19</sup> Schneiter and Middlebrooks,<sup>45</sup> Fu et al.,<sup>46</sup> and Arora et al.<sup>47</sup> have discussed various applications of RO for purification of water. This process is highly effective for removal of  $\text{F}^-$  and ensures constant water quality. Ndiaye et al.<sup>48</sup> have observed that, more than 98%  $\text{F}^-$  removal from water is possible by using RO technique. However, this process is expensive in comparison with other methods. Disposal of concentrated brine

discharges is also a problem. NF operates at lower pressures and the membranes used for this process have slightly larger pores (microporous) than those used for RO process. NF requires less energy compare to RO and removes high concentration of dissolved solids easily.<sup>29</sup> Applications of NF membranes in water and waste water treatment has been reviewed by Drioli et al.<sup>49</sup> Tahikt et al.<sup>50</sup> have studied the defluoridation of water using NF400 membrane as a nanofilter and the quality of water produced after filtration was satisfactory, especially for lower  $F^-$  concentrations. However, for higher  $F^-$  concentrations, a double pass is necessary to produce water with  $< 1.5 \text{ mg L}^{-1} F^-$ .

In the dialysis method, solutes are separated by transporting through a membrane whereas, in RO and NF methods water passes through a membrane to retain the solutes. The membranes used in dialysis method have pores which are much less restrictive than those used for NF. This is because of the fact that, here the solute can be driven through the membrane either by an applied electric field or by Donnan effect.<sup>30, 51</sup> Durmaz et al.<sup>52</sup> have used Donnan dialysis method for defluoridation of water with AHA anion exchange membrane and also studied the effects of pH of the solution, co-existing anions and initial  $F^-$  concentration on  $F^-$  removal efficiency. The  $F^-$  removal efficiency of AHA membrane were then compared with other membranes such as Neosepta AFN and polysulfone SB-6407 and found to be in the order of AFN > AHA > SB-6407.

Electrodialysis method is similar to RO method except that applied electric field is used as a driving force instead of high pressure for removing the ionic components of contaminated water through ion exchange membranes.  $F^-$  removal from water using electrodialysis method has been studied by various researchers, such as Lounici et al.<sup>42</sup>, Kabay et al.<sup>53</sup>, Anouar et al.<sup>54</sup>, Lahnid et al.<sup>55</sup> etc. Kabay et al.<sup>53</sup> have reported the separation performance of electrodialysis in terms of mass transfer and energy consumption. It has been observed that, with increasing initial  $F^-$  concentration in the influent solution, the separation performance can be increased by increasing the applied potential. Moreover, the separation of  $F^-$  was affected by presence of  $Cl^-$  but not by  $SO_4^{2-}$ . The authors did not find any change in separation performance of electrodialysis process with changing feed flow rate.

The factors which influence these processes are raw water quality, cost, rejection of significant water loss, recovery and pretreatment. RO, NF, dialysis and

electro dialysis processes are relatively expensive to install and operate in comparison to other methods (adsorption, precipitation-coagulation, ion exchange) and these processes are prone to membrane fouling, scaling or membrane degradation.<sup>19, 29</sup>

### 1.3.3. Ion-Exchange Method

Ion exchange resins have also been used for defluoridation of drinking water.<sup>56-59</sup> Removal of  $F^-$  from water can be performed by passing water through a strongly basic anion-exchange resin, containing quarternary ammonium functional groups. The mechanism of removal of  $F^-$  from water by this method can be explained using the following equation.<sup>29</sup>



$F^-$  ions present in water, replace  $\text{Cl}^-$  ions of the resin and this reaction continues until all the sites on the resin are occupied by  $F^-$ . To regenerate the active sites of resin, backwashing of the resin is required with supersaturated sodium chloride solution.  $\text{Cl}^-$  ions replace the  $F^-$  ions leading to recharge of the resin. The higher electronegativity of  $F^-$  is the driving force for replacing of  $\text{Cl}^-$  ions of resin.<sup>29</sup> Mohan Rao and Bhaskaran<sup>56</sup> studied the defluoridation of water by using ion exchange materials and aluminum sulfate solution (2- 4%) was used for regeneration of the materials. In a two way ion exchange cyclic process, Castel et al.<sup>58</sup> used two anion exchange columns for defluoridation of water effectively. Zhou et al.<sup>60</sup> used lanthanum impregnated cross linked gelatin for removal of  $F^-$  from water. Verssinina et al.<sup>61</sup> reported the effect of other anions on  $F^-$  removal efficiency in ion exchange process. The ion exchange method has the capability to remove  $F^-$  up to 90- 95 % and it retains the taste of the water intact. However, in this technique  $F^-$  removal efficiency is reduced in the presence of  $\text{SO}_4^{2-}$ ,  $\text{CO}_3^{2-}$  and  $\text{PO}_4^{3-}$ .

### 1.3.4. Adsorption

Among the defluoridation methods, adsorption is one of the widely used methods because of its effectiveness, adsorption capacity, convenience, cost effectiveness, ease of operation, number of useful cycles, possibility of regeneration etc.<sup>29, 31</sup> Fan et al.<sup>7</sup> have theoretically explained that  $F^-$  adsorption on solid particles normally takes place in three essential steps:

- (i) External mass transfer: Transport or diffusion of  $F^-$  ions from bulk solution to the external surface of the adsorbent.
- (ii) Adsorption of  $F^-$  onto solid particle surfaces.
- (iii) Exchange of adsorbed  $F^-$  ions with the structural elements inside solid particles, depending upon the chemistry of the solids or transfer of the adsorbed  $F^-$  ions into the internal surfaces of porous materials (intra particle diffusion).<sup>30</sup>

In many water treatment plants this method is frequently used in large scale because it can be operated at high flow rates and can produce good quality of water by removing contaminants from water very effectively without generating sludge.<sup>31</sup>

Reported results have indicated that, each of the defluoridation techniques can remove  $F^-$  under specific conditions.  $F^-$  removal efficiency of a technique depends on many site-specific chemical, geographical and economic conditions.<sup>29</sup> Any particular technique cannot be generalized as a universal method for  $F^-$  removal because, if one technique is suitable for a particular region, that may not meet the requirements for some other places. Among the various methods used for defluoridation of drinking water, adsorption processes appear to be attractive method, which offers satisfactory results and is also simple, eco-friendly and cost effective.<sup>29</sup> Hence, special emphasis has been given to adsorption process and detailed discussions about various aspects of this process have been presented.

### 1.4. $F^-$ adsorption mechanisms on adsorbents

The capacity, energy and kinetics of  $F^-$  adsorption by adsorbents are influenced by the adsorption mechanism. Understanding these mechanisms becomes helpful for optimization of the adsorption process in water treatment plants and the subsequent adsorbent regeneration process. Some of the important mechanisms, which have been

proposed for  $F^-$  adsorption are (1) Outer-sphere surface complexation by van der Waals forces, (2) Outer-sphere surface complexation through ion exchange, (3) Inner-sphere surface complexation via H-bonding, (4) Inner-sphere surface complexation by ligand exchange, and (5) chemical modification of the adsorbent surface.<sup>31</sup> As weak physical adsorption process is involved in the first two mechanisms, they are non-specific to  $F^-$ . Strong chemical adsorption specific to  $F^-$  plays a critical role for the third and fourth mechanisms. Both specific and non-specific adsorption play important roles in fifth mechanism.

In the case of first mechanism, as van der Waals forces are weak short range forces acting between two atoms larger sized adsorbents exhibit a greater force of attraction. Therefore, dissolved organic matters (which are having high molecular weight and high surface area) preferentially adsorb over  $F^-$  on the surface of activated carbon.<sup>62</sup> It has been reported that,  $F^-$  can be adsorbed on manganese oxide-coated alumina by van der Waals forces at high pH.<sup>63</sup>

In ion exchange mechanism, when any counter ion leaves the ion exchanger surface it is replaced by equivalent amount of another counter ion to maintain electro-neutrality. Here, the adsorption occurs due to electrostatic or coulombic attraction and ions retain their inner hydration shell. Ions, having higher valency, higher concentration and ions of smaller hydrated equivalent volume, are preferred counter ions in this process.<sup>64</sup> As reported by Helfferich, the order of selectivity for anions by anion exchange resins is as follows: citrate  $>$   $SO_4^{2-}$ , oxalate  $>$   $I^- >$   $NO_3^- >$   $CrO_4^{2-} >$   $Br^- >$   $SCN^- >$   $Cl^- >$  acetate  $>$   $F^-$ .<sup>64</sup> So  $F^-$  removal by this process is difficult. Fig. 1.1 represents  $F^-$  removal by ion exchange resin.

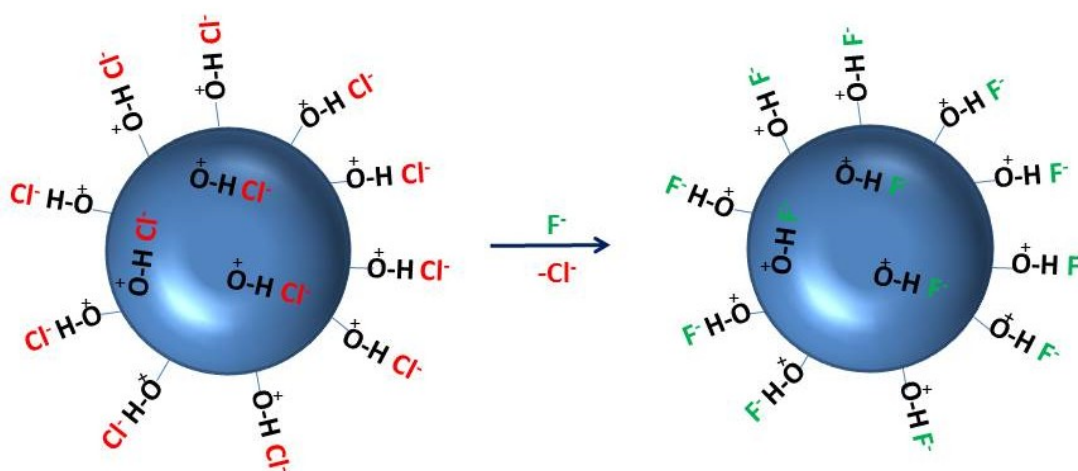


Fig. 1.1. Adsorption of  $F^-$  on the surface of ion exchange resin.<sup>31</sup>



In H-bonding mechanism, a strong dipole-dipole attraction between the strong electropositive H atom (which is present in adsorbent or adsorbate) and a strong electronegative atom or ion (e.g.  $F^-$ ) acts as driving force.<sup>65</sup> Here, the energy of adsorption is stronger than both van der Waals forces and ion exchange process but weaker than ligand exchange process. H-bonding mechanism is illustrated by Fig. 1.2.<sup>66-68</sup>

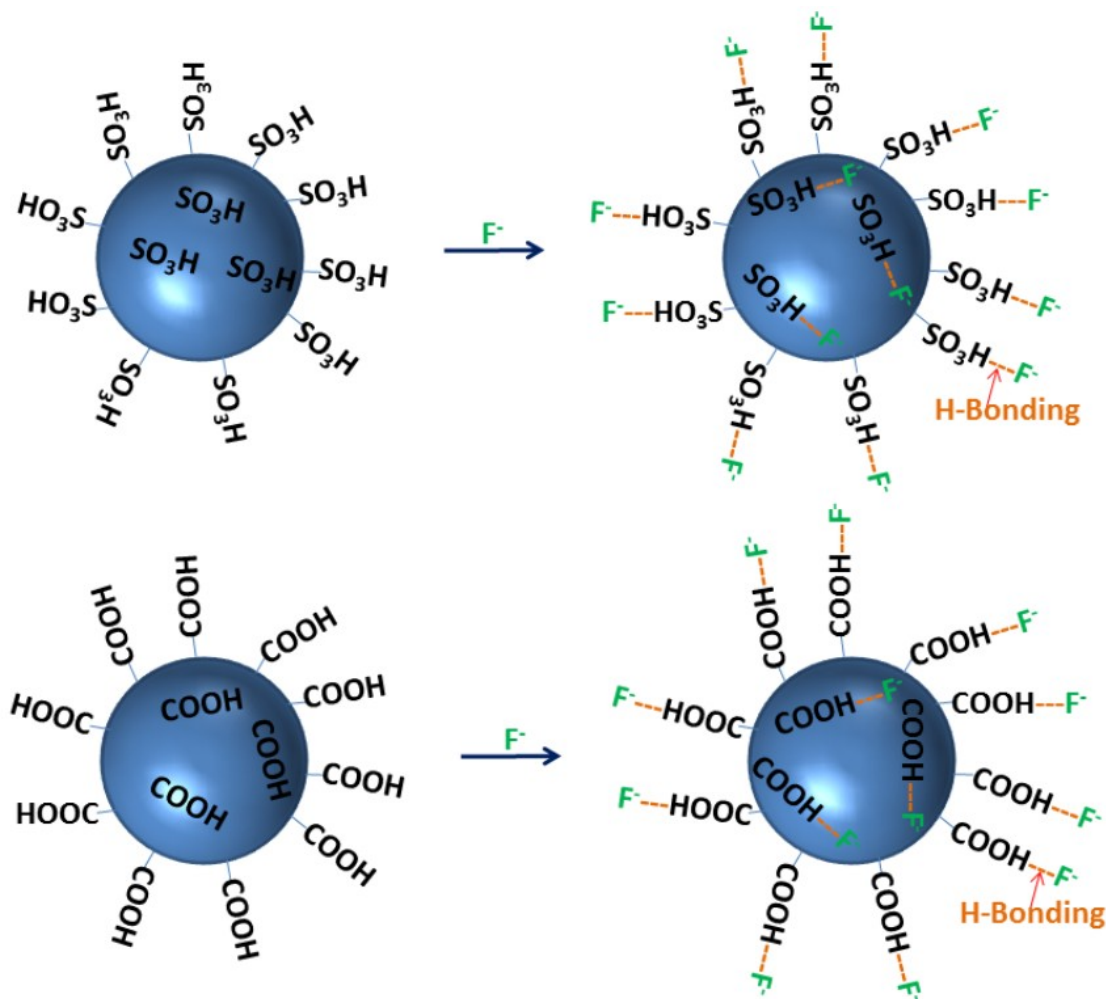


Fig. 1.2. Adsorption of  $F^-$  ion on the surface of adsorbent by H-bonding.<sup>31</sup>

In ligand exchange mechanism, a strong covalent bond forms between adsorbing anion ( $F^-$ ) and metallic cations, which are present at the surface of adsorbent. In this process other anions or  $H_2O$ , which were previously bonded to the metallic cation are released (Fig. 1.3). Thus,  $F^-$  specifically adsorbs on the adsorbent surface by forming an inner sphere complex. It has been reported that, during adsorption of  $F^-$  on the surface of several metal oxides near neutral pH results in

increase in pH of the solution.<sup>69, 70</sup> This is due to the release of  $\text{OH}^-$  ions, which were attached to adsorbents via ligand exchange mechanism. Adsorbents show high adsorption capacity with high selectivity for anions when adsorption proceeds via this mechanism. These adsorbents generally selectively remove the larger portion of targeted anions from very dilute solution even in the presence of competing anions with higher concentrations.<sup>70-72</sup>

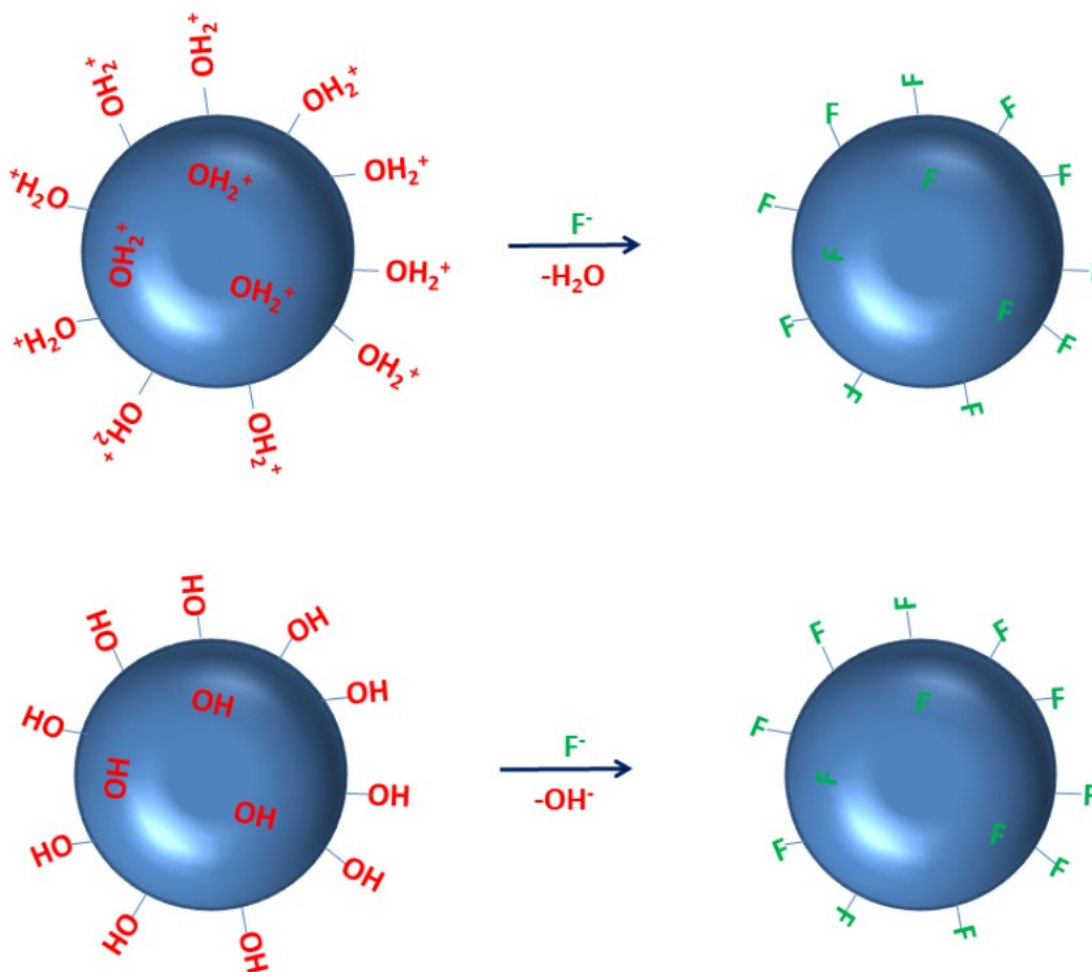


Fig. 1.3. Ligand exchange mechanism of  $\text{F}^-$  adsorption.<sup>31</sup>

Chemical modifications of surface of the adsorbents can also enhance the adsorption capacity of the adsorbents. Adsorbents with negatively charged surface tend to repel  $\text{F}^-$ . In these cases multivalent cations (such as  $\text{Zr}^{4+}$ ,  $\text{Ce}^{3+}$ ,  $\text{Al}^{3+}$ ,  $\text{La}^{4+}$ ,  $\text{Fe}^{3+}$  etc.) are impregnated onto the adsorbents, so that they can attract  $\text{F}^-$  ions by coulombic force.<sup>71, 73-78</sup> These metallic cations act as adsorption sites and form a

bridge between adsorbing  $F^-$  and adsorbent. This mechanism is shown below as Fig. 1.4.

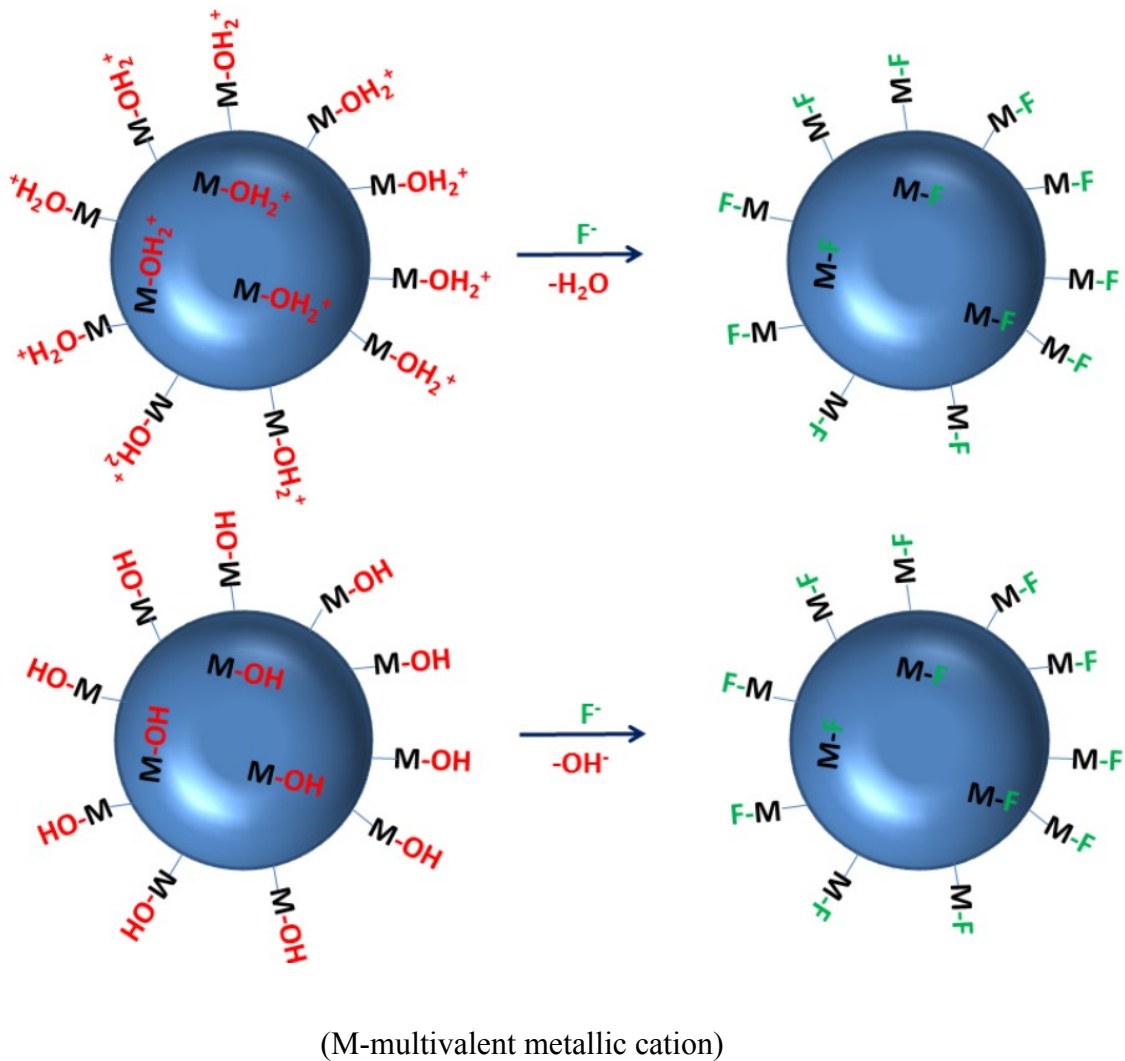


Fig. 1.4. Adsorption of  $F^-$  on the chemically modified adsorbent surface.<sup>31</sup>

When the adsorbents are porous in nature, adsorption generally proceeds in two steps: (i) initial rapid adsorption at the outer surface of adsorbent and (ii) when a pseudo equilibrium between solid- solution interface is reached then diffusion of  $F^-$  occurs into the interior pores and channels of adsorbent.<sup>31</sup> This second step is much slower than first step. Granular ferric hydroxide,<sup>79</sup> manganese oxide-coated alumina,<sup>63</sup> fly ash,<sup>80</sup> activated alumina<sup>81</sup> and alum sludge<sup>82</sup> are some examples of this type of adsorbent.

Ligand exchange mechanism is reported as the predominant mechanism for  $F^-$  adsorption for many inorganic adsorbents having high adsorption capacity. Whereas, H-bonding mechanism plays important role for organic adsorbents.<sup>31</sup>

#### 1.4.1. Factors influencing $F^-$ adsorption

It has been reported that, several factors play critical roles in the adsorption process of  $F^-$  on various adsorbents. Important factors are pH, co-existing anions and temperature. In the following sub sections we will discuss in details about the roles of these factors.

##### 1.4.1.1. pH

pH of the solution is one of the important factors which influence the adsorption of  $F^-$  on adsorbent. Though the pH at which maximum amount of  $F^-$  is adsorbed mostly depends upon the characteristic of adsorbent but generally it has been observed that, the pH range where  $F^-$  adsorption occurs in great extent lies in between 4 and 8.  $F^-$  adsorption has been found low at very low pH as well as at very high pH.<sup>31</sup> Point of zero charge (PZC) is one of the important properties of the adsorbent which influences the  $F^-$  adsorption capacity of adsorbents. For example, PZC of activated carbon is 3.9- 4.7 and it showed maximum  $F^-$  removal at pH 3- 4.<sup>83</sup> Similarly, Fe and Al oxides removed maximum amount of  $F^-$  at pH 6- 8, and their PZC values are around 7- 8.<sup>79, 81, 84</sup> The surface of the adsorbent becomes negatively charged when pH is higher than its PZC value, as a result adsorption of  $F^-$  on the adsorbent surface decreases. Whereas, when pH value is lower than the PZC value, the adsorbent surface becomes positively charged and  $F^-$  ions are adsorbed on the surface. However in some cases, at lower pH formation of positively charged AlF complexes occurred, which caused the reduction of  $F^-$  adsorption.<sup>84-86</sup>

##### 1.4.1.2. Co-existing anions

Several other anions (e.g.  $PO_4^{2-}$ ,  $Cl^-$ ,  $SO_4^{2-}$ ,  $Br^-$ ,  $HCO_3^-$ ,  $NO_3^-$  etc.) are generally present in natural water along with  $F^-$  and compete with  $F^-$  in adsorption process. The

concentration of competing anions and their affinity towards adsorbents greatly affect the  $F^-$  removal processes. As reported by Meenakshi et al.<sup>67</sup> when  $F^-$  is removed by an anion exchange resin increasing concentration of  $Cl^-$ ,  $SO_4^{2-}$ ,  $Br^-$ ,  $NO_3^-$ , and  $HCO_3^-$  caused to decrease  $F^-$  adsorption. On the contrary, when a chelating resin was used where  $F^-$  adsorption occurred selectively by H-bonding, it was observed that these anions had no effect on  $F^-$  adsorption.  $F^- > Cl^- > NO_3^- > SO_4^{2-}$  is the reported preferential order of anion adsorption on the chelating resin (Indion FR 10).<sup>67</sup> Solangi et al.<sup>66</sup> have reported that, when thio-urea incorporated amberlite resin was used for  $F^-$  removal in presence of various anions, then  $Br^-$ ,  $NO_2^-$  and  $PO_4^{3-}$  showed little interference whereas  $Cl^-$ ,  $SO_4^{2-}$ ,  $NO_3^-$ ,  $HCO_3^-$  and  $CO_3^{2-}$  exhibited no interference. This was because of strong H-bonding between  $F^-$  and amide groups of resin.

In case of multivalent metal oxide adsorbents, selective  $F^-$  adsorption occurs mostly via ligand exchange specific adsorption mechanism. In case of Al, Ti and Fe oxide containing alum sludge,  $F^-$  adsorption was reported to occur selectively in presence of  $SO_4^{2-}$  and  $NO_3^-$ .<sup>82</sup> For this adsorbent,  $F^-$  removal from a  $F^-$  solution (20 mg  $L^{-1}$ ) was reduced from 85% to 40% and 62% when  $SO_4^{2-}$  and  $NO_3^-$  (with concentration of 50 mg  $L^{-1}$ ) were present respectively. Presence of  $PO_4^{3-}$  and  $SeO_4^{2-}$  (20 mg  $L^{-1}$ ) reduced  $F^-$  adsorption up to 25%. So, the decreased order of competition of anions for  $F^-$  adsorption as reported by Sujana et al.<sup>82</sup> is  $PO_4^{3-} > SeO_4^{2-} > SO_4^{2-} > NO_3^-$ . Kumar et al.<sup>79</sup> have reported that, when granular ferric hydroxide was used as adsorbent, the presence of competing ions, such as  $Cl^-$ ,  $SO_4^{2-}$ ,  $BrO_3^-$ ,  $NO_3^-$ ,  $CO_3^{2-}$  and  $PO_4^{3-}$  (each having concentration 20-100 mg  $L^{-1}$ ), did not have much effect on  $F^-$  removal from a solution, having  $F^-$  concentration 20 mg  $L^{-1}$  and adsorbent dose of 10 g  $L^{-1}$ . This was attributed to the availability of plenty of adsorption sites. However, when adsorbent dose was low (5 g  $L^{-1}$ ) the presence of  $PO_4^{3-}$ ,  $CO_3^{2-}$  and  $SO_4^{2-}$  (concentration 100 mg  $L^{-1}$  of each anion) anions reduced  $F^-$  adsorption capacity by 35%, 25% and 20% respectively, whereas other anions did not show any interference. Similarly, according to Raichur and Basu, the presence of  $SO_4^{2-}$  or  $NO_3^-$  in water did not affect significantly  $F^-$  adsorption capacity of an adsorbent, composed of a mixture of rare earth oxides (oxides of La, Ce, Pr, Nd, Sm and Y).<sup>13</sup>

Generally, in case of adsorbents which are specific for  $F^-$  adsorption, the presence of non-specifically adsorbing anions ( $NO_3^-$ ,  $Cl^-$ ) does not affect significantly the  $F^-$  removal capacity of adsorbents.<sup>31</sup>  $PO_4^{3-}$  and  $SeO_4^{2-}$  are the specific anions

which compete with  $F^-$ . However, when  $F^-$  is adsorbed by non-specific adsorbent, the non-specifically adsorbing anions then compete with  $F^-$  in adsorption process.<sup>31</sup>

### 1.4.1.3. Temperature

Effect of temperature on  $F^-$  adsorption does not follow any consistent trend. Endothermic nature of adsorption has been reported for many adsorbents like granular ferric hydroxide,<sup>79</sup> fly ash,<sup>80</sup> calcined Mg/Al/CO<sub>3</sub> LDH,<sup>87</sup> Al<sub>2</sub>O<sub>3</sub>,<sup>88</sup> LDH/ chitosan,<sup>89</sup> and spent catalyst.<sup>86</sup> On the contrary, for some adsorbents, such as chelating resin,<sup>67</sup> alum sludge,<sup>82</sup> calcined Zn/Al LDH,<sup>8</sup> alkoxide origin Al<sub>2</sub>O<sub>3</sub>,<sup>90</sup> mesoporous Al<sub>2</sub>O<sub>3</sub>,<sup>91</sup> modified activated carbon,<sup>92</sup> nano zirconium chitosan composite,<sup>93</sup> geo-materials,<sup>94</sup> exothermic nature of adsorption has been reported. It has also been reported that, temperature has no significant influence on  $F^-$  adsorption process for some adsorbents (e.g., trivalent cations/ zeolite).<sup>75</sup>

Till date, the effect of temperature on  $F^-$  adsorption process is not well understood. However, nature of adsorbent, the temperature range at which experiments are conducted and other experimental parameters may dictate whether adsorption will be endothermic or exothermic in nature. When temperatures were low (5 °C and 10 °C) the rate of adsorption was found to be low, which might be due to the slow movement of  $F^-$  ions towards adsorption sites at these low temperatures. Lai and Liu<sup>86</sup> have observed that, on spent catalyst  $F^-$  adsorption increased significantly with increasing temperature from 5 °C to 25 °C, but a further rise in temperature up to 50 °C did not cause any significant increase of  $F^-$  adsorption. In case of alum sludge, exothermic adsorption of  $F^-$  was reported.<sup>82</sup> This might be because rising temperature has increased the escaping tendency of  $F^-$  from adsorbent. Another explanation might be that at higher temperature increasing thermal energy of adsorbed  $F^-$  caused increased desorption.

### 1.4.2. Adsorption kinetics

Several mechanisms have been proposed by researchers to explain the adsorption kinetics of  $F^-$  onto solid adsorbents.<sup>63, 81, 87</sup> Generally, the factors which govern the adsorption kinetics are diffusion or transport of  $F^-$  from bulk solution to exterior

surface of adsorbent, surface adsorption, movement and attachment of  $F^-$  at the sites of the interior surface and pores through sorption, complexation or precipitation etc. Several factors, such as structural (including surface) properties of adsorbents, initial concentration of  $F^-$  in solution, interaction between  $F^-$  and adsorption sites etc. play important roles in determining the adsorption kinetics. Two important kinetic models which are widely used to explain the adsorption kinetics of  $F^-$  on solid adsorbents are pseudo first order adsorption kinetic model (equation 2) and pseudo second order adsorption kinetic model (equation 3).

Pseudo first order adsorption kinetic model<sup>95</sup>:

$$\log(q_e - q_t) = \log q_e - (k_1/2.303)t \quad (2)$$

Pseudo second order adsorption kinetic model<sup>96</sup>:

$$t/q_t = 1/(k_2q_e^2) + (1/q_e)t \quad (3)$$

where,  $q_t$  is the amount of  $F^-$  adsorbed on adsorbent ( $mg\ g^{-1}$ ) at time  $t$  (min),  $q_e$  is the amount of  $F^-$  adsorbed on adsorbent ( $mg\ g^{-1}$ ) at equilibrium,  $k_1$  is the rate constant ( $min^{-1}$ ) for pseudo first order kinetics and  $k_2$  is the rate constant ( $g\ mg^{-1}min^{-1}$ ) for pseudo second order kinetics. When adsorption proceeds through pseudo second order kinetics, it has been believed that,  $F^-$  adsorption occurred via chemisorption process.<sup>69, 97, 98</sup>

### 1.4.3. Adsorption isotherms

Adsorption isotherms provide important information about the adsorption processes. It has been observed that, most of the reported defluoridation experiments are confined to batch adsorption studies, which only suggest the feasibility of sorption by an adsorbent and renders its adsorption capacity through best-fitting isotherms and some kinetic models. Although many theories of adsorption isotherm models have been put forward to explain the phenomena of adsorption, Freundlich<sup>99</sup> and Langmuir models<sup>100</sup> have been widely used. Freundlich and Langmuir isotherms are used in adsorption to understand the extent and degree of favorability of adsorption.

Freundlich model indicates the heterogeneity of the adsorbent surface and considers multilayer adsorption. The Freundlich model can be represented as equation 4.

$$\log q_e = \log K_f + (1/n) \log C_e \quad (4)$$

where,  $K_f$  is the Freundlich constant related to adsorption capacity and  $1/n$  is the Freundlich constant related to adsorption intensity and it is a measure of surface heterogeneity, ranging between 0 to 1, becoming more heterogeneous as its value gets closer to zero.

In the Langmuir adsorption isotherm model, the following assumptions are considered (i) all adsorption sites are identical, (ii) each site retains one molecule of the given compound (mono layered adsorption) and (iii) all sites are energetically and sterically independent of the adsorbed quantity. The Langmuir model can be represented in linear form as equation 5.

$$C_e/q_e = 1/(Q_0b) + C_e/Q_0 \quad (5)$$

where,  $q_e$  is amount of  $F^-$  adsorbed at equilibrium ( $mg\ g^{-1}$ ),  $C_e$  is equilibrium  $F^-$  concentration ( $mg\ L^{-1}$ ),  $b$  ( $L\ mg^{-1}$ ) is the Langmuir constant related to sorption energy and  $Q_0$  ( $mg\ g^{-1}$ ) is maximum  $F^-$  adsorption capacity.

### 1.5. Different adsorbents used for defluoridation of water

Several adsorbent materials have been utilized in the past to identify an efficient and economical adsorbent to remove  $F^-$  from ground water. Some of them are activated alumina (AA),<sup>81, 84, 88, 101-105</sup> metal oxide loaded or impregnated alumina,<sup>63, 69, 98, 106-110</sup> mesoporous alumina based adsorbents,<sup>91, 111-113</sup> alum impregnated AA,<sup>114</sup> alkoxide origin  $Al_2O_3$ ,<sup>90</sup> hydrous alumina,<sup>115</sup> alumina cement granules,<sup>97, 116</sup> acidic alumina,<sup>117</sup> aluminum hydroxides,<sup>118</sup> nano particle based adsorbents (nano  $Al_2O_3$ ,<sup>119</sup> nano  $AlOOH$ ,<sup>120</sup> alumina nanofibers,<sup>121</sup> nano  $MgO$ ,<sup>122, 123</sup> nano goethite,<sup>124</sup>  $CaO$  nanoparticles,<sup>125</sup> Mg-doped nano  $Fe_2O_3$ ,<sup>126</sup> sulphate doped  $Fe_2O_3/ Al_2O_3$  nanoparticles,<sup>127</sup> zirconium-based nanoparticle,<sup>128</sup> nano- zirconium-carbon hybrid,<sup>129</sup> nano sized hydrous zirconium oxide encapsulated polystyrene anion exchanger,<sup>130</sup>



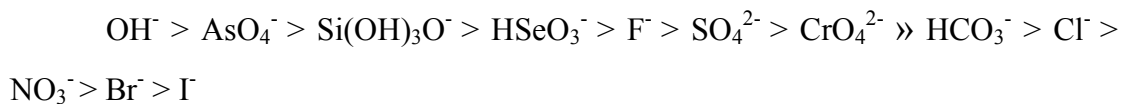
iron-doped titanium oxide nanoadsorbent,<sup>131</sup> nanohydroxyapatite,<sup>132, 133</sup> CeO<sub>2</sub>-ZrO<sub>2</sub> nanocages,<sup>134</sup> Mg-doped nano ferrihydrite,<sup>135</sup> nano-hydroxyapatite/ chitin composite,<sup>136</sup> mixed-phase nano iron oxides<sup>137</sup>), carbon based materials (activated carbon (AC), KMnO<sub>4</sub> modified AC,<sup>92</sup> Al impregnated AC,<sup>83</sup> aligned carbon nanotubes,<sup>15</sup> Al<sub>2</sub>O<sub>3</sub> loaded CNT,<sup>138</sup> titanium and lanthanum oxides impregnated on granular AC,<sup>139</sup> bio char,<sup>140</sup> bone char<sup>141</sup> and carbon black<sup>9</sup>), zeolites (zeolite,<sup>142</sup> Al, La, Zr loaded natural zeolites,<sup>71</sup> Al loaded synthetic zeolites,<sup>76</sup> Al, La loaded synthetic zeolites<sup>75</sup>), layered double hydroxides (LDH) (MgAl-CO<sub>3</sub> LDHs,<sup>87, 143, 144</sup> Zn/ Al LDH,<sup>8</sup> Li-Al LDHs,<sup>145</sup> Mg-Cr-Cl LDH,<sup>146</sup> Mg-Al-LDH nanoflake impregnated magnetic alginate beads<sup>147</sup>), clays (clay minerals,<sup>148</sup> bentonite clay,<sup>149</sup> magnesium incorporated bentonite clay<sup>150</sup>), Fe-Al mixed oxide/ hydroxide adsorbents,<sup>151-156</sup> metal- organic frameworks,<sup>157</sup> Zr loaded collagen fiber,<sup>73</sup> ceramics,<sup>158, 159</sup> Al-Ce hybrid adsorbent,<sup>160</sup> calcium aluminate,<sup>161</sup> Fe-Al-Ce trimetal oxide,<sup>162-166</sup> granular ferric hydroxide,<sup>167</sup> hydrous ferric oxide,<sup>168</sup> hydrous zirconium oxide,<sup>169</sup> porous zirconium alginate beads,<sup>170</sup> chitosan derivatives and composites,<sup>171-173</sup> rare earth oxides,<sup>13</sup> hydrous cerium oxide,<sup>174</sup> bauxite,<sup>175</sup> Mg-Al hydrous oxides,<sup>176</sup> Mg-Al-La triple-metal hydrous oxide,<sup>177</sup> Zn/ Al hydrotalcite-like compound,<sup>8</sup> Fe-Ce-Ni nanoporous adsorbent,<sup>178</sup> laterite,<sup>179</sup> calcite,<sup>180</sup> natural soil,<sup>181</sup> Al-Zr impregnated cellulose,<sup>182</sup> etc. The most commonly used adsorbent for defluoridation of water is either activated Al<sub>2</sub>O<sub>3</sub> or Al<sub>2</sub>O<sub>3</sub> based materials. Different Al<sub>2</sub>O<sub>3</sub> based adsorbents and nano particle based adsorbents which are reported for F<sup>-</sup> removal are discussed in details in the following sections.

### 1.5.1. Al<sub>2</sub>O<sub>3</sub> based adsorbents

#### 1.5.1.1. Activated Alumina (AA)

AA is the most extensively used adsorbent for defluoridation of drinking water, because of its high affinity and selectivity for F<sup>-</sup> ions.<sup>63, 69, 70, 102, 183</sup> F<sup>-</sup> adsorption capacity of AA varies with the surface properties, crystal structure and morphology. For instance, for F<sup>-</sup> removal  $\gamma$ - Al<sub>2</sub>O<sub>3</sub> is 10 times more efficient than  $\alpha$ - Al<sub>2</sub>O<sub>3</sub>.<sup>29</sup> Ghorai and Pant have investigated the mechanism of F<sup>-</sup> adsorption on Al<sub>2</sub>O<sub>3</sub>.<sup>81, 103</sup> The authors have also investigated F<sup>-</sup> removal using AA (commercial Grade OA- 25) in continuous and batch operations.<sup>103</sup> When AA was treated with the solution having higher F<sup>-</sup> concentrations at a high flow rate, lower F<sup>-</sup> removal and early saturation was

observed. 85% efficiency was reported for regenerated AA and F<sup>-</sup> uptake capacity of AA was decreased marginally after each regeneration cycle. After 5 cycles, only 5% reduction of F<sup>-</sup> uptake capacity was observed. Sorption of different anions on AA in the pH range 5.5- 8.5 was studied by Johnston and Heijnen and the following selectivity sequence was proposed.<sup>29, 184</sup>



Lopez Valdivieso et al.<sup>104</sup> have investigated the defluoridation mechanism of Al<sub>2</sub>O<sub>3</sub> by determining the zeta potential of α- Al<sub>2</sub>O<sub>3</sub>. The effects of temperature and pH on α- Al<sub>2</sub>O<sub>3</sub>/ aqueous solution interface were investigated by conducting electrophoretic mobility measurements and adsorption experiments. It was observed that, F<sup>-</sup> adsorption on Al<sub>2</sub>O<sub>3</sub> followed Langmuir adsorption isotherm. F<sup>-</sup> adsorption was affected by the electric charge at α- Al<sub>2</sub>O<sub>3</sub>/ aqueous solution interface and the surface density of OH<sup>-</sup> groups. Such adsorption occurred through an exchange between F<sup>-</sup> and surface OH<sup>-</sup>. The authors have concluded that, with increasing pH and temperature, the deprotonation of Al<sub>2</sub>O<sub>3</sub> surface as well as the stability of the surface OH<sup>-</sup> groups were increased, as a result F<sup>-</sup> adsorption was decreased. The interaction of F<sup>-</sup> with Al<sub>2</sub>O<sub>3</sub> was due to their chemical affinity and electrostatic attraction between F<sup>-</sup> and surface AlOH<sub>2</sub><sup>+</sup> and AlOH sites. pH range of 5 to 6 was found to be suitable to remove F<sup>-</sup> from aqueous solution effectively. Farrah et al.<sup>185</sup> have also investigated F<sup>-</sup> ion interaction with Al<sub>2</sub>O<sub>3</sub>, amorphous Al(OH)<sub>3</sub>, and gibbsite in the pH range of 3- 8 with F<sup>-</sup> concentrations from 0.1 to 1 mM. pH range of 5.5- 6.5 has been reported for maximum F<sup>-</sup> adsorption (up to 9 mol kg<sup>-1</sup>). The importance of activation of adsorbent for defluoridation of water was investigated by Shimelis et al.<sup>186</sup> They have compared the activity of untreated hydrated Al<sub>2</sub>O<sub>3</sub> (UHA) with thermally treated hydrated Al<sub>2</sub>O<sub>3</sub> (THA), which was obtained from hydrolysis of Al<sub>2</sub>(SO<sub>4</sub>)<sub>3</sub>. It has been reported that, F<sup>-</sup> removal efficiency of the adsorbents was increased with increasing adsorbent dosage. With increasing thermal treatment temperature up to 200 °C, F<sup>-</sup> removal efficiency was increased, but further temperature increase resulted in decrease in F<sup>-</sup> removal efficiency. Maximum F<sup>-</sup> removal efficiency was achieved in the pH range of 4- 9 by both UHA and THA adsorbents. The F<sup>-</sup> adsorption data fitted well to the Freundlich isotherm model and F<sup>-</sup> adsorption capacity of THA and UHA was 23.7 mg g<sup>-1</sup> and 7

mg g<sup>-1</sup> respectively. The authors have also reported that, by using THA adsorbent in continuous packed bed column, 6 L of 20 mg L<sup>-1</sup> F<sup>-</sup> containing water can be treated using 4.5 g of THA before breakthrough. Ku and Chiou<sup>84</sup> have used AA as an adsorbent and investigated the effect of pH, temperature and presence of other competing ions on F<sup>-</sup> removal efficiency. Equilibrium behaviors of the adsorption processes were well described by Langmuir and Freundlich isotherm models. Based on the low values of activation energy, which was determined experimentally, authors concluded that F<sup>-</sup> removal by Al<sub>2</sub>O<sub>3</sub> occurred by nonspecific adsorption. Bahena et al.<sup>187</sup> have studied the effect of zeta potential of  $\alpha$ - Al<sub>2</sub>O<sub>3</sub> on F<sup>-</sup> adsorption. It was observed that, under conditions close to and above pHPZC (9.2), the specific adsorption of F<sup>-</sup> onto  $\alpha$ - Al<sub>2</sub>O<sub>3</sub> occurred by replacing OH<sup>-</sup> from positively charged surfaces and through H-bonding. Defluoridation of water by using metallurgical grade Al<sub>2</sub>O<sub>3</sub> (MGA) under different experimental conditions was investigated by Pietrelli.<sup>188</sup> Maximum F<sup>-</sup> removal by MGA occurred between pH 5 and 6. At higher pH values, its F<sup>-</sup> removal capacity was decreased drastically.

Kumar et al.<sup>119</sup> have studied the F<sup>-</sup> sorption on nano- Al<sub>2</sub>O<sub>3</sub> ( $\gamma$ -Al<sub>2</sub>O<sub>3</sub>) under different experimental conditions. Authors did not find any changes in the X-ray diffraction (XRD) pattern and scanning electron micrograph (SEM) of nano-Al<sub>2</sub>O<sub>3</sub> before and after F<sup>-</sup> adsorption. But Fourier-Transformed Infra-Red (FTIR) spectra of F<sup>-</sup> sorbed sorbent indicated the possible interactions between F<sup>-</sup> and nano- Al<sub>2</sub>O<sub>3</sub>. It was suggested that, F<sup>-</sup> sorption on nano- Al<sub>2</sub>O<sub>3</sub> occurred via formation of a monolayer coverage by adsorbed F<sup>-</sup> on the surface of the adsorbent. The predominant mechanism behind the F<sup>-</sup> adsorption was the replacement of OH<sup>-</sup> ions by F<sup>-</sup> resulting in the formation of the AlF complexes. The authors also observed that, F<sup>-</sup> adsorption was strongly pH dependent and maximum F<sup>-</sup> adsorption occurred at pH 6.15. This is due to the fact that, as pHPZC of nano-Al<sub>2</sub>O<sub>3</sub> is ~7.2 so, when pH of solution was below pHPZC value, the surface of Al<sub>2</sub>O<sub>3</sub> became positively charged. Zhang et al.<sup>189</sup> have studied the interaction of fluorine on  $\gamma$ - Al<sub>2</sub>O<sub>3</sub> surface by multinuclear MAS NMR spectroscopy to identify the fluorine species on the fluorinated  $\gamma$ - Al<sub>2</sub>O<sub>3</sub>. The spectroscopy analysis indicated that, F<sup>-</sup> enters the surface of Al<sub>2</sub>O<sub>3</sub> by substituting OH<sup>-</sup> groups without breaking the bridging Al-O-Al bonds. At higher F<sup>-</sup> loadings bridging Al-O-Al bonds broke down to adsorb more F<sup>-</sup> due to strong electron-withdrawing effect of fluorine.<sup>119</sup> Leyva-Ramos et al.<sup>102</sup> have prepared AA by using

pseudo-boehmite. It was reported that,  $F^-$  adsorption capacity of AA was decreased considerably with increasing pH of the solution from 4 to 11.  $F^-$  adsorption equilibrium was irreversible at pH 5 but reversible at pH 11. Here, adsorption of  $F^-$  on AA adsorbent occurred by electrostatic interactions as well as chemisorption between the  $F^-$  in solution and the basic sites of the AA surface but not by ion exchange. Wang et al.<sup>120</sup> have investigated the potential of nano-sized aluminum oxide hydroxide (nano-  $AlOOH$ ) as sorbent for removal of  $F^-$ . The authors have reported that, its  $F^-$  adsorption was increased with increasing pH of the solution and reached maximum of 96.7% at pH 6.8, then decreased with further increase in pH. Desorption studies showed that,  $F^-$  could easily be desorbed from sorbent at pH 13.

Gong et al.<sup>88</sup> have synthesized five different aluminas at different pH ranging from 5 to 9 and calcination temperatures (60- 500 °C).  $F^-$  adsorption isotherms of all five aluminas were fitted well to both Langmuir and Freundlich models. Thermodynamic studies showed that,  $F^-$  adsorption on  $Al_2O_3$  was spontaneous and endothermic. It was also observed that, acidity or basicity of  $Al_2O_3$  exhibited significant effect on  $F^-$  adsorption behavior and the process of ion exchange in  $F^-$  removal. Acidic  $Al_2O_3$  exhibited higher  $F^-$  adsorption capacity and faster  $F^-$  adsorption than basic  $Al_2O_3$  due to its higher ion exchange capacity and more positive charge on the surface. For acidic  $Al_2O_3$ , more  $Cl^-$  was exchanged with  $F^-$  and adsorption/ release of  $OH^-$  was dependent on the initial  $F^-$  concentration. Whereas in case of basic  $Al_2O_3$ , most of the exchange sites were provided by  $OH^-$  and  $F^-$  removal occurred through the exchange between  $F^-$  and  $OH^-$ . Dash et al.<sup>190</sup> have studied the defluoridation of ground water using  $\gamma-Al_2O_3$  coated on ceramic honeycomb (having 400 channels per square inch) which adsorbed  $F^-$  rapidly and effectively. Coatings on ceramic honeycomb were prepared using a sol of dispersible precursor of boehmite and it was calcined at 500 °C. It was observed that,  $F^-$  removal by the adsorbent was low at high flow rate. The specific  $F^-$  uptake capacity was found to be 15.4 mg  $g^{-1}$  from de-ionised water whereas in case of ground water the capacity was 11.08 mg  $g^{-1}$ . The regeneration of the adsorbent was performed by passing a dilute solution of  $Al_2(SO_4)_3$  solution. A  $F^-$  removal kit, consisting of 5 ceramic honeycombs in series, was evaluated to defluoridate ground water. Around 200 liters of ground water (initial  $F^-$  concentration of 5 mg  $L^{-1}$ ) was defluoridated to the permissible level of  $F^-$  concentration ( $< 1.5$  mg  $L^{-1}$ ).

### 1.5.1.2. Mesoporous Al<sub>2</sub>O<sub>3</sub>

According to the IUPAC definition, solids that contain pores with pore diameter (i) > 50 nm are called as macroporous, (ii) between 2- 50 nm are mesoporous and (iii) < 2 nm are microporous.<sup>191, 192</sup>

Based on the synthesis strategy, the synthesized mesoporous alumina may possess amorphous walls or crystalline walls.<sup>193, 194</sup> Alumina exists in different crystalline phases such as  $\gamma$ ,  $\eta$ ,  $\delta$ , and  $\alpha$ .<sup>193, 195</sup>  $\gamma$ -Al<sub>2</sub>O<sub>3</sub> transforms to  $\alpha$ -Al<sub>2</sub>O<sub>3</sub> when heated at higher temperature.<sup>195, 196</sup> However, collapse of mesoporous framework walls was observed at elevated temperatures.<sup>197, 198</sup>  $\gamma$ -Al<sub>2</sub>O<sub>3</sub> can be obtained by heat treatment of Al(OH)<sub>3</sub> or AlOOH at intermediate temperatures.<sup>199</sup> Several researchers have reported different synthetic routes for preparation of mesoporous Al<sub>2</sub>O<sub>3</sub>. Naik and Ghosh<sup>192</sup> have summarized the methods which are used for synthesis of mesoporous Al<sub>2</sub>O<sub>3</sub> and described the mechanisms of formation of mesoporous Al<sub>2</sub>O<sub>3</sub>. Various factors, such as starting materials (e.g. alkoxides, metal salts etc.), surfactants (as structure directing agent) and reaction parameters (e.g. pH, temperature, solvent, co-solvent etc.) influence the formation of porous alumina.<sup>192, 200</sup> Some of the typical methodologies are discussed below:

Baumann et al.<sup>201</sup> and Hao et al.<sup>202</sup> have used aluminum salts, propylene oxide and ethanol to prepare  $\gamma$ -Al<sub>2</sub>O<sub>3</sub> through calcination at 800 °C. Cejka et al.<sup>199</sup> reported the synthesis of organized mesoporous aluminas by using carboxylic acid surfactants (lauric acid and stearic acids). Length of the hydrophobic hydrocarbon chain of carboxylic acids played important role in the synthesis. Lee et al.<sup>112</sup> have synthesized two different kinds of mesoporous Al<sub>2</sub>O<sub>3</sub> (MA-1 and MA-2) by adopting the methods used by Ray et al.<sup>203</sup> and Cejka et al.<sup>199</sup> using aluminum tri-sec-butoxide as an aluminum source. MA-1 was synthesized by using cetyl trimethyl ammonium bromide, as pore structure directing agent, in 2- butanol medium and autoclaving the mixture at 100 °C for 24 h. MA-2 was synthesized using stearic acid as a structure directing agent and 1- propanol as solvent. Jagtap et al.<sup>91</sup> have synthesized mesoporous Al<sub>2</sub>O<sub>3</sub> using chitosan as template and aluminum nitrate as source of aluminum. Precursor was prepared by the addition of NH<sub>4</sub>OH solution dropwise to the Al-Chitosan mixture with continuous stirring. The precursor was calcined at different temperatures ranging from 350- 550 °C in air atmosphere for 6 h to obtain

porous  $\text{Al}_2\text{O}_3$  spheres with high specific surface area. Li et al.<sup>113</sup> have synthesized highly ordered mesoporous  $\text{Al}_2\text{O}_3$  using sol-gel method. In this method, triblock copolymer pluronic P123 was used as soft template and aluminum isopropoxide was used as aluminum source. Yang et al.<sup>111</sup> have synthesized highly ordered and disordered mesoporous aluminas using different aluminum salts as a source of aluminum. They have used aluminum isopropoxide, aluminum nitrate nonahydrate and aluminum chloride as source of aluminum,  $\text{EO}_{20}\text{PO}_{70}\text{ED}_{20}$  (P123) as surfactant and ethanol as a solvent. Mesoporous  $\text{Al}_2\text{O}_3$  was obtained by calcining the precursors at different temperatures ranging from 400- 1000 °C. Camacho et al.<sup>98</sup> have synthesized granular AA beads by sol-gel method, where a stable boehmite sol was prepared using aluminum tri-sec-butoxide. Granular beads were prepared by dropping boehmite sol droplets through paraffin oil. Camacho et al. modified the synthesized granular AA beads using CaO and  $\text{MnO}_2$  to enhance the defluoridation property.  $\text{CaCl}_2$  and  $\text{MnCl}_2$  were used as source for calcium and manganese. Gong et al.<sup>88</sup> have synthesized five different aluminas at different pH and calcination temperatures by using  $\text{AlCl}_3 \cdot 6\text{H}_2\text{O}$  as aluminum source. The precursors were prepared with pH 5, 7, 9 and the powders were calcined at 150 °C or 500 °C to get different phases of  $\text{Al}_2\text{O}_3$ .

Yang et al.<sup>111</sup> have developed highly ordered and disordered mesoporous aluminas and studied their  $\text{F}^-$  adsorption performances. The synthesized mesoporous  $\text{Al}_2\text{O}_3$  possesses large pore size distribution of 7- 14 nm and high surface areas in the range of 163- 338  $\text{m}^2 \text{g}^{-1}$ . The porous structure is beneficial for transportation of  $\text{F}^-$  from solution to the interconnected mesoporous channels and  $\text{F}^-$  can be anchored on the surface. Highly ordered mesoporous  $\text{Al}_2\text{O}_3$  exhibited extremely faster adsorption kinetics and 90%  $\text{F}^-$  removal occurred within 20 min with an optimal pH of 6. Jagtap et al.<sup>91</sup> have synthesized mesoporous  $\text{Al}_2\text{O}_3$  using a biopolymer, called chitosan, as a template and calcination temperatures were 350 °C, 450 °C and 550 °C. The authors studied the effect of calcination temperature on  $\text{F}^-$  adsorption capacity of mesoporous  $\text{Al}_2\text{O}_3$  and found that, the mesoporous  $\text{Al}_2\text{O}_3$ , which was prepared by calcining at 450 °C, showed higher  $\text{F}^-$  removal efficiency than other materials. The synthesized adsorbent can be used over a wide range of pH 3 to 9. The mechanism involved for  $\text{F}^-$  adsorption on adsorbent was reported as complex in nature and both surface adsorption as well as intra-particle diffusion contributed to the rate determining step. Thermodynamic study revealed that,  $\text{F}^-$  adsorption on synthesized adsorbent was

spontaneous and exothermic process. The assessment of field water quality showed that,  $F^-$  ion concentration was reduced to prescribed limit after treatment with  $Al_2O_3$ , which was prepared by calcining at 450 °C.

Lee et al.<sup>112</sup> have prepared two different kinds of high surface area mesoporous  $Al_2O_3$  using aluminum tri-sec-butoxide in presence of either cetyl trimethyl ammonium bromide (MA-1) or stearic acid (MA-2) as a structure directing agent. These mesoporous aluminas have demonstrated significantly enhanced  $F^-$  adsorption capacity and faster kinetics than that of commercial aluminas. MA-2 adsorbent showed higher  $F^-$  adsorption capacity (14.26 mg  $g^{-1}$ ) and higher initial adsorption rate than those of a commercial  $\gamma$ -  $Al_2O_3$ . The authors have reported that, the textural features of higher surface area and relatively smaller pore size in MA-2 compared to activated aluminas were responsible for this enhancement in  $F^-$  adsorption process.

Lai and Liu<sup>86</sup> have studied the defluoridation of water using a by-product of the petrochemical industry, called spent catalyst, consisting of mainly porous  $Al_2O_3$  and  $SiO_2$  (specific surface area: 130  $m^2 g^{-1}$ , PZC 5.2). Its maximum  $F^-$  adsorption capacity at pH 4 was 28 mg  $g^{-1}$  at 25 °C as well as at 50 °C. Since the activation energy calculated from Arrhenius equation was very low (3.2 J  $mol^{-1}$ ), the mechanism of  $F^-$  adsorption was considered to be non- specific adsorption involving coulombic forces.

### 1.5.1.3. Modified Activated Alumina

AA is one of the generally used adsorbents for removal of  $F^-$  from drinking water. However, the slow rate of  $F^-$  adsorption limits the usage of commercially available AA for treating water. Hence, to enhance  $F^-$  adsorption efficacy of AA, researchers have modified  $Al_2O_3$  surface by depositing metal/ metal oxides.<sup>2, 29, 31, 69, 106-108</sup>

Li et al.<sup>113</sup> have synthesized highly ordered mesoporous aluminas and calcium doped aluminas. These mesoporous adsorbents showed strong affinity towards  $F^-$  ions and extremely high  $F^-$  adsorption capacities. Samples prepared at 400 °C possessed amorphous pore walls and showed higher  $F^-$  adsorption capacities than that of the sample prepared at 900 °C. Ca- doped mesoporous  $Al_2O_3$  showed higher  $F^-$  adsorption capacity than that of mesoporous  $Al_2O_3$ . At lower initial  $F^-$  concentrations (below 150

mg L<sup>-1</sup>), F<sup>-</sup> removal occurred due to monolayer adsorption onto the positively charged surface of the adsorbents. At higher initial F<sup>-</sup> concentrations, high F<sup>-</sup> adsorption capacities were observed for Ca- doped mesoporous Al<sub>2</sub>O<sub>3</sub>, which could be due to the formation of CaF<sub>2</sub> precipitates. These mesoporous adsorbents also showed high arsenic removal ability. Camacho et al.<sup>98</sup> have prepared AA and calcium oxide and manganese oxide coated AA (CaO-AA and MnO<sub>2</sub>-AA) for defluoridation. CaO-AA adsorbed 5 and 10 times more F<sup>-</sup> than that of AA and MnO<sub>2</sub>-AA and chemisorption was responsible for F<sup>-</sup> adsorption. Kamble et al.<sup>90</sup> have investigated the effectiveness of alkoxide origin Al<sub>2</sub>O<sub>3</sub> ( $\gamma$ - Al<sub>2</sub>O<sub>3</sub> containing small amounts of Fe<sub>2</sub>O<sub>3</sub> and SiO<sub>2</sub> as well as activated carbon in its pores) for removal of F<sup>-</sup> from drinking water using batch and continuous mode operations. Maximum F<sup>-</sup> removal efficiency was observed in the pH range of 5- 7. Thermodynamic study revealed that, adsorption of F<sup>-</sup> by this adsorbent was an exothermic and spontaneous process. Alkoxide origin Al<sub>2</sub>O<sub>3</sub> showed lower equilibrium F<sup>-</sup> concentration in the treated water as compared to AA. The reason for increased F<sup>-</sup> adsorption was attributed to the increased electropositivity and the small hydrophobicity which was retained on the alkoxide origin Al<sub>2</sub>O<sub>3</sub>. Maliyekkal et al.<sup>106</sup> have prepared magnesia-amended AA (MAAA) for removal of F<sup>-</sup> from drinking water. MAAA was prepared by calcining Mg(OH)<sub>2</sub> impregnated AA at 450 °C. MAAA adsorbent showed much higher and faster F<sup>-</sup> removal compared to AA. An optimum F<sup>-</sup> removal was observed in the pH range of 5- 7.5, which was very reasonable in real situations. Most of the common interfering ions showed insignificant effect on F<sup>-</sup> sorption by MAAA. The authors concluded that, F<sup>-</sup> uptake by MAAA was a complex process involving both surface sorption as well as intraparticle diffusion.

Maliyekkal et al.<sup>69</sup> have modified the surface of AA by coating with manganese oxide and studied its F<sup>-</sup> removal efficiency. F<sup>-</sup> removal capacity of manganese oxide coated alumina (MOCA) was found to be much faster than that of AA. Regeneration of MOCA adsorbent was performed using 2.5% NaOH solution. MOCA adsorbent has the capability to bring down F<sup>-</sup> concentration of drinking water below 1.5 mg L<sup>-1</sup> (WHO permissible limit). Tripathy and Raichur<sup>109</sup> have also studied the defluoridation of drinking water by using manganese dioxide coated AA. This adsorbent was able to bring down F<sup>-</sup> concentration to 0.2 mg L<sup>-1</sup> when the initial F<sup>-</sup> concentration of water was 10 mg L<sup>-1</sup>. The authors have concluded that, removal of F<sup>-</sup>



by manganese dioxide coated AA occurred through physical adsorption as well as initial intraparticle diffusion at the porous surface. Teng et al.<sup>63</sup> have studied the efficiency of hydrous manganese oxide coated  $\text{Al}_2\text{O}_3$  (HMOCA) for removal of  $\text{F}^-$  from water. HMOCA adsorbent was prepared by coating hydrous manganese oxide onto  $\text{Al}_2\text{O}_3$  surface by employing a redox process. HMOCA adsorbent could reduce  $\text{F}^-$  concentration from  $6 \text{ mg L}^{-1}$  to  $0.4 \text{ mg L}^{-1}$  at an initial pH of 5.2, while the removal efficiency was 45% for pure AA under the same condition. The mechanism of  $\text{F}^-$  adsorption on HMOCA was explained by anion exchange between  $\text{OH}^-$  and  $\text{F}^-$  in the acidic pH range. After  $\text{F}^-$  adsorption, pH of the solution was increased due to liberation of  $\text{OH}^-$  from adsorbent. When pH was  $> 6$ ,  $\text{F}^-$  adsorption occurred by van der Waals forces. The surface of HMOCA adsorbent was considered to be electronegative when the initial pH was above 6. Since the  $\text{pH}_{\text{PZC}}$  of HMOCA was 5.9, the negatively charged surface of HMOCA prevented the movement of  $\text{F}^-$  towards HMOCA surface due to coulombic repulsion force. The authors have also performed the column studies and reported that for the influent, having initial  $\text{F}^-$  concentration of  $5 \text{ mg L}^{-1}$ ,  $\text{F}^-$  concentration was decreased to below  $1 \text{ mg L}^{-1}$  after treatment with HMOCA. Alemu et al.<sup>204</sup> have synthesized aluminum oxide-manganese oxide (AOMO) composite and its  $\text{F}^-$  removal efficiency was found to be varied with the percentage of manganese oxide. AOMO showed higher equilibrium adsorption capacity at pH 5- 7, which is comparable with most of the reported  $\text{Al}_2\text{O}_3$  based adsorbents and other adsorbents.

To enhance the  $\text{F}^-$  removal efficiency of mesoporous  $\text{Al}_2\text{O}_3$ , Bansiwali et al.<sup>107</sup> have modified the surface of mesoporous  $\text{Al}_2\text{O}_3$  by coating with copper oxide. The copper oxide coated  $\text{Al}_2\text{O}_3$  was prepared by calcining  $\text{CuSO}_4$  impregnated  $\text{Al}_2\text{O}_3$  at  $450 \text{ }^\circ\text{C}$ . Coating of copper oxide has enhanced the  $\text{F}^-$  adsorption capacity of pure mesoporous  $\text{Al}_2\text{O}_3$  from  $2.32$  to  $7.77 \text{ mg g}^{-1}$ , probably due to the increase in zeta potential to more positive values with the coating of copper oxide. Only a slight variation in  $\text{F}^-$  removal efficiency was observed in the pH range 4- 9. Tripathy et al.<sup>114</sup> have studied the defluoridation of water by impregnating alum on  $\text{Al}_2\text{O}_3$ .  $\text{F}^-$  adsorption capacity of alum impregnated  $\text{Al}_2\text{O}_3$  was increased with increasing pH and reached a maximum of 92.6% at pH 6.5, but thereafter decreased with further increase in pH. It was proposed that,  $\text{F}^-$  was superficially adsorbed on alum impregnated AA and the reaction might not be due to adsorption but simply surface precipitation.

Regeneration of the adsorbent was performed by rinsing the  $F^-$  sorbed adsorbent with 0.1 M NaOH solution followed by neutralizing the adsorbent with 0.1 M HCl. Shi et al.<sup>205</sup> have synthesized a  $F^-$  adsorbent by impregnating lanthanum oxide on commercially available granulated AA (LAA).  $F^-$  adsorption on LAA occurred via ligand exchange between  $F^-$  and surface hydroxyl groups. Teutli-Sequeira et al.<sup>108</sup> have studied  $F^-$  removal from aqueous solutions and drinking water by using aluminum modified hematite, zeolite tuff and calcite.  $F^-$  adsorption kinetics was explained by using pseudo second order and Elovich models. It was observed that, higher  $F^-$  sorption capacities (10.25 and 1.16  $mg\ g^{-1}$  for aqueous solutions and drinking water respectively) were obtained for aluminum modified zeolite with an adsorbent dose of 10  $g\ L^{-1}$  and an initial  $F^-$  concentration of 9  $mg\ L^{-1}$  and 8.29  $mg\ L^{-1}$  for aqueous and drinking water respectively. Final  $F^-$  concentrations after treatment become 0.08 and 0.7  $mg\ L^{-1}$  respectively. The authors have proposed that, the main mechanism involved in this  $F^-$  sorption was chemisorption on heterogeneous materials. Aluminum modified zeolite tuff showed the best characteristics for the adsorption of  $F^-$  from drinking water.

La(III) and Y(III) impregnated  $Al_2O_3$  have also shown very promising results for removal of  $F^-$  from water.<sup>206</sup>  $F^-$  removal selectivity of impregnated  $Al_2O_3$  in presence of other anions was in the order:  $F^- > PO_4^{2-} > AsO_4^{3-} > SeO_3^{2-}$ .  $La(OH)_3$  supported on  $Al_2O_3$  has also been studied for removal of  $F^-$  from water.<sup>207</sup>  $F^-$  adsorption capacity of  $La(OH)_3$  impregnated  $Al_2O_3$  (0.35  $mM\ g^{-1}$ ) was found to be much higher than  $Al_2O_3$  (0.17- 0.19  $mM\ g^{-1}$ ). The mechanism of  $F^-$  removal was explained by ion exchange process between  $F^-$  and  $OH^-$  present on the surface of the adsorbent.  $F^-$  concentration was decreased from 7  $mM$  to 0.003  $mM$  after treating with adsorbent in the pH range of 5.7- 8.  $F^-$  removal capacity of the adsorbent was decreased in the presence of  $PO_4^{2-}$  and  $SO_4^{2-}$  whereas presence of  $Cl^-$ ,  $Br^-$ ,  $I^-$  and  $NO_3^-$  did not show any significant decrease in  $F^-$  removal capacity.

Some of the alumina based adsorbents which are utilized for defluoridation of water are listed in the Table 1.1. Caution needs to be exercised in comparing  $F^-$  adsorption capacities of different adsorbents because different parameters (such as initial  $F^-$  concentration range, adsorbent dose, pH, temperature etc.) were used by different researchers.

Table 1.1 Various alumina based adsorbents used for defluoridation of water.

Adsorbent	Initial F <sup>-</sup> concentration, (adsorbent dose)	Contact time, Temperature	pH	F <sup>-</sup> adsorption capacity (mg g <sup>-1</sup> )	Applicable kinetic models	Applicable Isotherm models	Important observation	Ref.
Activated Al <sub>2</sub> O <sub>3</sub>	2.5- 30 mg L <sup>-1</sup> , (5 g L <sup>-1</sup> )	10 h, 30 °C	7	1.08	pseudo second order	Langmuir	-At low pH, F <sup>-</sup> sorption capacity was less due to the formation of week hydrofluoric acid. -At alkaline pH range, reduction in F <sup>-</sup> adsorption was due to the competition between OH <sup>-</sup> and F <sup>-</sup> for active sites of Al <sub>2</sub> O <sub>3</sub> .	[69]
Activated Al <sub>2</sub> O <sub>3</sub>	1-1000 mg L <sup>-1</sup> , (6.6 g L <sup>-1</sup> )	48 h, 25 °C	5.5	24	pseudo second order; intraparticle diffusion	Freundlich	-Chemisorption was responsible for F <sup>-</sup> adsorption on activated Al <sub>2</sub> O <sub>3</sub> .	[98]
Activated Al <sub>2</sub> O <sub>3</sub> (γ-Al <sub>2</sub> O <sub>3</sub> )	15-100 mg L <sup>-1</sup> , (12.5 g L <sup>-1</sup> )	16- 24h, 30 °C	5-7	16.34	-	Langmuir, Freundlich	-Presence of SO <sub>4</sub> <sup>2-</sup> inhibited the F <sup>-</sup> adsorption by the formation of aluminum-sulfate complexes.	[84]

Activated Al <sub>2</sub> O <sub>3</sub>	2.5- 14 mg L <sup>-1</sup> , -	--	7	2.41	pseudo first order; intraparticle diffusion	Langmuir, Freundlich	-F <sup>-</sup> adsorption on AA occurred by ion exchange as well as adsorption process.	[81]
Activated Al <sub>2</sub> O <sub>3</sub>	1-20 mg L <sup>-1</sup> , -	3 days, 25 °C	7	2.69	-	Freundlich	-Maximum F <sup>-</sup> adsorption occurred at pH 4 (8.27 mg g <sup>-1</sup> ).	[102]
Activated Al <sub>2</sub> O <sub>3</sub> (grade OA-25)	2.5- 14 mg L <sup>-1</sup> , (4 g L <sup>-1</sup> )	--	7	1.45	-	-	- At pH > 7, OH <sup>-</sup> and silicates strongly compete with F <sup>-</sup> for active sites of Al <sub>2</sub> O <sub>3</sub> . - At pH < 7, soluble AlF complexes (AlF <sup>2+</sup> , AlF <sub>2</sub> <sup>+</sup> ) were formed.	[103]
Alkoxide origin Al <sub>2</sub> O <sub>3</sub>	0- 25 mg L <sup>-1</sup> , (5 g L <sup>-1</sup> )	24 h, 30 °C	7	2	pseudo second order	Langmuir	-At acidic pH, the surface of the adsorbent was highly protonated. -Surface acquires negative charge in alkaline pH and OH <sup>-</sup> competes with F <sup>-</sup> leading to decrease in its F <sup>-</sup> uptake.	[90]
Nano-Al <sub>2</sub> O <sub>3</sub>	1- 100 mg L <sup>-1</sup> , (1 g L <sup>-1</sup> )	24 h, 25 °C	6.15	14.0	pseudo second order	Langmuir	-Interaction of F <sup>-</sup> and Al <sub>2</sub> O <sub>3</sub> was endothermic in nature. -F <sup>-</sup> sorption was decreased in presence of PO <sub>4</sub> <sup>3-</sup> , CO <sub>3</sub> <sup>-</sup> , and SO <sub>4</sub> <sup>2-</sup> .	[119]

nano- AlOOH	3- 35 mg L <sup>-1</sup> , (5 g L <sup>-1</sup> )	6 h, 25 °C	7	3.26	pseudo second order	Langmuir	-F <sup>-</sup> sorption capacity decreased in the presence of PO <sub>4</sub> <sup>3-</sup> and SO <sub>4</sub> <sup>2-</sup> .	[120]
Al <sub>2</sub> O <sub>3</sub> nanofibers ( $\alpha$ - Al <sub>2</sub> O <sub>3</sub> )	10-100 mg L <sup>-1</sup> , (5 g L <sup>-1</sup> )	1 h, 25 °C	7	1.2	pseudo second order	Freundlich	-F <sup>-</sup> adsorption may be due to the combined effect of both chemical and electrostatic interactions between the Al <sub>2</sub> O <sub>3</sub> surface and F <sup>-</sup> and also the availability of active sites on the Al <sub>2</sub> O <sub>3</sub> surface.	[121]
Metallurgical grade Al <sub>2</sub> O <sub>3</sub> (MGA)	-	-, 20 °C	5- 6	12.57	-	Langmuir, Freundlich	-At higher pH values, F <sup>-</sup> adsorption capacity decreased drastically because of the competition between F <sup>-</sup> and OH <sup>-</sup> for the active sites of MGA.	[188]
Acidic Al <sub>2</sub> O <sub>3</sub>	2- 15 mg L <sup>-1</sup> , (1 g L <sup>-1</sup> )	24 h, 25 °C		8.4	pseudo second order	Langmuir	-F <sup>-</sup> adsorption onto Al <sub>2</sub> O <sub>3</sub> was due to surface adsorption.  -The order of anions reducing the F <sup>-</sup> removal efficiency is HCO <sub>3</sub> <sup>-</sup> > CO <sub>3</sub> <sup>2-</sup> > SO <sub>4</sub> <sup>2-</sup> > NO <sub>3</sub> <sup>-</sup> > Cl <sup>-</sup>	[117]

Mesoporous Al <sub>2</sub> O <sub>3</sub>	5- 50 mg L <sup>-1</sup> , (2 g L <sup>-1</sup> )	24 h, 30 °C	6.8	8.26	pseudo second order	Langmuir	-Order of anions reducing the F <sup>-</sup> removal was HCO <sub>3</sub> <sup>-</sup> > SO <sub>4</sub> <sup>2-</sup> > NO <sub>3</sub> <sup>-</sup> > Cl <sup>-</sup> . -Maximum F <sup>-</sup> adsorption occurred at pH 3.	[91]
Mesoporous Al <sub>2</sub> O <sub>3</sub>	5-200 mg L <sup>-1</sup> , (0.6 g L <sup>-1</sup> )	12 h, 25 °C	6	135	pseudo second order	Langmuir	-F <sup>-</sup> adsorption occurred by chemisorption mechanism through ligand exchange. -F <sup>-</sup> adsorption capacity decreased in the presence of HCO <sub>3</sub> <sup>-</sup> and SO <sub>4</sub> <sup>2-</sup> .	[111]
Mesoporous Al <sub>2</sub> O <sub>3</sub>	20-250 mg L <sup>-1</sup> , (12 g L <sup>-1</sup> )	24 h, 30 °C	6	14.26	pseudo second order	Langmuir	-Mesoporous Al <sub>2</sub> O <sub>3</sub> with higher surface area and narrow pore size showed faster response time for F <sup>-</sup> adsorption.	[112]
Mesoporous Al <sub>2</sub> O <sub>3</sub>	2-1000 mg L <sup>-1</sup> , (0.1 g L <sup>-1</sup> )	12 h, 25 °C	6.5	300	-	-	- The sample calcined at 400 °C with amorphous pore walls showed higher F <sup>-</sup> adsorption capacity than that of sample calcined at 900 °C.	[113]
Ca doped mesoporous Al <sub>2</sub> O <sub>3</sub>	2-1000 mg L <sup>-1</sup> , (0.1 g L <sup>-1</sup> )	12 h, 25 °C	6.5	450	-	-	- At lower initial F <sup>-</sup> concentrations (below 150 mg L <sup>-1</sup> ), the F <sup>-</sup> adsorption isotherm follows Langmuir model. -At higher initial F <sup>-</sup> concentrations, the	[113]

							higher F <sup>-</sup> removal occurred due to the formation of CaF <sub>2</sub> .	
MnO <sub>2</sub> coated Al <sub>2</sub> O <sub>3</sub>	2.5- 30 mg L <sup>-1</sup> , (5 g L <sup>-1</sup> )	3 h, 30 °C	7	2.85	pseudo second order	Langmuir	-Optimum F <sup>-</sup> removal occurred between pH range of 4- 7.	[69]
MnO <sub>2</sub> - modified AA	1-1000 mg L <sup>-1</sup> , (6.6 g L <sup>-1</sup> )	48 h, 25 °C	5.5	10.18	pseudo second order; intraparticle diffusion	Langmuir	-Chemisorption was responsible for F <sup>-</sup> adsorption on MnO <sub>2</sub> -AA.	[98]
CaO- modified AA	1-1000 mg L <sup>-1</sup> (6.6 g L <sup>-1</sup> )	48 h, 25 °C	5.5	101.01	pseudo second order; intraparticle diffusion	Langmuir	-Chemisorption was responsible for F <sup>-</sup> adsorption on CaO-AA. -Alkalinity of the adsorbent was found to influence the F <sup>-</sup> adsorption capacity.	[98]
Hydrous MnO <sub>2</sub> coated Al <sub>2</sub> O <sub>3</sub>	10- 70 mg L <sup>-1</sup> , (5 g L <sup>-1</sup> )	1 h, 30 °C	5.2	7.09	pseudo second order	Langmuir	-Optimum F <sup>-</sup> removal occurred between pH range of 4- 6.	[63]
Magnesia amended AA	5- 150 mg L <sup>-1</sup> , (4 g L <sup>-1</sup> )	-, 30 °C	6.5- 7	10.12	pseudo second order	Sips model	-Surface sorption as well as intraparticle diffusion plays a significant role in the F <sup>-</sup> sorption process.	[106]

<b>Al<sub>2</sub>O<sub>3</sub> cement granules (ALC)</b>	<b>2.5-100 mgL<sup>-1</sup>, (2 g L<sup>-1</sup>)</b>	<b>3 h, 27 °C</b>	<b>6.5-7</b>	<b>34.36</b>	<b>-</b>	<b>Freundlich</b>	<b>-F<sup>-</sup> removal was spontaneous and endothermic process. -F<sup>-</sup> removal occurred by chemisorption mechanism.</b>	<b>[97]</b>
<b>Alum impregnated Al<sub>2</sub>O<sub>3</sub></b>	<b>1- 35 mg L<sup>-1</sup>, (8 g L<sup>-1</sup>)</b>	<b>3 h, room temperature</b>	<b>6.5</b>	<b>40.68</b>	<b>-</b>	<b>Bradley equation</b>	<b>-Can remove F<sup>-</sup> effectively (up to 0.2 mgL<sup>-1</sup>) from water containing 20 mg L<sup>-1</sup> F<sup>-</sup>.</b>	<b>[114]</b>
<b>Lanthanum-impregnated AA</b>	<b>0- 100 mg L<sup>-1</sup>, (1 g L<sup>-1</sup>)</b>	<b>24 h, 25 °C</b>	<b>7</b>	<b>16.9</b>	<b>-</b>	<b>Langmuir</b>	<b>-F<sup>-</sup> adsorption occurred by ligand exchange mechanism between F<sup>-</sup> and surface hydroxyl groups.</b>	<b>[205]</b>



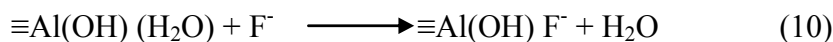
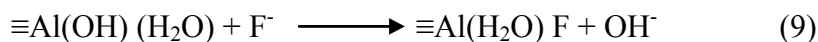
### 1.5.2. Mechanism of F<sup>-</sup> adsorption on Al<sub>2</sub>O<sub>3</sub> based adsorbents

Presence of hydroxyl groups on the surface of adsorbent play critical role in determining the F<sup>-</sup> adsorption behavior of Al<sub>2</sub>O<sub>3</sub>. Protonation and deprotonation of these surface hydroxyl groups cause electrical charge promoting adsorption.<sup>151</sup> The mechanisms involved in F<sup>-</sup> adsorption on Al<sub>2</sub>O<sub>3</sub> have been reported by Leyva-Ramos et al.<sup>83</sup> and Sujana et al.<sup>151</sup> It has been proposed that, the surface groups present on the active sites of alumina are ≡Al-OH<sub>2</sub><sup>+</sup>, ≡Al-OH and ≡Al-O<sup>-</sup>. Ligand exchange model and ion exchange model have been utilized to explain F<sup>-</sup> adsorption on Al<sub>2</sub>O<sub>3</sub> in aqueous medium and it can be described by the following equations (6-10):<sup>83,97</sup>

Ion exchange model:



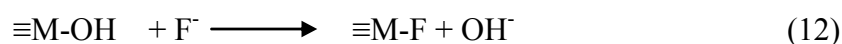
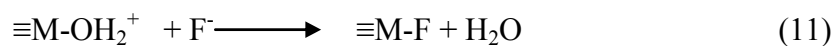
Ligand exchange model:



According to Ku and Chiou<sup>84</sup> and Hao and Huang,<sup>115</sup> formation of various F<sup>-</sup> complexes (e. g, AlF<sup>2+</sup>, AlF<sub>2</sub><sup>+</sup>, AlF<sub>3</sub>, AlF<sub>4</sub><sup>-</sup>) also plays important role on adsorption of F<sup>-</sup> on Al<sub>2</sub>O<sub>3</sub>. The disadvantage associated with AA is that, maximum F<sup>-</sup> removal occurs only when pH value of solution is below 6 and this factor limits the practical applicability of AA for this purpose. Moreover, it has also been reported that Al<sub>2</sub>O<sub>3</sub> begins to leach below pH 6 and poses severe threat to human health.<sup>39</sup>

It has been reported by various researchers that, F<sup>-</sup> adsorption capacity of Al<sub>2</sub>O<sub>3</sub> can be increased by chemical modification of its surfaces. F<sup>-</sup> ion is classified as hard base due to its high electronegativity and small ionic size. So, it has a strong affinity towards electropositive multivalent metal ions like Zr<sup>4+</sup>, Fe<sup>3+</sup>, Ca<sup>2+</sup>, La<sup>3+</sup>, Ce<sup>4+</sup> etc.<sup>98, 208, 209</sup> Impregnation of positively charged cations (such as Zr<sup>4+</sup>, Ca<sup>2+</sup>, Mg<sup>2+</sup>, La<sup>4+</sup>, Fe<sup>3+</sup>, Ce<sup>4+</sup> etc.) onto the adsorbent helps to create positive charges on the

adsorbent surface which attracts  $F^-$  (equation (11) and (12)) and improves  $F^-$  adsorption capacity.<sup>31</sup> These metallic cations act as a bridge in between adsorbed  $F^-$  and  $Al_2O_3$  surface. The chemistry involved in this type of adsorption can be presented by equations 11 and 12:



( $\equiv M$  represents the multivalent metallic cation surfaces)

### 1.5.3. Nano particle based adsorbents

Nanoparticles have proven themselves as excellent adsorbents due to their unique features namely, large surface area and large number of active sites for interaction with different contaminants.<sup>210-214</sup> Exploring these properties several researchers have developed different nano particle based adsorbents. One of the strategies, which have been adopted to fabricate adsorbents, is to impregnate nanoparticles on the surface or inside the pores of solid porous support matrix.

Maliyekkal et al.<sup>123</sup> have tested the potential of MgO nanoparticles for defluoridation of aqueous solutions. The adsorbent was synthesized by self-propagated combustion of magnesium nitrate trapped in cellulose fibers. The synthesized MgO nanoparticles were crystalline in nature with high phase purity and particle size was varied in the range of 3- 7 nm. The authors have explained the mechanism of  $F^-$  adsorption on MgO nanoparticles by using the data obtained from spectroscopic, microscopic and macroscopic studies. The sorption of  $F^-$  on nano MgO was attributed to the isomorphic substitution of  $OH^-$  by  $F^-$  in brucite lattice. This reaction was found to be possible since both  $F^-$  and  $OH^-$  ions are of similar size, iso-electronic in nature and possess comparable ionic radii. Devi et al.<sup>122</sup> have studied  $F^-$  adsorption feasibility of nano sized magnesium oxide (nano- MgO) from aqueous solution. Maximum 90%  $F^-$  removal was obtained by using  $0.6 \text{ g L}^{-1}$  dosage of nano-MgO. From equilibrium studies it was observed that, Freundlich model was better fitted than Langmuir model, which indicated the multilayer  $F^-$  adsorption on nano-MgO. Patel et al.<sup>125</sup> have performed defluoridation experiments employing CaO nanoparticles, prepared by sol-gel technique, as sorbent. The percentage of  $F^-$  removal

was decreased from 98 to 89% with increasing temperature from 25 to 55 °C, when initial F<sup>-</sup> concentration was 100 mg L<sup>-1</sup>. The main cause for decrease of F<sup>-</sup> removal at higher temperature was attributed to the escaping tendency of the ions from the interface. Sorption of F<sup>-</sup> on CaO nanoparticles have occurred via conversion of CaO to Ca(OH)<sub>2</sub> in water and then sorption of F<sup>-</sup> by surface chemical reaction, where OH<sup>-</sup> ions of Ca(OH)<sub>2</sub> were replaced rapidly by F<sup>-</sup> and formed CaF<sub>2</sub>. F<sup>-</sup> sorption capacity of CaO nanoparticles was found to be almost constant in the pH range of 2- 8. A progressive decrease in F<sup>-</sup> uptake by this sorbent above pH 8 was observed and attributed to the electrostatic repulsion of F<sup>-</sup> to negatively charged surface and the competition for active sites by an excessive amount of OH<sup>-</sup> ions. Competitive anions such as SO<sub>4</sub><sup>2-</sup> and NO<sub>3</sub><sup>-</sup> did not affect the F<sup>-</sup> sorption on CaO nanoparticles.

Pathak et al.<sup>215</sup> have synthesized variety of nano sized inorganic oxides (Fe<sub>3</sub>O<sub>4</sub>, Al<sub>2</sub>O<sub>3</sub> and ZrO<sub>2</sub>) through thermolysis of a polymeric based aqueous precursor method. The obtained Fe<sub>3</sub>O<sub>4</sub>, Al<sub>2</sub>O<sub>3</sub> and ZrO<sub>2</sub> nanosized oxide powders were incorporated on activated charcoal matrix through adsorption and used as an adsorbent for removal of trace amount of F<sup>-</sup> and various other pollutants. These adsorbents were also able to remove As (III) and As (V) ions also from the industrial waste water up to 0.01- 0.02 mg L<sup>-1</sup> levels. Zhao et al.<sup>216</sup> have developed a nano sized adsorbent Fe<sub>3</sub>O<sub>4</sub>@Al(OH)<sub>3</sub>. It exhibited strong F<sup>-</sup> adsorption in the pH range of 5- 7. The maximum F<sup>-</sup> sorption capacity was found to be 88.48 mg g<sup>-1</sup> at pH 6.5. From XPS (X-ray photoelectron spectroscopy) data and experimental results it was confirmed that, F<sup>-</sup> sorption was driven by both electrostatic attraction and surface complexation. Pan et al.<sup>130</sup> have fabricated a composite, nano sized hydrous zirconium oxide encapsulated within a commercial porous polystyrene anion exchanger D 201 (HZO-201), for removal of F<sup>-</sup> from water. HZO-201 showed higher F<sup>-</sup> removal capacity than AA and D 201 when competing anions (Cl<sup>-</sup>, SO<sub>4</sub><sup>2-</sup>, NO<sub>3</sub><sup>-</sup> and HCO<sub>3</sub><sup>-</sup>) coexisted at relatively high concentrations. Fixed column adsorption experiments indicated that, the effective treatable volume of water with HZO-201 was ~ 7- 14 times larger than D 201, irrespective of whether synthetic solution or ground water was the feeding solution. Sundaram et al.<sup>136, 217, 218</sup> have investigated the defluoridation property of nano-hydroxyapatite (nHAp). For enhancement of F<sup>-</sup> adsorption capacity of nHAp, nHAp was coated on chitin and chitosan. Treatment of water sampled from a F<sup>-</sup> endemic village (in India), having F<sup>-</sup> concentration of 2.33

mg L<sup>-1</sup> with nHAp-chitosan composite resulted in reduction in F<sup>-</sup> concentration to 0.26 mg L<sup>-1</sup>.<sup>217</sup> The authors have also studied the F<sup>-</sup> removal capacity of nHAp-chitin composite and obtained higher F<sup>-</sup> adsorption capacity than those of nHAp<sup>218</sup> and nHAp-chitosan composite.<sup>136</sup>

Considering the advantages of magnetic separation process and potential of activated Al<sub>2</sub>O<sub>3</sub> for defluoridation of water, Chang et al.<sup>219</sup> have synthesized nano-scale bayerite/ SiO<sub>2</sub>/ Fe<sub>3</sub>O<sub>4</sub> adsorbents. The authors have synthesized two types of aluminum-type adsorbents via three sequential steps: (i) chemical precipitation of Fe<sub>3</sub>O<sub>4</sub>, (ii) coating of SiO<sub>2</sub> on Fe<sub>3</sub>O<sub>4</sub>, and (iii) formation of aluminum-type adsorbents, bayerite (Al(OH)<sub>3</sub>) on SiO<sub>2</sub>/ Fe<sub>3</sub>O<sub>4</sub>, by adopting sol-gel (denoted as MASG) or homogeneous precipitation (called as MAHP) methods. The F<sup>-</sup> adsorption potential of the prepared sorbents was compared with commercial activated Al<sub>2</sub>O<sub>3</sub> (CA). Langmuir adsorption isotherm explained well the equilibrium F<sup>-</sup> adsorption on CA, MASG and MAHP. MASG sorbent was found to be the most effective sorbent with F<sup>-</sup> adsorption capacity of 38 g kg<sup>-1</sup>. This value is comparable with CA even at a higher pH value. The F<sup>-</sup> adsorption on MASG and MAHP was attributed to the functional groups on MASG and MAHP surface which adsorbed F<sup>-</sup>. Chang et al.<sup>220</sup> have used nano-sized ZrO<sub>2</sub>/ SiO<sub>2</sub>/ Fe<sub>3</sub>O<sub>4</sub> as an adsorbent for removal of F<sup>-</sup> from water and simulated industrial wastewater. F<sup>-</sup> sorption capacity of 14.7 mg g<sup>-1</sup> was achieved at constant pH 4. The adsorbent can be regenerated by using 0.001 N NaOH solution. Swaina et al.<sup>221</sup> have reported the preparation of a sorbent composite, composed of binary metal oxide (Fe(III)- Zr(IV)) in an alginate matrix. Maximum F<sup>-</sup> sorption capacity determined from Langmuir adsorption model was 0.98 mg g<sup>-1</sup>. Thermodynamic parameter, ΔG°, was negative, which indicated the spontaneity of F<sup>-</sup> adsorption process.

Li et al.<sup>222</sup> have used carbon nanotubes (CNTs) as support to deposit Al<sub>2</sub>O<sub>3</sub> and investigated the potential application of Al<sub>2</sub>O<sub>3</sub>/ CNTs for F<sup>-</sup> removal from drinking water. CNTs were prepared by pyrolysis of a propylene-hydrogen mixture with Ni particles as catalyst. The F<sup>-</sup> adsorption capacity of Al<sub>2</sub>O<sub>3</sub>/ CNTs was about 13.5 times higher than AC-300 carbon, 4 times higher than γ-Al<sub>2</sub>O<sub>3</sub> and also higher than that of amberlite IRA-410 polymeric resin. The F<sup>-</sup> removal efficiency of aligned carbon nanotubes (ACNTs) was investigated by Li et al.<sup>15</sup> The authors have reported that, both surface and inner cavities of ACNTs were readily accessible for F<sup>-</sup> sorption.

ACNTs exhibited higher  $F^-$  adsorption capacity than AC, even though the ACNTs possessed much lower specific surface area and pore volume than AC. However,  $F^-$  adsorption capacity of ACNTs was high, but the cost of preparation of the adsorbent was too high which limits its commercial utilization. In a later study, Li et al.<sup>138</sup> have modified CNTs with  $Al_2O_3$  and investigated the effects of calcination temperature,  $Al_2O_3$  loading on CNTs and pH on  $F^-$  removal capacity. It was observed that, in the pH range of 6- 9 at 25 °C, the  $F^-$  adsorption capacity of CNTs was increased from 2.3  $mg\ g^{-1}$  to 9.6  $mg\ g^{-1}$  when 30 wt.%  $Al_2O_3$  was loaded onto CNTs and calcined to 450 °C. For this material, ligand exchange mechanism was responsible when the surface was positively charged and ion exchange mechanism was dominant when the surface was neutral. Some of the nano particle based adsorbents, which are utilized for defluoridation of water, are listed in Table 1.2.

Table 1.2. Various nano particle based adsorbents used for defluoridation of water.

Adsorbent (particle size)	Initial F <sup>-</sup> concentration, (adsorbent dose)	Contact time, Temperature	pH	Adsorption Capacity (mg/g)	Applicable kinetic models	Applicable Isotherm models	Important observation	Ref.
Nano MgO (< 50 nm)	5- 100 mg L <sup>-1</sup> , (0.6 g L <sup>-1</sup> )	2 h, 25 °C	10-11	14	pseudo second order	Freundlich	Less sensitive to pH variations. Order of anions reducing the F <sup>-</sup> removal was OH <sup>-</sup> > SO <sub>4</sub> <sup>2-</sup> > HCO <sub>3</sub> <sup>-</sup> > Cl <sup>-</sup> .	[122]
Nano MgO (3- 7 nm)	5- 200 mg L <sup>-1</sup> , (0.5 g L <sup>-1</sup> )	-, 30 °C	7	-	pseudo second order	Freundlich	Less sensitive to pH variations. PO <sub>4</sub> <sup>3-</sup> was more competitor for F <sup>-</sup> followed by HCO <sub>3</sub> <sup>-</sup> and NO <sub>3</sub> <sup>-</sup> .	[123]
Sulfate doped Fe <sub>3</sub> O <sub>4</sub> / Al <sub>2</sub> O <sub>3</sub> nanoparticles (15-20 nm)	2- 16 mg L <sup>-1</sup> , (1 g L <sup>-1</sup> )	7h, 25 °C	7	70	Elovich	Two site Langmuir Model	F <sup>-</sup> removal inhibited by the presence of PO <sub>4</sub> <sup>3-</sup> . Optimum pH range for F <sup>-</sup> removal was 4-10.	[127]
Nano sized hydrous zirconium oxide encapsulated within polystyrene anion exchanger	-, (0.5 g L <sup>-1</sup> )	12 h, 25 °C	6.8 3.5	24.2 134.2	pseudo second order and intraparticle diffusion	Langmuir	Order of anions reducing the F <sup>-</sup> removal was HCO <sub>3</sub> <sup>-</sup> ≈ SO <sub>4</sub> <sup>2-</sup> > NO <sub>3</sub> <sup>-</sup> > Cl <sup>-</sup> .	[130]

CaO nanoparticles (< 15 nm)	10-100 mg L <sup>-1</sup> , (0.6 g L <sup>-1</sup> )	30 min, 25 °C		163	pseudo first order	Freundlich, Langmuir, D-R isotherm	Sorption of F <sup>-</sup> occurred by surface chemical reaction with the formation of CaF <sub>2</sub> .	[125]
Nano zirconium- carbon hybrid (Zr(IV)-oxalate: < 100 nm)	0.1- 60 mg L <sup>-1</sup> , (3.33 g L <sup>-1</sup> )	7 days, 25 °C	7	17.7	-	Langmuir, Freundlich	F <sup>-</sup> adsorption mechanism: (i) hydroxyl exchange from Zr-oxalate surface sites (ii) F <sup>-</sup> interaction with the positive charge of zirconium ions in Zr=O groups.	[129]
CeO <sub>2</sub> -ZrO <sub>2</sub> nanocages (80- 100 nm)	1- 100 mg L <sup>-1</sup> , (0.2 g L <sup>-1</sup> )	24 h, room temperature	4	175	pseudo second order	Langmuir	Anion exchange and electrostatic interaction play key roles in F <sup>-</sup> removal.	[134]
Nano Fe-Ce-Al (40 nm)	0.001 M, (5 g L <sup>-1</sup> )	36 h, 25 °C	7	2.22	-	-	300 bed volumes can be treated with the effluent less than 1.0 mg L <sup>-1</sup> at an initial F <sup>-</sup> concentration of 5.5 mg L <sup>-1</sup> .	[166]
Nano hydroxyapatite (200 nm)	10 mg L <sup>-1</sup> , (5 g L <sup>-1</sup> )	30 min, 30 °C	-	1.29	pseudo second order	Langmuir	The mechanism of F <sup>-</sup> removal of n-HAp follows both adsorption and ion-exchange mechanism.	[218]
Nano hydroxyapatite/ chitin composite	6- 12 mg L <sup>-1</sup> , (2 g L <sup>-1</sup> )	30 min, 30 °C	7	2.84	pseudo second order, pore diffusion model	Freundlich	The nature of the F <sup>-</sup> sorption process was spontaneous and endothermic.	[136]

Nano hydroxyapatite/ chitosan composite	9- 15 mg L <sup>-1</sup> , (5 g L <sup>-1</sup> )	-, 30 °C	7	2.04	pseudo second order, pore diffusion model	Langmuir	F <sup>-</sup> removal capacity was decreased in the presence of HCO <sub>3</sub> <sup>-</sup> .  The nature of the F <sup>-</sup> sorption process is spontaneous and endothermic.	[217]
Nano goethite ( $\alpha$ -FeOOH) (1-10 nm)	10-150 mg L <sup>-1</sup> , (1 g L <sup>-1</sup> )	2 h, 30 °C	5.75	59	pseudo second order	Freundlich	Optimum F <sup>-</sup> removal occurred between pH range of 6- 8.  Presence of Cl <sup>-</sup> , SO <sub>4</sub> <sup>2-</sup> adversely affected F <sup>-</sup> removal.	[124]
Al <sub>2</sub> O <sub>3</sub> / CNTs	-, (2 g L <sup>-1</sup> )	12 h, 25 °C	6	28.7	-	Freundlich	Higher F <sup>-</sup> adsorption capacity could be mainly due to the amorphous structure of Al <sub>2</sub> O <sub>3</sub> .  Optimum F <sup>-</sup> removal occurred between pH range of 5- 9.	[222]
Aligned carbon nanotubes (diameter 20-80 nm)	20 mg L <sup>-1</sup> , (0.5 g L <sup>-1</sup> )	3 h, 25 °C	7	4.5	-	Freundlich	Active sites on the surface caused by defects and amorphous carbon, inner cavities and internanotube space contribute to high F <sup>-</sup> removal capability.	[15]



## 1.6. Gap in existing research

Though, it is a well known fact that a significant portion of human population all around the world is suffering from consumption of  $F^-$  contaminated ground water, but till date defluoridation of drinking water is a major challenge. Amongst several techniques, adsorption based methods are found to be more convenient and cost effective. Though, variety of adsorbents have been developed for this purpose,  $Al_2O_3$  based materials have exhibited their high  $F^-$  removal capacity from water. Several types of alumina have been reported as adsorbent for defluoridation of water, but in most of the cases to prepare  $Al_2O_3$ , aluminum alkoxides are used as aluminum source and alcohol as solvent. Aluminum alkoxides are not only costly but also reactive to the moisture. The use of alcohol as solvent and sometimes autoclave as reactor makes these synthesis processes difficult and expensive. However, the disadvantage associated with activated  $Al_2O_3$  is that optimum  $F^-$  removal capacity occurs only at a pH value of the solution below 6.0, which limits the practical applications of activated  $Al_2O_3$  heavily. Moreover, it has also been reported that  $Al_2O_3$  begins to leach below pH 6 and poses severe threat to human health.<sup>39</sup> So, there is a need to develop a simple but cost effective method to prepare an adsorbent which can act as an efficient adsorbent to remove  $F^-$  from water.

Modifications of  $Al_2O_3$  significantly enhance the  $F^-$  removal capacity of the adsorbents. However, their complicated preparation methodologies and small scale of production, limit their usage only in laboratory scale. Therefore, there is a need to develop an adsorbent which is not only cost effective but also capable of  $F^-$  removal from water (at least up to the permissible limit) so that clean drinkable water can be served to the human community particularly those who are economically challenged.

## 1.7. Objectives

The objectives of thesis work aims at:

1. Development of a simple but cost-effective aqueous solution based method for synthesis of mesoporous  $Al_2O_3$  based adsorbents.
2. Incorporation of metal oxide nanoparticle ( $ZrO_2$ ,  $MgO$  and  $CaO$ ) into  $Al_2O_3$  matrix with different loadings (wt. %) and optimization of composition of the oxides for better adsorption capacity.

3. Investigations on crystal structure, surface area and pore size distribution and morphology of the synthesized adsorbents.
4. (a) Investigations on effect of various processing parameters on F<sup>-</sup> adsorption property of synthesized materials. The processing parameters are
  - (i) Composition of adsorbents, (ii) Contact time, (iii) Initial pH of the solution, (iv) Adsorbent dose, (v) Initial F<sup>-</sup> concentration of the solution.(b) Studies on fluoride ion adsorption kinetics and adsorption isotherms of synthesized materials.
5. Establish the correlation between structure, morphology, compositions of the synthesized adsorbents and their fluoride ion adsorption property.

### **1.8. Characterization details**

The synthesized adsorbents were characterized by the following techniques:

#### **(a) X-Ray Diffraction (XRD) Analysis**

Powder X-ray diffraction (XRD) patterns of the samples were recorded using a Rigaku powder X-ray diffractometer (Mini FlexII, Rigaku, Japan) using Cu K<sub>α</sub> radiation. The diffractograms were recorded in the 2θ ranges 10 - 80° with a scanning speed of 3°/ min.

#### **(b) Nitrogen adsorption-desorption analysis**

Nitrogen adsorption-desorption isotherms of the synthesized materials were obtained by using a surface area and porosity analyzer (Micromeritics Tristar 3000, USA) to determine Brunauer-Emmett-Teller (BET) surface area and Barrett-Joyner-Halenda (BJH) pore size. Prior to the adsorption measurements all samples were out gassed using nitrogen flow at 200 °C for 10 h.

#### **(c) High resolution transmission electron microscopy technique**

High Resolution Transmission Electron micrographs (HRTEM) of the synthesized samples were obtained using HRTEM (FEI, Tecnai G2 30 S-Twin, USA) operated at 300 kV.

#### (d) Determination of $\text{pH}_{\text{PZC}}$ of the adsorbents

$\text{pH}_{\text{PZC}}$  plays an important role in the surface characterization of metal oxides/hydroxides. In the adsorption process,  $\text{pH}_{\text{PZC}}$  determines how easily a substrate can adsorb ions present in solution.  $\text{pH}_{\text{PZC}}$  of the adsorbents can be determined by using the salt addition method.<sup>223, 224</sup> For determination of  $\text{pH}_{\text{PZC}}$  of the synthesized materials, a solution of 0.01 M NaCl was prepared, and its pH was adjusted in between 3 and 12 by using calculated amount of 0.01 M HCl and 0.01 M NaOH solutions and pH of the mixture was measured using a pH meter (EUTECH instruments pH 700). 10 mL of 0.01 M NaCl solutions having different pH were taken in 15 mL centrifuge tubes and 30 mg of adsorbent was added in each of these solutions. These tubes were then kept on a mechanical shaker (Neolab instruments, Mumbai, India) at  $(30 \pm 2)$  °C for 24 h and the equilibrium (final) pH of the solutions were recorded.  $\Delta\text{pH}$  (the difference between initial and final pH) values were plotted against their initial pH values. The  $\text{pH}_{\text{initial}}$  at which  $\Delta\text{pH}$  was zero was considered as  $\text{pH}_{\text{PZC}}$ .

### 1.9. Fluoride adsorption experiments

In order to determine the effect of different controlling parameters (such as adsorbent dose, contact time, initial  $\text{F}^-$  concentration, pH and co-existing anions) on  $\text{F}^-$  adsorption capacity of the synthesized adsorbents, batch adsorption experiments were performed. All adsorption experiments were carried out at  $(30 \pm 2)$  °C. A stock solution containing  $1000 \text{ mg L}^{-1} \text{ F}^-$  was prepared by dissolving 2.23 g of sodium fluoride in 1000 mL of RO water. Working solutions were prepared by diluting this stock solution. In a typical experiment, 30 mg of adsorbent was mixed with 10 mL of  $\text{F}^-$  solution in a 15 mL capped centrifuge tube. The mixture was placed in a mechanical shaker and agitation at a speed of 120 rpm. When equilibrium was reached, the adsorbent was separated from the mixture by centrifuging at 4000 rpm for 10 min. The concentration of  $\text{F}^-$  present in the solution after treatment with adsorbent was determined using UV-Vis spectrophotometer. The amount of  $\text{F}^-$  adsorbed by the adsorbent,  $q_e$  ( $\text{mg g}^{-1}$ ), was calculated using the following equation:

$$q_e = (C_0 - C_e)(V/m) \quad (13)$$

where  $C_0$  and  $C_e$  are initial and equilibrium concentrations of  $F^-$  in solution ( $mg L^{-1}$ ) respectively,  $V$  is the volume of solution (L) and  $m$  is mass of the adsorbent (g).

The effect of adsorbent dose on  $F^-$  adsorption was investigated by varying the adsorbent dose from  $0.1 g L^{-1}$  to  $8 g L^{-1}$ . The effect of contact time was examined with initial  $F^-$  concentration of  $30 mg L^{-1}$  and adsorbent dose of  $5 g L^{-1}$ . Adsorption kinetic experiments were carried out by using  $3 g L^{-1}$  of the adsorbent with different  $F^-$  concentrations ranging from  $5 mg L^{-1}$  to  $30 mg L^{-1}$ . At a designed interval time, the samples were centrifuged and residual  $F^-$  concentrations were determined. The effect of initial  $F^-$  concentration and the adsorption isotherms were studied using solutions having various  $F^-$  concentrations varying from  $5 mg L^{-1}$  to  $100 mg L^{-1}$ . The effect of pH was investigated by adjusting the solution pH from 4 to 10, using 0.01 M HCl and 0.01 M NaOH for a solution having initial  $F^-$  concentration  $30 mg L^{-1}$ . Reproducibility of measurements was determined in triplicate and average values are reported here.

### 1.10. Fluoride analysis

In the literature available methods for  $F^-$  analysis are ion selective electrode method, ion chromatography and UV-Vis spectroscopy etc.<sup>3</sup> Amongst these methods use of UV-Vis spectroscopic technique is simpler. In the present study we have determined the concentration of  $F^-$  ion in aqueous solution using UV-Vis spectroscopy.<sup>225</sup>

$F^-$  concentrations in the solutions (before and after treatment with adsorbent) were measured using UV-Visible spectrophotometer (V-570, Jasco, Japan) at 550 nm with a zirconium-xylene orange complex reagent.<sup>225</sup> Xylene orange dye (sodium salt of 3,3'-bis[N,N-di(carboxymethyl)-aminomethyl]-o-cresolsulphonphthalein) forms an orange colored complex with  $Zr^{4+}$ . Zr-xylene orange was prepared by mixing the dye with depolymerized zirconium solution in HCl. This complex decolorizes when it reacts with  $F^-$  ions. During the reaction, fluoride ions dissociate the zirconyl-xylene orange complex and forms colorless zirconium fluoride. This reaction was used for the spectrophotometric determination of  $F^-$ .<sup>226, 227</sup> At the time of analysis, 1 mL of reagent solution was added to 4 mL of  $F^-$  solution (1: 4 volume ratio).<sup>225</sup> Absorbance of different  $F^-$  solutions with known  $F^-$  concentration (ranging from 0-  $1 mg L^{-1}$ ) was measured at  $\lambda_{max} = 550 nm$ . Calibration curve was constructed by plotting absorbance vs.  $F^-$  concentration.  $R^2$  value of the calibration curve was 0.99.

### 1.11. Outlay of thesis

The thesis is divided into six chapters and each chapter is followed by a summary.

Chapter 1 describes the various types of methodologies employed for defluoridation of water. In depth discussions about different proposed mechanisms for  $F^-$  adsorption, factors which influence the adsorption process, different types of adsorbents (particularly  $Al_2O_3$  based adsorbents) and recently developed nanoparticle based adsorbents and performance of various adsorbents have been described here. Different synthesis routes employed for preparation of mesoporous alumina have been discussed. Identification of research gaps based on literature review and the objective of the present research work have also been discussed.

Chapter 2 describes the simple aqueous solution based chemical methodology for preparation of mesoporous alumina and investigations on their fluoride removal performance from water.

Chapter 3 describes the preparation of  $ZrO_2$  nanoparticle loaded mesoporous  $Al_2O_3$  based adsorbents and investigations on their fluoride removal performance from water.

Chapter 4 describes the preparation of  $MgO$  nanoparticle loaded mesoporous  $Al_2O_3$  based adsorbents and investigations on their fluoride removal performance from water.

Chapter 5 describes the preparation of  $CaO$  nanoparticle loaded mesoporous  $Al_2O_3$  based adsorbents and investigations on their fluoride removal performance from water.

In Chapter 6, the conclusions and future scope of research work have been presented along with a comparative summary of results for the synthesized adsorbents.

## CHAPTER 2

# Preparation of mesoporous $Al_2O_3$ and their fluoride removal performance from water

### 2.1. Experimental procedure for materials synthesis

#### 2.1.1. Materials used

Aluminium nitrate nonahydrate was procured from Fisher Scientific, India; triethanol amine (TEA) and sodium fluoride were procured from Merck, India; stearic acid, sodium hydroxide and hydrochloric acid from S.d fine-chem limited, India. All chemicals were used as received. Activated alumina (grade: AD101-F) was procured from ACE Manufacturing and Marketing, Baroda, India. Reverse Osmosis (RO) water was used for conducting all experiments.

#### 2.1.2. Synthesis of mesoporous $Al_2O_3$ <sup>228</sup>

This synthesis methodology involves five steps.

Step 1: *Preparation of an aqueous mixture of TEA and stearic acid having molar ratio 1:0.1*: 16 mL of TEA was mixed with 30 mL of  $H_2O$ . In this mixture desired amount of stearic acid was mixed with continuous stirring till a clear solution was obtained.

Step 2: In the mixture of TEA and stearic acid an aqueous solution containing 14.716 g  $Al(NO_3)_3 \cdot 9H_2O$  and 20 mL  $H_2O$  was mixed. This mixture was warmed at 80 °C. In this mixture molar ratio of  $Al(NO_3)_3 \cdot 9H_2O$ : stearic acid: TEA was 1:0.3:3. During stirring of this reaction mixture a white precipitate was formed.

Step 3: This reaction mixture was transferred in a Teflon bottle, closed it tightly and allowed to age for 24 h at 90 °C.

Step 4: The white gel thus obtained was filtered and washed thoroughly with RO water and dried at  $90^\circ\text{C}$ .

Step 5: To obtain mesoporous  $\text{Al}_2\text{O}_3$ , this precursor was calcined at  $550^\circ\text{C}$  for 4 h.

## 2.2. Results and discussions

### 2.2.1. Characterization of adsorbents

#### 2.2.1.1. X-ray diffraction analysis<sup>228</sup>

Wide angle powder XRD patterns of synthesized  $\text{Al}_2\text{O}_3$  and commercial  $\text{Al}_2\text{O}_3$  are shown in Fig. 2.1. For synthesized  $\text{Al}_2\text{O}_3$  as well as commercial  $\text{Al}_2\text{O}_3$ , diffraction peaks corresponding to (111), (311), (400), (511) and (440) planes of  $\gamma$ - $\text{Al}_2\text{O}_3$  (ICDD Card 10-0425) were observed. This confirms that synthesized  $\text{Al}_2\text{O}_3$  and commercial  $\text{Al}_2\text{O}_3$  are  $\gamma$ - $\text{Al}_2\text{O}_3$  in nature. However, crystallite size determination of these materials using scherrer's equation (for (440) plane) showed that, the crystallite size of commercial  $\text{Al}_2\text{O}_3$  (6.4 nm) is larger than that of synthesized  $\text{Al}_2\text{O}_3$  (5.3 nm), which indicated relatively poor crystalline nature of synthesized  $\gamma$ - $\text{Al}_2\text{O}_3$ .

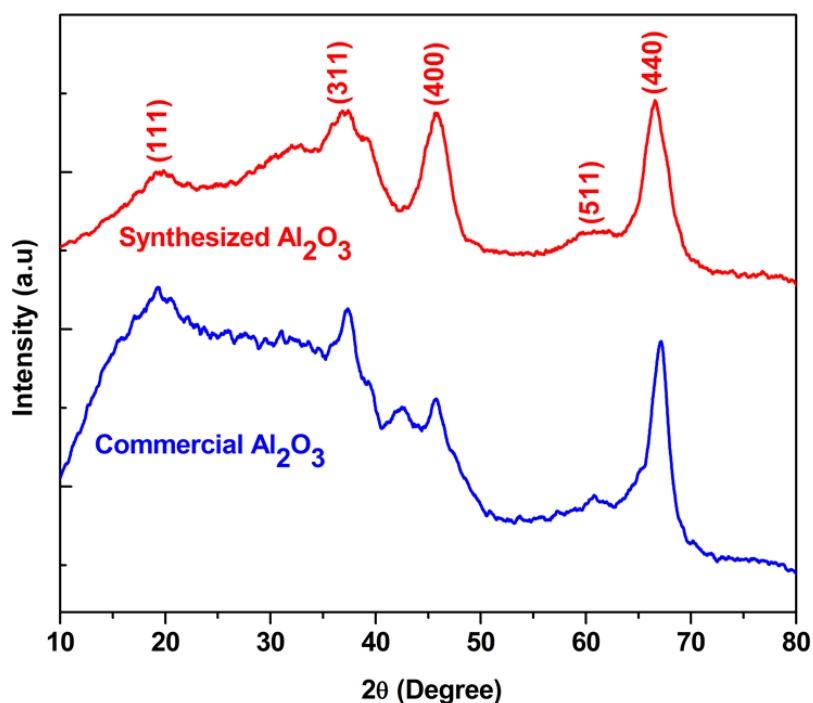


Fig. 2.1. Room temperature powder XRD pattern of synthesized  $\text{Al}_2\text{O}_3$  and commercial  $\text{Al}_2\text{O}_3$ .

### 2.2.1.2. N<sub>2</sub> adsorption-desorption analysis<sup>228</sup>

Nitrogen adsorption-desorption analysis of synthesized Al<sub>2</sub>O<sub>3</sub> showed Type IV physisorption isotherm with H2 hysteresis loop characteristic, which indicates the mesoporous nature of synthesized Al<sub>2</sub>O<sub>3</sub> (Fig. 2.2). Presence of H2 type hysteresis loop for the isotherm suggested the presence of pores with narrow necks and wide bodies (often referred to as ink bottle pores) in the sample.<sup>229</sup> However, in case of commercial Al<sub>2</sub>O<sub>3</sub>, type-IV isotherm and H4 type hysteresis loop were observed indicating the presence of narrow slit like pores.<sup>229</sup> Synthesized Al<sub>2</sub>O<sub>3</sub> possessed BET surface area of 358.7 m<sup>2</sup> g<sup>-1</sup>, with a narrow pore size distribution having average pore diameter 7.5 nm and pore volume of 0.78 cm<sup>3</sup> g<sup>-1</sup>, whereas BET surface area, average pore diameter and pore volume of commercial Al<sub>2</sub>O<sub>3</sub> were 198 m<sup>2</sup> g<sup>-1</sup>, 4.7 nm and 0.26 cm<sup>3</sup> g<sup>-1</sup> respectively.

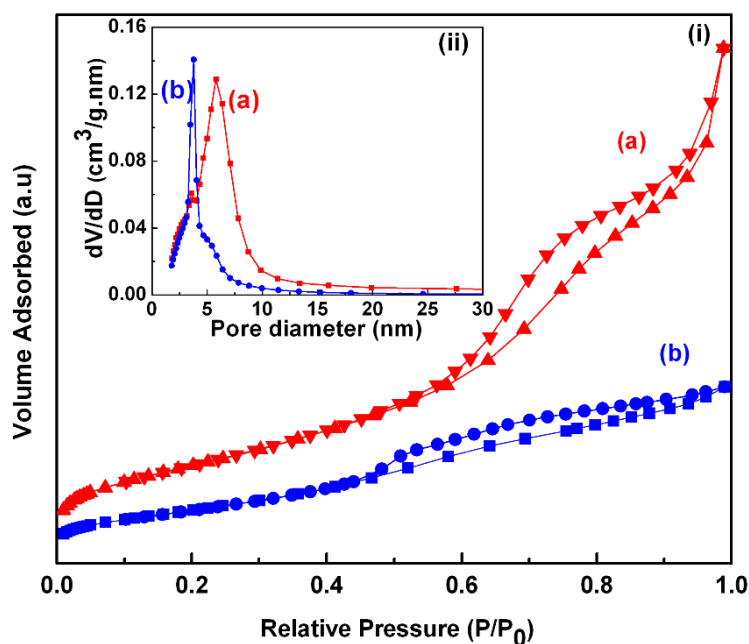


Fig. 2.2. (i) N<sub>2</sub> adsorption- desorption isotherms and (ii) pore size distribution of (a) synthesized Al<sub>2</sub>O<sub>3</sub> and (b) commercial Al<sub>2</sub>O<sub>3</sub>.

### 2.2.1.3. HRTEM analysis<sup>228</sup>

HRTEM image of synthesized Al<sub>2</sub>O<sub>3</sub> (Fig. 2.3) depicted a wormhole-like morphology with highly interconnected porous system but pores are disorder in nature.



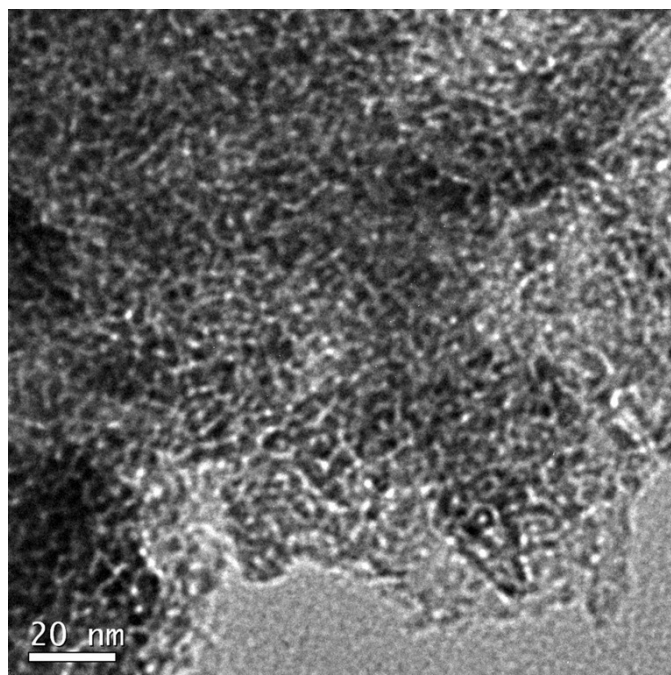


Fig. 2.3. HRTEM image of synthesized  $\text{Al}_2\text{O}_3$ .

#### 2.2.1.4. Analysis of $\text{pH}_{\text{PZC}}$ of the adsorbents

In aqueous solution, PZC of an adsorbent plays an important role in the adsorption process. The  $\text{pH}_{\text{PZC}}$  indicates the pH at which the net surface charge on adsorbent is zero. When pH of the solution is  $< \text{pH}_{\text{PZC}}$  of adsorbent, the net surface charge on solid surface of adsorbent is positive because of the adsorption of excess  $\text{H}^+$ . This situation favours the adsorption of anions on the surface of adsorbent due to coulombic attraction. When pH of the solution is  $> \text{pH}_{\text{PZC}}$  of adsorbent, the net surface charge of the adsorbent becomes negative due to desorption of  $\text{H}^+$ . Now, adsorption of anions on the negatively charged surface of adsorbent competes with coulombic repulsion.<sup>223, 224</sup> The  $\text{pH}_{\text{PZC}}$  values were determined from  $\Delta\text{pH}$  (the difference between initial and final pH) versus  $\text{pH}_{\text{initial}}$  plots, as pH at which  $\Delta\text{pH}$  is zero, that is,  $\text{pH}_{\text{initial}} = \text{pH}_{\text{final}}$ . The  $\text{pH}_{\text{PZC}}$  values for commercial  $\text{Al}_2\text{O}_3$  and synthesized  $\text{Al}_2\text{O}_3$  were found to be 8.1 and 8.2 respectively (Fig. 2.4).

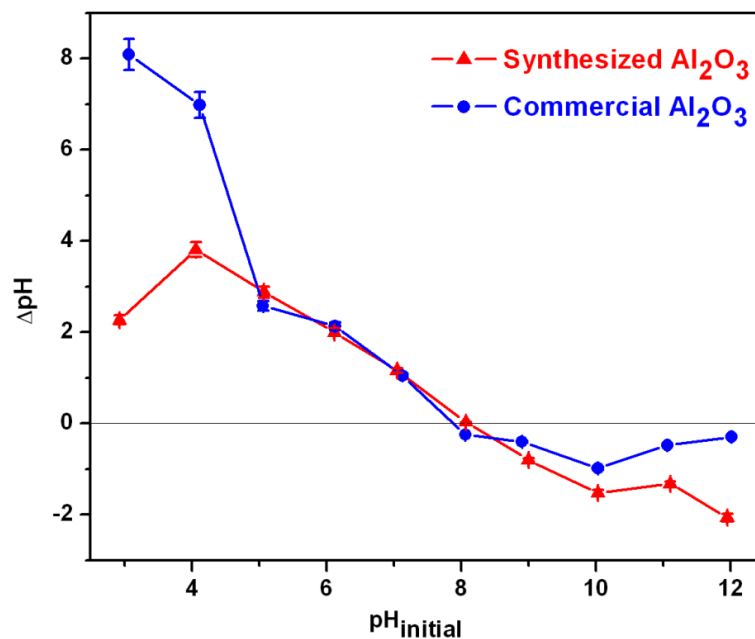


Fig. 2.4. Plot for determination of  $\text{pH}_{\text{PZC}}$  of commercial  $\text{Al}_2\text{O}_3$  and synthesized  $\text{Al}_2\text{O}_3$ .

## 2.2.2. Fluoride adsorption studies<sup>228, 230</sup>

### 2.2.2.1. Determination of unknown $\text{F}^-$ concentration

The unknown  $\text{F}^-$  concentration in the solution (after treatment with adsorbent) was determined using the calibration curve which was constructed by plotting absorbance vs known  $\text{F}^-$  concentration (Fig. 2.5).

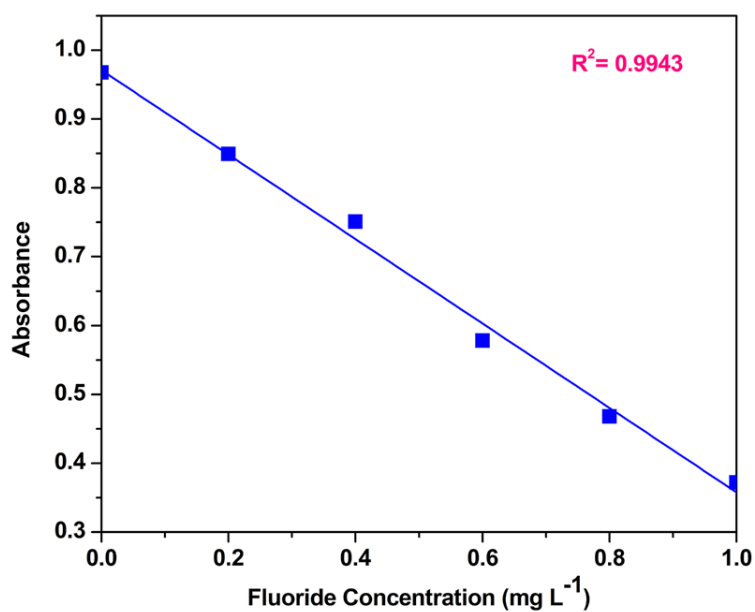


Fig. 2.5. Calibration curve for determining the unknown  $\text{F}^-$  concentrations ( $\lambda_{\text{max}} = 550$  nm).

### 2.2.2.2. Effect of contact time

The sorption of F<sup>-</sup> on synthesized Al<sub>2</sub>O<sub>3</sub> and commercial Al<sub>2</sub>O<sub>3</sub> was investigated as a function of contact time at initial F<sup>-</sup> concentration of 5 mg L<sup>-1</sup>. It was noticed that, F<sup>-</sup> removal increased with time (Fig. 2.6). Both the adsorbents exhibited an initial rapid uptake of F<sup>-</sup> followed by a slower fluoride removal rate that gradually reached an equilibrium concentration. In case of synthesized Al<sub>2</sub>O<sub>3</sub>, ~ 79% F<sup>-</sup> removal was attained within 1 h contact time and equilibrium was reached in 6 h with ~ 92% F<sup>-</sup> removal. In case of commercial Al<sub>2</sub>O<sub>3</sub>, ~ 24% F<sup>-</sup> was removed in 1 h and the equilibrium was reached in 10 h with ~39% F<sup>-</sup> removal. The reason for higher F<sup>-</sup> removal capacity of synthesized Al<sub>2</sub>O<sub>3</sub> is high surface area and porous structure of synthesized mesoporous Al<sub>2</sub>O<sub>3</sub> (358.7 m<sup>2</sup> g<sup>-1</sup>) than the commercial Al<sub>2</sub>O<sub>3</sub> (198 m<sup>2</sup> g<sup>-1</sup>).

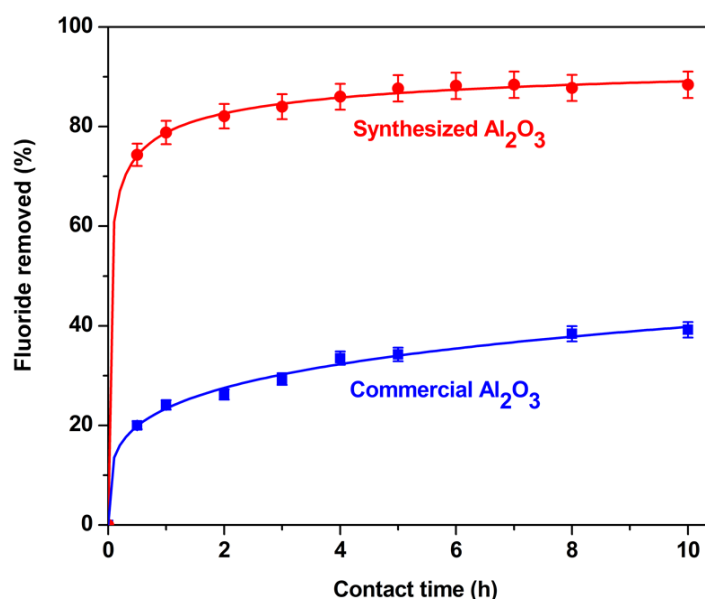


Fig. 2.6. Effect of contact time on F<sup>-</sup> removal of synthesized Al<sub>2</sub>O<sub>3</sub> and commercial Al<sub>2</sub>O<sub>3</sub>. (C<sub>0</sub> = 5 mg L<sup>-1</sup>, adsorbent dose = 5 g L<sup>-1</sup>, pH = 6.8 ± 0.2).

### 2.2.2.3. Effect of adsorbent dose

The influence of adsorbent dose on F<sup>-</sup> removal at a fixed initial F<sup>-</sup> concentration of 10 mg L<sup>-1</sup> is shown in Fig. 2.7. It was noticed that percentage of F<sup>-</sup> removal increased from 11.5 to ~ 70% with an increase in adsorbent dose from 0.1 to 8 g L<sup>-1</sup>. However,

after a dosage of  $3 \text{ g L}^{-1}$ , there was no significant change in the percentage removal of  $F^-$ . Therefore,  $3 \text{ g L}^{-1}$  of  $Al_2O_3$  was used in all the tests.

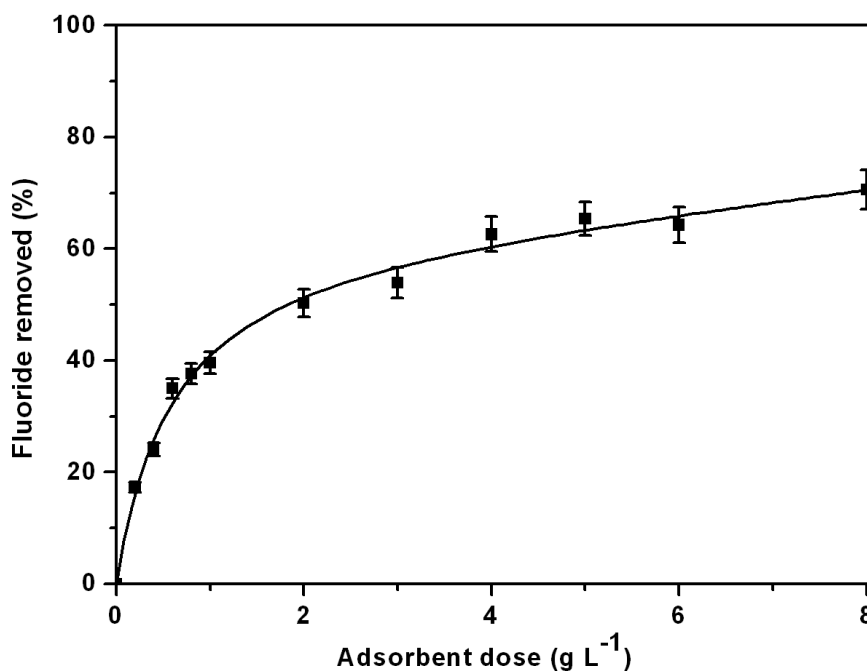


Fig. 2.7. Effect of adsorbent dose on  $F^-$  removal of synthesized  $Al_2O_3$ . ( $C_0 = 10 \text{ mg L}^{-1}$ , contact time = 8 h,  $\text{pH} = 6.8 \pm 0.2$ ).

#### 2.2.2.4. Adsorption kinetics

In this study adsorption kinetics of synthesized  $Al_2O_3$  were investigated using an adsorbent dose of  $3 \text{ g L}^{-1}$  and initial  $F^-$  concentration of 5, 10, 20 and  $30 \text{ mg L}^{-1}$ . Fig. 2.8 shows the change of adsorption capacity ( $q_t$ ) of synthesized  $Al_2O_3$  with change in contact time ( $t$ ) and initial  $F^-$  concentration.

The kinetic data obtained were analyzed using Lagergren's pseudo-first order kinetic model<sup>95</sup> (equation 2) and Ho's pseudo-second order kinetic model<sup>96</sup> (equation 3) (Chapter 1, page no.14). For pseudo-first order kinetic model, the adsorption rate constant ( $k_1$ ) was calculated from the slope of the linear plot of  $\log (q_e - q_t)$  versus  $t$  (Fig. 2.9(i)). In case of pseudo second order kinetic model, kinetic data were plotted  $t/q_t$  versus  $t$ .  $k_2$  was calculated from the intercept and slope of the plot (Fig. 2.9(ii)). Pseudo-second order kinetic model was selected as a best fit model based on the match of the  $q_e$  values between experimental ( $q_{e(\text{exp})}$ ) and theoretical ( $q_{e(\text{cal})}$ ) values and linear correlation coefficient ( $R^2$ ) values (Table 2.1). The values obtained by

pseudo-second order model were found to be mostly in good agreement with experimental data. Pseudo-second order kinetics suggests that chemisorption might be responsible for  $\text{F}^-$  adsorption on synthesized  $\text{Al}_2\text{O}_3$ .<sup>69, 98, 112, 119</sup>

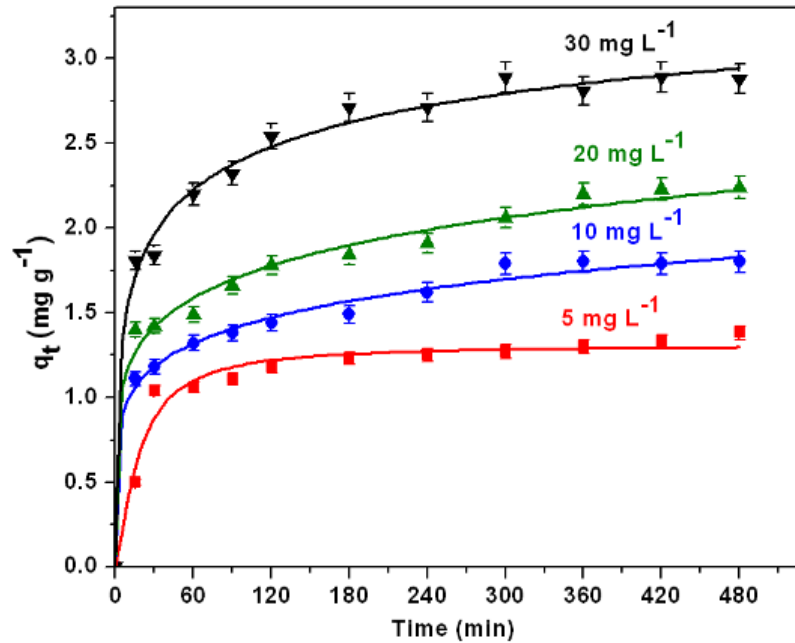


Fig. 2.8. Adsorption kinetic curves of  $\text{F}^-$  at different initial  $\text{F}^-$  concentrations (adsorbent dose =  $3 \text{ g L}^{-1}$ ;  $C_0 = 5, 10, 20, 30 \text{ mg L}^{-1}$ ,  $\text{pH} = 6.8 \pm 0.2$ ).

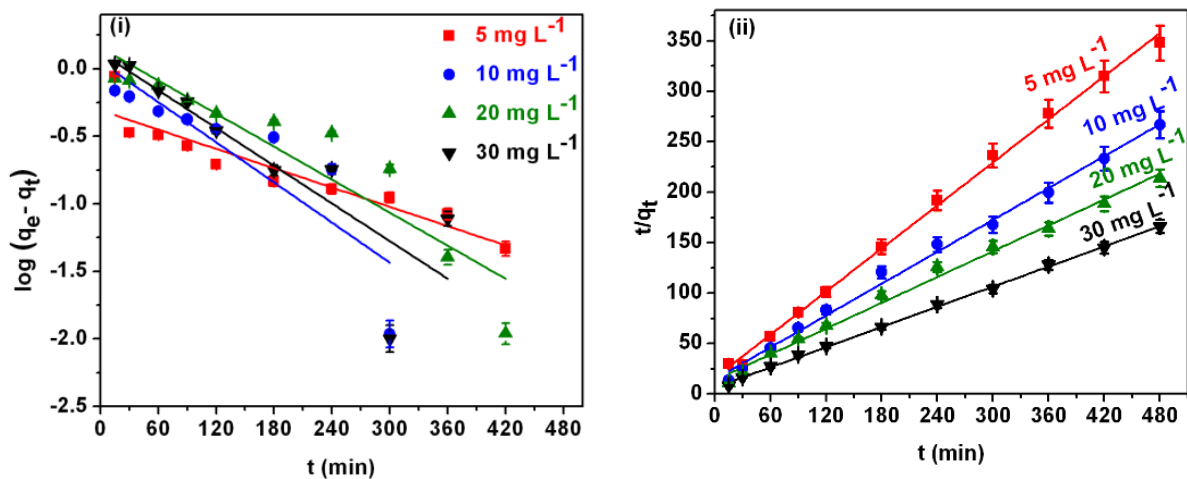


Fig. 2.9. (i) Pseudo-first order kinetic and (ii) Pseudo-second order kinetic fit for  $\text{F}^-$  adsorption on synthesized  $\text{Al}_2\text{O}_3$  at  $C_0 = 5, 10, 20, 30 \text{ mg L}^{-1}$ , adsorbent dose =  $3 \text{ g L}^{-1}$ ,  $\text{pH} = 6.8 \pm 0.2$ .

Table 2.1. Comparison of pseudo-first order and pseudo-second order kinetic models parameters, and calculated  $q_{e(cal)}$  and experimental  $q_{e(exp)}$  values for different initial F<sup>-</sup> concentrations of synthesized Al<sub>2</sub>O<sub>3</sub>.

C <sub>0</sub> (mg L <sup>-1</sup> )	q <sub>e(exp)</sub> (mg g <sup>-1</sup> )	Pseudo first order			Pseudo second order		
		q <sub>e(cal)</sub> (mg g <sup>-1</sup> )	k <sub>1</sub> (min <sup>-1</sup> )	R <sup>2</sup>	q <sub>e(cal)</sub> (mg g <sup>-1</sup> )	k <sub>2</sub> (g mg <sup>-1</sup> min <sup>-1</sup> )	R <sup>2</sup>
5	1.38	0.49	0.0055	0.8740	1.40	0.0315	0.9976
10	1.80	1.12	0.0114	0.7113	1.89	0.0191	0.9943
20	2.24	1.43	0.0094	0.8488	2.35	0.0131	0.9919
30	2.89	1.31	0.0107	0.7336	3.00	0.0169	0.9985

#### 2.2.2.5. Effect of initial fluoride concentration

The effect of initial F<sup>-</sup> concentration on F<sup>-</sup> adsorption capacity by synthesized Al<sub>2</sub>O<sub>3</sub> and commercial Al<sub>2</sub>O<sub>3</sub> was studied by keeping all other parameters constant (adsorbent dose 3 g L<sup>-1</sup>, contact time = 8 h) as shown in Fig. 2.10. It was found that the sorption capacity at equilibrium (q<sub>e</sub>) gradually increased with the increase in initial F<sup>-</sup> concentration (C<sub>0</sub>). The gradual rise indicates the availability of sites for F<sup>-</sup> adsorption during the initial phase. However, adsorption site saturation occurred as F<sup>-</sup> concentration increased and a plateau was reached indicating the saturation of adsorption sites.

#### 2.2.2.6. Adsorption isotherm study

In the present study two well known isotherm models, viz, Freundlich isotherm<sup>99</sup> and Langmuir isotherm<sup>100</sup> (Chapter 1, page no.15) were used. The values of K<sub>f</sub> and 1/n were obtained from the slope and intercept of the linear Freundlich plot of log q<sub>e</sub> vs log C<sub>e</sub> shown in Fig. 2.11 (i). The values of Langmuir parameters Q<sub>0</sub> and b were calculated from the slope and intercept of the linear Langmuir plot of C<sub>e</sub>/q<sub>e</sub> vs C<sub>e</sub> (Fig. 2.11 (ii)). Parameters obtained from Freundlich and Langmuir isotherms are listed in Table 2.2. These results indicated that, both Freundlich and Langmuir isotherm models fitted the experimental data reasonably well. However, the present data fitted slightly better to the Freundlich equation according to the correlation coefficient (R<sup>2</sup>)

indicating multilayer adsorption of  $\text{F}^-$  on the surface of  $\text{Al}_2\text{O}_3$ .<sup>88, 91, 97, 120</sup> Since the mesoporous  $\text{Al}_2\text{O}_3$  have different active binding sites (sites on the adsorbent surface and the sites inside the pores),  $\text{F}^-$  adsorption occurs through multilayer adsorption and on the heterogeneous surface.  $\text{F}^-$  sorption capacities of synthesized  $\text{Al}_2\text{O}_3$  and commercial  $\text{Al}_2\text{O}_3$  were found to be 5.13 and 2.18  $\text{mg g}^{-1}$  respectively.  $\text{F}^-$  adsorption capacity of the synthesized  $\text{Al}_2\text{O}_3$  is higher than that of some of the reported aluminas and commercial  $\text{Al}_2\text{O}_3$ .<sup>69, 90, 102</sup>

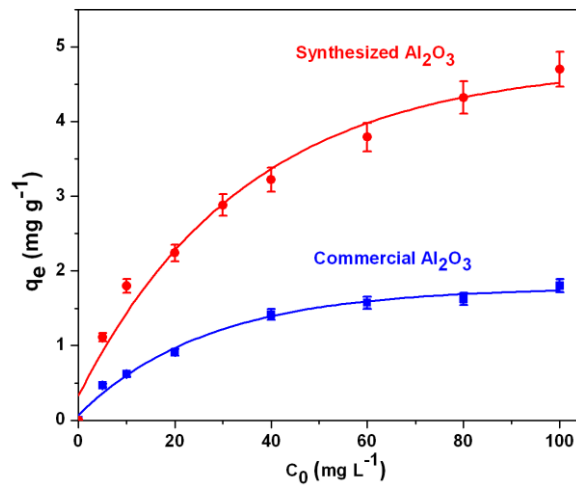


Fig. 2.10. Effect of initial  $\text{F}^-$  concentration on  $\text{F}^-$  adsorption capacity of synthesized  $\text{Al}_2\text{O}_3$  and commercial  $\text{Al}_2\text{O}_3$  (initial  $\text{F}^-$  concentration = 5 to 100  $\text{mg L}^{-1}$ , adsorbent dose = 3  $\text{g L}^{-1}$ , contact time = 10 h,  $\text{pH} = 6.8 \pm 0.2$ ).

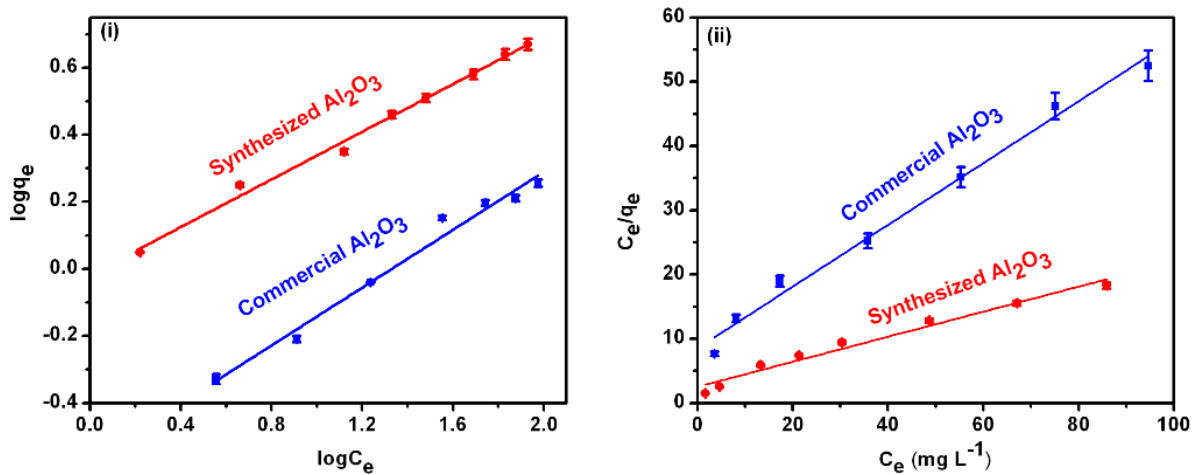


Fig. 2.11. (i) Freundlich adsorption isotherm and (ii) Langmuir adsorption isotherm fits for adsorption of  $\text{F}^-$  on synthesized  $\text{Al}_2\text{O}_3$  and commercial  $\text{Al}_2\text{O}_3$ . (adsorbent dose = 3  $\text{g L}^{-1}$ ,  $C_0 = 5$  to 100  $\text{mg L}^{-1}$ ,  $\text{pH} = 6.8 \pm 0.2$ ).

Table 2.2. Freundlich and Langmuir isotherm constants for F<sup>-</sup> adsorption on synthesized Al<sub>2</sub>O<sub>3</sub> and commercial Al<sub>2</sub>O<sub>3</sub> at pH of 6.8 ± 0.2.

	Langmuir isotherm			Freundlich isotherm		
	Q <sub>0</sub> (mg g <sup>-1</sup> )	b (l mg <sup>-1</sup> )	R <sup>2</sup>	K <sub>f</sub>	1/n	R <sup>2</sup>
Synthesized Al <sub>2</sub> O <sub>3</sub>	5.13	0.08	0.9707	0.96	0.36	0.9918
Commercial Al <sub>2</sub> O <sub>3</sub>	2.08	0.06	0.9798	0.27	0.43	0.9881

To examine whether F<sup>-</sup> sorption on Al<sub>2</sub>O<sub>3</sub> is favorable or not, the value of ‘r’ (separation factor or equilibrium parameter) was calculated using the following equation.<sup>90, 91, 119, 231</sup>

$$r = 1/(1+bC_0) \quad (14)$$

where C<sub>0</sub> and b are the initial F<sup>-</sup> concentration and Langmuir isotherm constant respectively. It is well reported that the ‘r’ value indicates that the type of isotherm be irreversible (r = 0), favorable (0 < r < 1), linear (r = 1) or unfavorable (r > 1). In the present case, ‘r’ values were < 1 (varies from 0.769 to 0.11 with the variation of C<sub>0</sub> from 5 to 100 mg L<sup>-1</sup>), indicating the favorable adsorption of F<sup>-</sup> on synthesized Al<sub>2</sub>O<sub>3</sub> and commercial Al<sub>2</sub>O<sub>3</sub>.

#### 2.2.2.7. Effect of initial pH

The effect of pH on F<sup>-</sup> removal by synthesized Al<sub>2</sub>O<sub>3</sub> was investigated over a pH range from 4 to 10, with a fixed adsorbent dose of 3 g L<sup>-1</sup>, C<sub>0</sub> of 30 mg L<sup>-1</sup> and contact time 8 h. Fig. 2.12 shows the effect of pH on F<sup>-</sup> adsorption. It was observed that, adsorption capacity of synthesized Al<sub>2</sub>O<sub>3</sub> decreased with increasing pH. The adsorption of F<sup>-</sup> on synthesized Al<sub>2</sub>O<sub>3</sub> does not change much within the pH range of 4 to 9. However, when initial pH was 10, the F<sup>-</sup> adsorption capacity of synthesized Al<sub>2</sub>O<sub>3</sub> was decreased, which might be either due to electrostatic repulsion from the negatively charge surface of Al<sub>2</sub>O<sub>3</sub> or to a competition between excess OH<sup>-</sup> and F<sup>-</sup> (pH<sub>pzc</sub> value of mesoporous Al<sub>2</sub>O<sub>3</sub> is 8.2 which is < 10).<sup>91</sup>



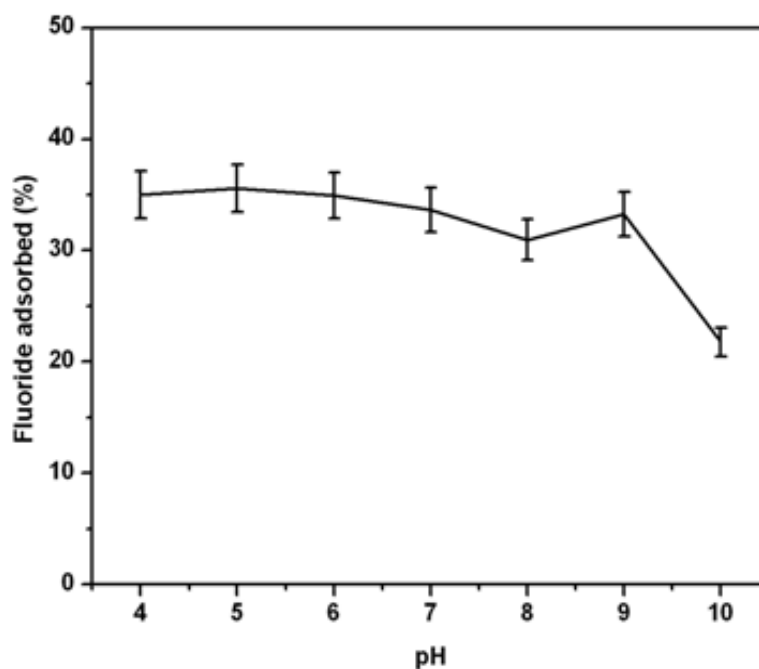


Fig. 2.12. Effect of initial pH on  $F^-$  adsorption capacity of synthesized  $Al_2O_3$  (adsorbent dose =  $3\text{ g L}^{-1}$ ,  $C_0 = 30\text{ mg L}^{-1}$ , contact time = 8 h).

#### 2.2.2.8. Effect of co-existing anions

Besides fluoride ions the natural ground water always contains various other ions, which may compete with fluoride during adsorption and affect the efficiency of the adsorbent. To study the effect of co-existing anions on  $F^-$  adsorption on synthesized adsorbents,  $10\text{ mg L}^{-1}$  and  $100\text{ mg L}^{-1}$  initial concentrations of  $Cl^-$ ,  $NO_3^-$ ,  $SO_4^{2-}$  and  $HCO_3^-$  were used while keeping the initial  $F^-$  concentration as  $10\text{ mg L}^{-1}$ . The effect of co-ions on the  $F^-$  removal efficiency of  $Al_2O_3$  is shown in Fig. 2.13. It was observed that the presence of  $Cl^-$  did not affect the  $F^-$  removal capacity of the adsorbents. Presence of  $NO_3^-$  ( $10$  and  $100\text{ mg L}^{-1}$ ) and  $SO_4^{2-}$  ( $10\text{ mg L}^{-1}$ ) ions slightly decreased ( $\sim 2\text{-}3\%$ )  $F^-$  removal capacity of the adsorbent, whereas  $\sim 8\text{-}9\%$  decrease was observed when  $HCO_3^-$  was present. This is due to the competition between  $HCO_3^-$  and  $F^-$  for the adsorption on active sites of the adsorbent.

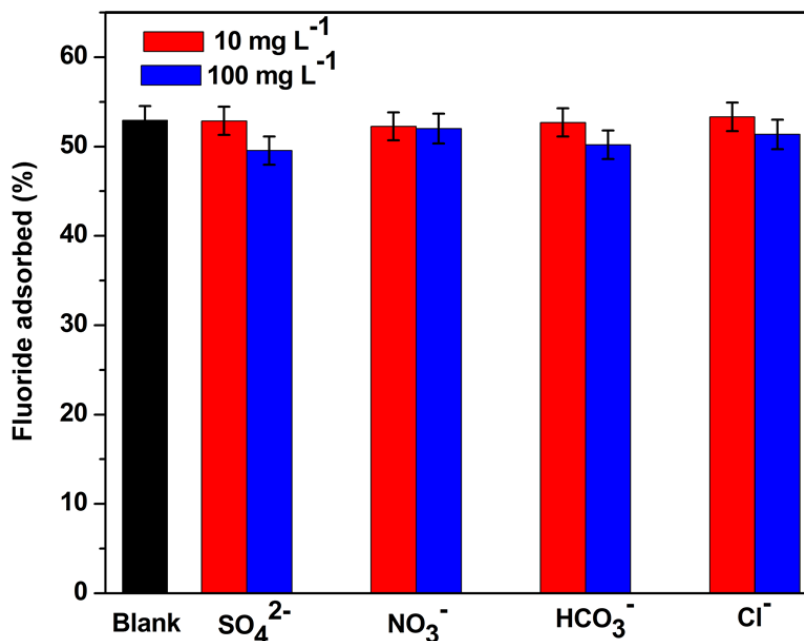


Fig. 2.13. Effect of co-existing anions on  $\text{F}^-$  adsorption capacity of  $\text{Al}_2\text{O}_3$  (adsorbent dose =  $3 \text{ g L}^{-1}$ ,  $C_0 = 10 \text{ mg L}^{-1}$ , contact time = 8 h).

### 2.3. Summary of results

- i. Mesoporous  $\gamma\text{-Al}_2\text{O}_3$  was prepared by using an aqueous solution based chemical method. In this method, stearic acid in combination with TEA was used as pore structure directing agent.
- ii. This synthetic method offers the following advantages
  - a. Simplicity of the method, only mixing of aqueous solutions of the reagents was required.
  - b. Aluminum nitrate was used as starting material instead of costly and reactive aluminum alkoxides.
  - c. Water was used as solvent instead of commonly used solvent, alcohol.
- iii. Use of cheap aluminum nitrate instead of aluminum alkoxides (which are generally used in sol-gel, hydrothermal technique) and water as solvent helps to make this process cost-effective and simple.
- iv.  $\sim 92\%$   $\text{F}^-$  was removed by the synthesized  $\text{Al}_2\text{O}_3$  from a  $\text{F}^-$  solution (having initial  $\text{F}^-$  concentration  $5 \text{ mg L}^{-1}$ ) whereas, commercial  $\text{Al}_2\text{O}_3$  removed only  $\sim 39\%$   $\text{F}^-$ . Synthesized  $\text{Al}_2\text{O}_3$  exhibited better  $\text{F}^-$  removal efficiency than commercial  $\text{Al}_2\text{O}_3$ .

## CHAPTER 3

# Preparation of ZrO<sub>2</sub> nanoparticle loaded mesoporous Al<sub>2</sub>O<sub>3</sub> based adsorbents and their fluoride removal performance from water

### 3.1. Experimental procedure for materials synthesis

#### 3.1.1. Materials used

Aluminium nitrate nonahydrate, nitric acid, sodium hydroxide, Liquor Ammonia and sodium sulphate were procured from Fisher Scientific, India; triethanol amine (TEA), sodium hydrogen carbonate, sodium chloride, sodium nitrate, ZrOCl<sub>2</sub>.8H<sub>2</sub>O and sodium fluoride were procured from Merck, India; stearic acid, and hydrochloric acid from S.d fine-chem. limited, India. All these chemicals were used as received.

#### 3.1.2. Synthesis of mesoporous Al<sub>2</sub>O<sub>3</sub>

Mesoporous Al<sub>2</sub>O<sub>3</sub> was synthesized as per the procedure described in Chapter 2, section 2.1.2.

#### 3.1.3. Preparation of ZrO<sub>2</sub> nanoparticle loaded mesoporous Al<sub>2</sub>O<sub>3</sub><sup>232</sup>

ZrO<sub>2</sub> nanoparticle loaded mesoporous aluminas were synthesized using a wet impregnation technique with different loading percentages (5, 10, 15 and 20 wt.%) of ZrO<sub>2</sub> on mesoporous Al<sub>2</sub>O<sub>3</sub>. For synthesis of ZrO<sub>2</sub> loaded mesoporous Al<sub>2</sub>O<sub>3</sub>, ZrOCl<sub>2</sub>.8H<sub>2</sub>O was used as a zirconium source. In a typical synthesis, calculated amount of ZrOCl<sub>2</sub>.8H<sub>2</sub>O were dissolved in water, followed by dropwise addition of aqueous ammonia under continuous stirring by magnetic stirrer until the pH becomes ~10. The precipitate thus obtained was filtered and washed with water until free from chloride ions. Aqueous nitric acid was added to white precipitate until the precipitate was completely dissolved. To this solution, desired amount of synthesized mesoporous Al<sub>2</sub>O<sub>3</sub> was added and then stirred for 12 h. The mixture was then dried on

a hot plate at 90 °C and then calcined at 550 °C for 4h in air atmosphere to obtain ZrO<sub>2</sub> loaded mesoporous Al<sub>2</sub>O<sub>3</sub>. 5, 10, 15 and 20 wt.% ZrO<sub>2</sub> loaded mesoporous Al<sub>2</sub>O<sub>3</sub> are now onwards will be referred as 5ZrO<sub>2</sub>@Al<sub>2</sub>O<sub>3</sub>, 10ZrO<sub>2</sub>@Al<sub>2</sub>O<sub>3</sub>, 15ZrO<sub>2</sub>@Al<sub>2</sub>O<sub>3</sub> and 20ZrO<sub>2</sub>@Al<sub>2</sub>O<sub>3</sub> respectively.

## 3.2. Results and discussion

### 3.2.1. Characterization of adsorbents

#### 3.2.1.1. X-ray diffraction analysis<sup>232</sup>

Wide angle powder XRD patterns of calcined ZrO<sub>2</sub> nanoparticle loaded mesoporous Al<sub>2</sub>O<sub>3</sub> samples was carried out to identify their crystalline phase and shown in Fig. 3.1. Though the XRD patterns of the materials showed poor crystalline structure with broad diffraction peaks, characteristic peaks of  $\gamma$ -Al<sub>2</sub>O<sub>3</sub> were identified (ICDD card no. 10-0425). However, the samples containing ZrO<sub>2</sub> loading up to 10 wt.% did not show any characteristic peaks of ZrO<sub>2</sub>. For the samples having ZrO<sub>2</sub> content 15 and 20 wt.%, small diffraction peaks at  $2\theta = 30.2^\circ$ ,  $50.3^\circ$  and  $60.2^\circ$  corresponding to (111), (112) and (121) planes of tetragonal ZrO<sub>2</sub> (ICDD card no: 50-1089) were observed along with the peaks of  $\gamma$ -Al<sub>2</sub>O<sub>3</sub>.

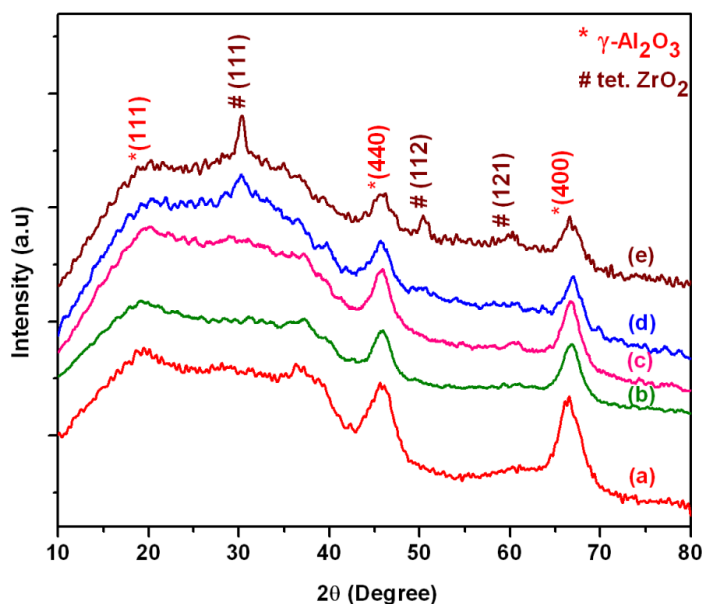


Fig. 3.1. XRD pattern of (a) Al<sub>2</sub>O<sub>3</sub>, (b) 5ZrO<sub>2</sub>@Al<sub>2</sub>O<sub>3</sub>, (c) 10 ZrO<sub>2</sub>@Al<sub>2</sub>O<sub>3</sub>, (d) 15ZrO<sub>2</sub>@Al<sub>2</sub>O<sub>3</sub>, (e) 20ZrO<sub>2</sub>@Al<sub>2</sub>O<sub>3</sub>.

### 3.2.1.2. N<sub>2</sub> adsorption-desorption analysis<sup>232</sup>

Nitrogen adsorption-desorption isotherms (Fig. 3.2) indicated that all isotherms of synthesized samples are typically type IV with H2 hysteresis loops, which means synthesized adsorbents possess mesoporous structure. H2 hysteresis loops for these isotherms suggested the presence of pores with narrow necks with wide bodies (often referred to as ink bottle pores).<sup>229</sup> Large hysteresis loop for pure mesoporous Al<sub>2</sub>O<sub>3</sub> can be attributed to its large pores.<sup>199</sup> Pore size distribution of all the synthesized samples also confirmed the mesoporosity of the materials (Fig. 3.2 (ii)). Surface area and pore size parameters of the synthesized adsorbents are summarized in Table 3.1. It was observed that BET surface area, average pore size and pore volume of ZrO<sub>2</sub> loaded aluminas decreased with increasing ZrO<sub>2</sub> loading on mesoporous Al<sub>2</sub>O<sub>3</sub>. Decrease of pore volume also indicated that ZrO<sub>2</sub> particles are incorporated into the pores of Al<sub>2</sub>O<sub>3</sub>.

Table 3.1. Surface area and pore size parameters obtained by means of N<sub>2</sub> adsorption-desorption study.

Sample	BET Surface area (m <sup>2</sup> /g)	BJH average pore size (nm)	BJH pore volume (cm <sup>3</sup> /g)
Al <sub>2</sub> O <sub>3</sub>	284	7.4	0.7
5ZrO <sub>2</sub> @Al <sub>2</sub> O <sub>3</sub>	189	5.1	0.28
10ZrO <sub>2</sub> @Al <sub>2</sub> O <sub>3</sub>	181	4.9	0.25
15ZrO <sub>2</sub> @Al <sub>2</sub> O <sub>3</sub>	170	4.4	0.23
20ZrO <sub>2</sub> @Al <sub>2</sub> O <sub>3</sub>	135	4.3	0.17

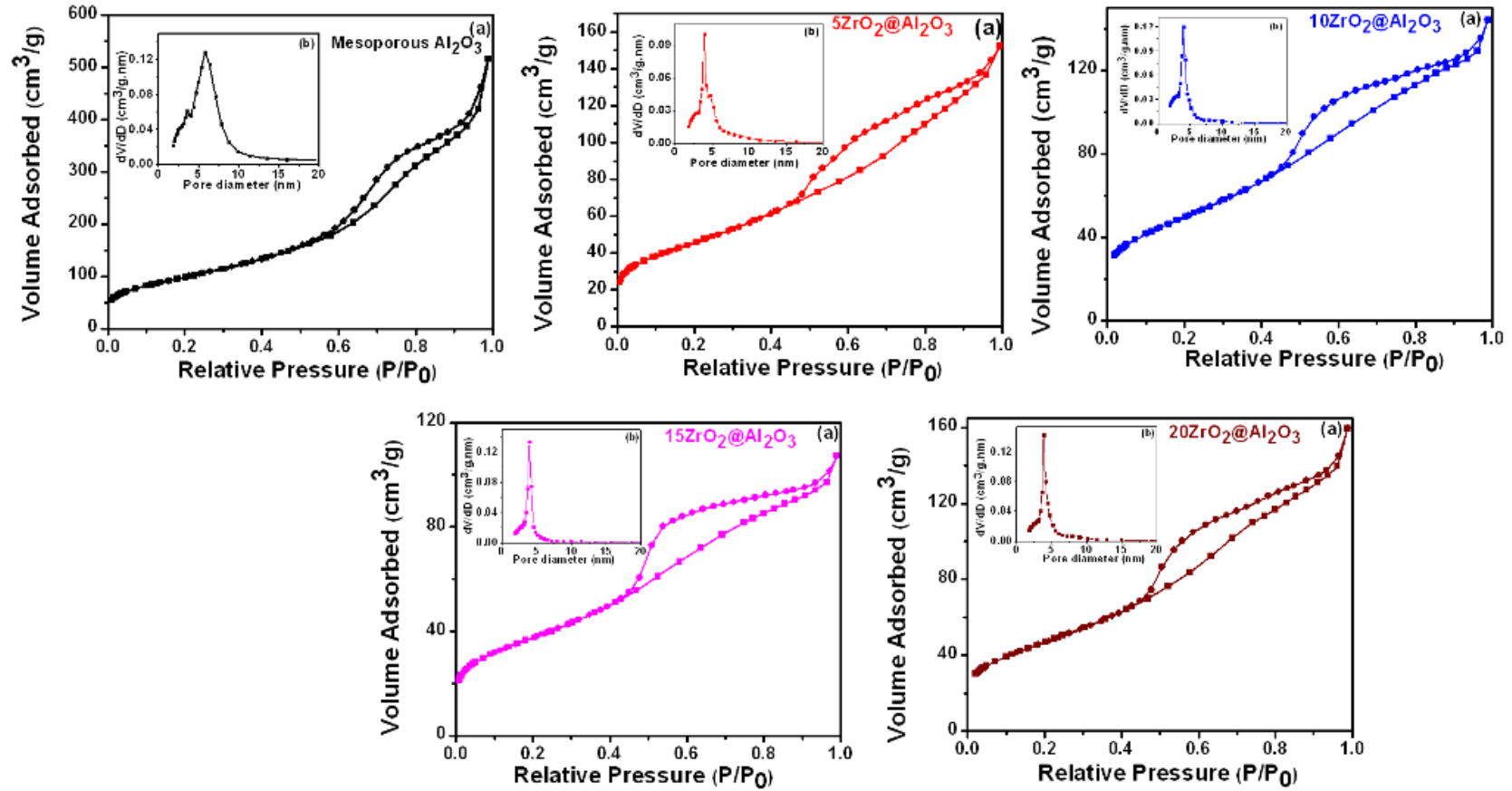


Fig. 3.2. (a)  $N_2$ -adsorption-desorption isotherms and (b) Pore size distributions (Inset) of pure  $Al_2O_3$  and  $ZrO_2$  loaded aluminas.

### 3.2.1.3. HRTEM analysis<sup>232</sup>

HRTEM of pure mesoporous Al<sub>2</sub>O<sub>3</sub> and 15ZrO<sub>2</sub>@Al<sub>2</sub>O<sub>3</sub> particles are shown in Fig. 3.3. The micrographs revealed the wormhole-like, highly connected porous structure of the Al<sub>2</sub>O<sub>3</sub> matrix. However, the pores are disordered in nature. Presence of ZrO<sub>2</sub> nanoparticles (< 8 nm) on mesoporous Al<sub>2</sub>O<sub>3</sub> matrix were observed for ZrO<sub>2</sub> loaded Al<sub>2</sub>O<sub>3</sub> samples (Fig. 3.3 (b, c)).

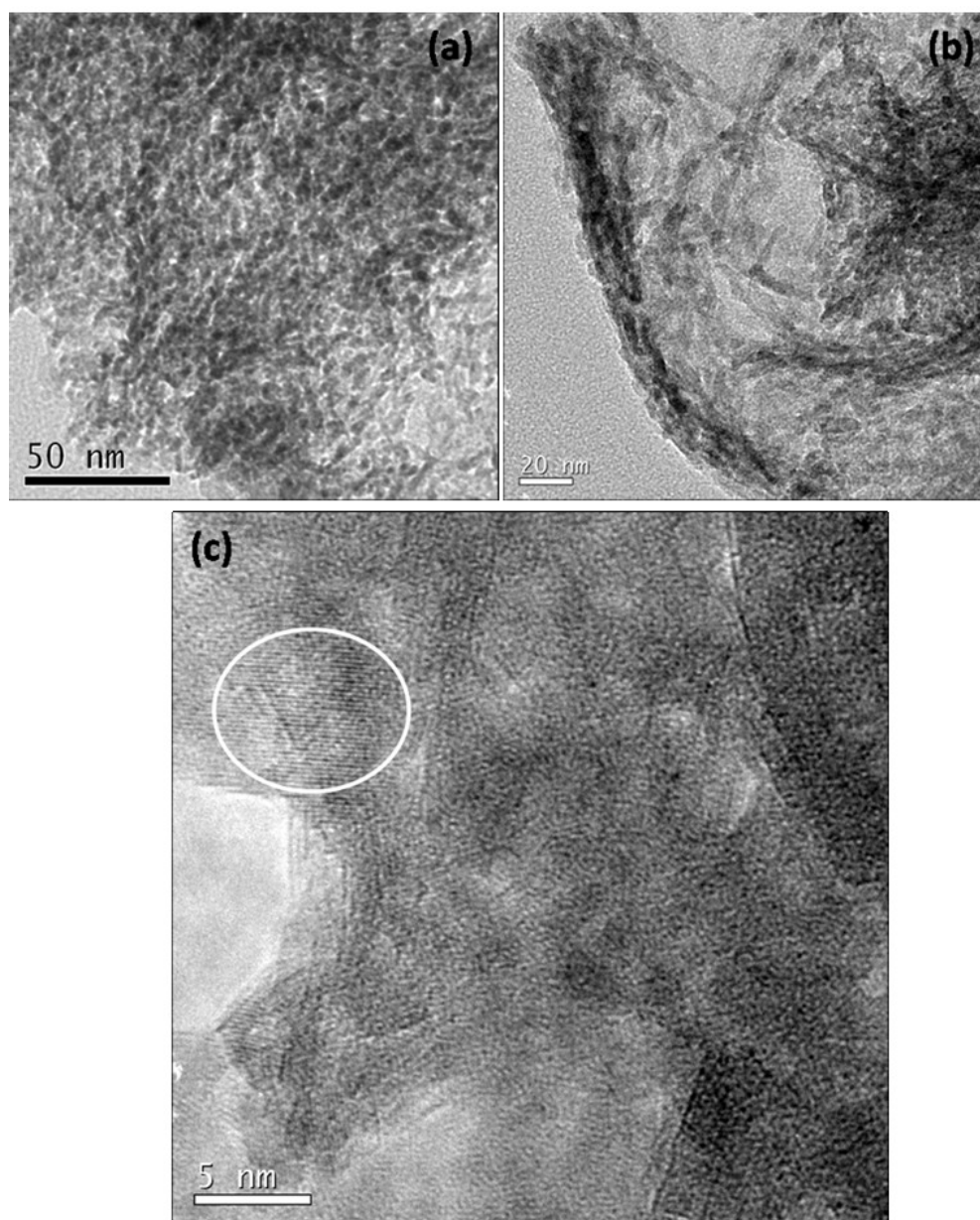


Fig. 3.3. HRTEM images of (a) Al<sub>2</sub>O<sub>3</sub>, (b) 15ZrO<sub>2</sub>@Al<sub>2</sub>O<sub>3</sub> and (c) shows 15ZrO<sub>2</sub>@Al<sub>2</sub>O<sub>3</sub> with higher magnification, showing the fringes of ZrO<sub>2</sub> nanoparticle.

### 3.2.1.4. Analysis of pHPZC of the adsorbents<sup>232</sup>

The pHPZC values for pure Al<sub>2</sub>O<sub>3</sub> and 15ZrO<sub>2</sub>@Al<sub>2</sub>O<sub>3</sub> were found to be 8.2 and 7.0 respectively (Fig. 3.4). Below the pHPZC value, the surface of the adsorbent is positive which favours the adsorption of F<sup>-</sup> on the surface of adsorbent due to columbic attraction.

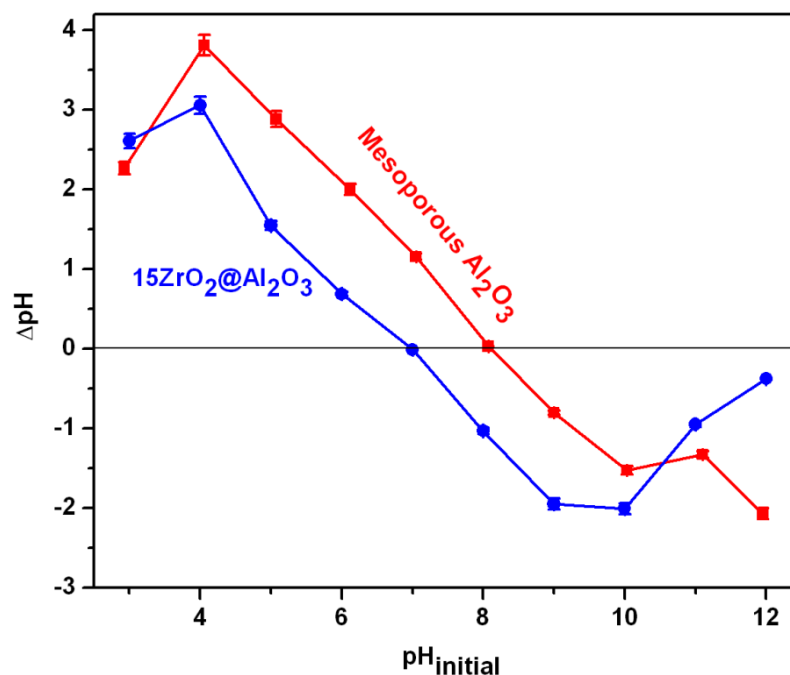


Fig. 3.4. Plot for determination of pHPZC of Al<sub>2</sub>O<sub>3</sub> and 15ZrO<sub>2</sub>@Al<sub>2</sub>O<sub>3</sub>.

### 3.2.2. Fluoride adsorption studies<sup>232</sup>

#### 3.2.2.1. Optimization of adsorbent composition

F<sup>-</sup> adsorption studies of various amount of ZrO<sub>2</sub> nanoparticle loaded aluminas were performed using a solution having initial fluoride concentration 30 mg L<sup>-1</sup> and adsorbent dose of 3 g L<sup>-1</sup>. It was clearly observed that, presence of ZrO<sub>2</sub> enhanced the F<sup>-</sup> adsorption capacity of the adsorbents. For instance, pure Al<sub>2</sub>O<sub>3</sub> adsorbed 28% F<sup>-</sup> whereas adsorbent having 15 wt.% ZrO<sub>2</sub> adsorbed ~48% F<sup>-</sup>. Several factors such as exchange of -OH groups (which are present on the surface of ZrO<sub>2</sub>) with F<sup>-</sup>, electrostatic interaction between Zr<sup>4+</sup> and F<sup>-</sup>, formation of zirconium oxyfluoro complexes etc. played important role on the enhancement of F<sup>-</sup> adsorption capacity of ZrO<sub>2</sub> loaded Al<sub>2</sub>O<sub>3</sub> adsorbents.<sup>169</sup> However, when ZrO<sub>2</sub> loading exceeded 15 wt.%,



much enhancement in F<sup>-</sup> adsorption capacity of adsorbents was not observed. So, further studies were conducted using 15ZrO<sub>2</sub>@Al<sub>2</sub>O<sub>3</sub>.

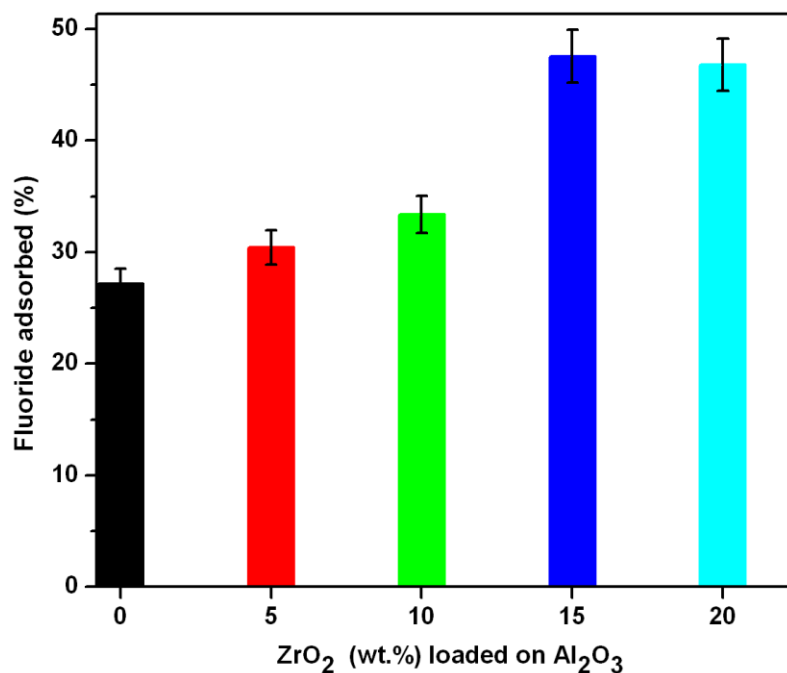


Fig. 3.5. Effect of ZrO<sub>2</sub> loading on mesoporous Al<sub>2</sub>O<sub>3</sub> for removal of F<sup>-</sup>. (C<sub>0</sub> = 30 mg L<sup>-1</sup>, adsorbent dose = 3 g L<sup>-1</sup>, contact time = 8 h, pH = 6.8 ± 0.2).

### 3.2.2.2. Effect of adsorbent dose

The effect of adsorption dose on removal of F<sup>-</sup> using pure Al<sub>2</sub>O<sub>3</sub> and 15ZrO<sub>2</sub>@Al<sub>2</sub>O<sub>3</sub> is shown in Fig. 3.6, in which percent of F<sup>-</sup> removal is plotted against adsorbent dose. It was observed that, initially percent of F<sup>-</sup> removal increased rapidly with the increase of adsorbent dose and maximum F<sup>-</sup> removal occurred when adsorbent was 3 g L<sup>-1</sup>. The percent of fluoride removal increased from 19% to 91% with increase of 15ZrO<sub>2</sub>@Al<sub>2</sub>O<sub>3</sub> dose from 0.25 to 8 g L<sup>-1</sup> at C<sub>0</sub> 10 mg L<sup>-1</sup>. However, when the adsorbent dose was more than 3 g L<sup>-1</sup>, not much increase in F<sup>-</sup> removal was observed with increasing adsorbent dose. Hence, 3 g L<sup>-1</sup> of adsorbent dose of Al<sub>2</sub>O<sub>3</sub> and 15ZrO<sub>2</sub>@Al<sub>2</sub>O<sub>3</sub> was considered for further studies. It was observed that 3 g L<sup>-1</sup> of pure Al<sub>2</sub>O<sub>3</sub> removed ~56% F<sup>-</sup> from a solution having F<sup>-</sup> concentration of 10 mg L<sup>-1</sup> whereas, 15ZrO<sub>2</sub>@Al<sub>2</sub>O<sub>3</sub> removed ~70% fluoride from the same solution.

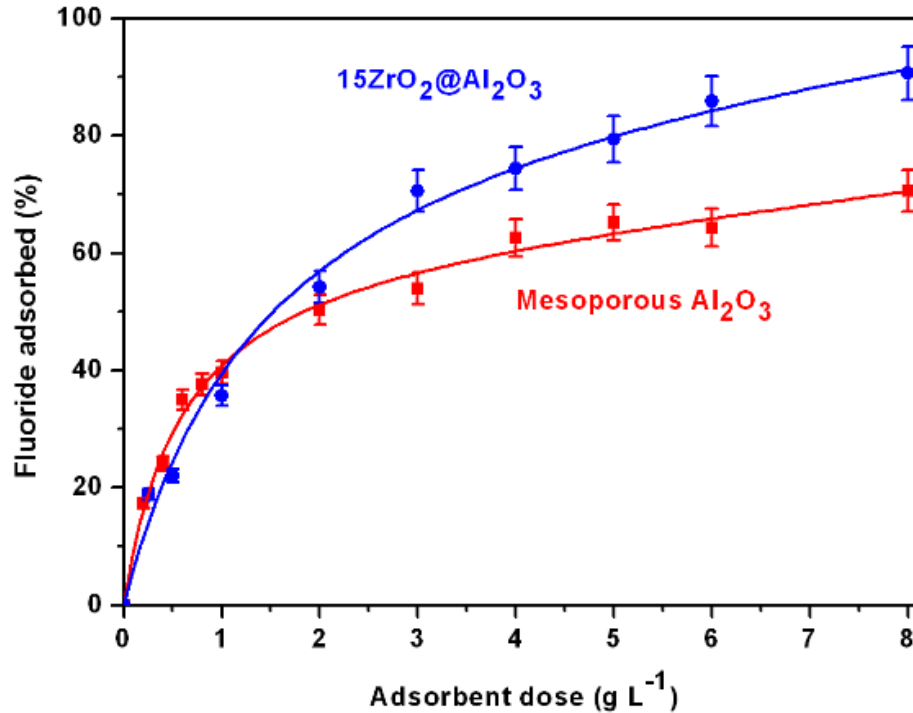


Fig. 3.6. Effect of adsorbent dose on  $F^-$  adsorption capacity of adsorbents. ( $C_0 = 10 \text{ mg L}^{-1}$ , contact time = 8 h,  $\text{pH} = 6.8 \pm 0.2$ ).

### 3.2.2.3. Effect of contact time

$F^-$  sorption on  $Al_2O_3$  and  $15ZrO_2@Al_2O_3$  was investigated as a function of time using a solution having initial  $F^-$  concentration  $30 \text{ mg L}^{-1}$  and adsorbent dose was  $3 \text{ g L}^{-1}$ . It was observed that,  $F^-$  adsorption by  $Al_2O_3$  and  $15ZrO_2@Al_2O_3$  was increased with time (Fig. 3.7). Initially, fluoride adsorption on adsorbents occurred fast, followed by slower adsorption till the equilibrium was reached. In case of  $Al_2O_3$ ,  $\sim 23\%$   $F^-$  sorption occurred within 90 min contact time and equilibrium reached in 300 min and  $\sim 29\%$   $F^-$  was adsorbed. In case of  $15ZrO_2@Al_2O_3$ ,  $\sim 34\%$   $F^-$  was adsorbed within 90 min and the equilibrium was reached in 480 min with  $\sim 52\%$   $F^-$  adsorption, hence equilibrium time of 480 min was applied for further studies.

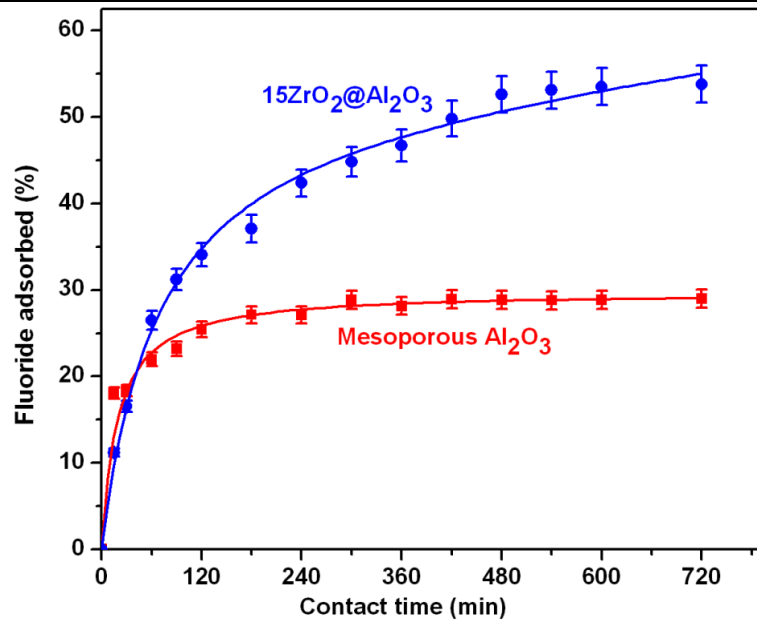


Fig. 3.7. Effect of contact time on F<sup>-</sup> adsorption capacity of adsorbents.

(C<sub>0</sub> = 30 mg L<sup>-1</sup>, adsorbent dose = 3 g L<sup>-1</sup>, pH = 6.8 ± 0.2).

#### 3.2.2.4. Adsorption kinetics

The rate of F<sup>-</sup> adsorption depends on the structure of the adsorbents and the interaction between F<sup>-</sup> and the active sites of adsorption.<sup>233</sup> The adsorption kinetics of F<sup>-</sup> adsorption on pure Al<sub>2</sub>O<sub>3</sub> and 15ZrO<sub>2</sub>@Al<sub>2</sub>O<sub>3</sub> were studied using C<sub>0</sub> of 5, 10, 20 and 30 mg L<sup>-1</sup> and adsorbent dose of 3 g L<sup>-1</sup> at room temperature. The adsorption kinetics of F<sup>-</sup> on 15ZrO<sub>2</sub>@Al<sub>2</sub>O<sub>3</sub> is shown in Fig. 3.8.

The kinetics of F<sup>-</sup> adsorption on Al<sub>2</sub>O<sub>3</sub> and 15ZrO<sub>2</sub>@Al<sub>2</sub>O<sub>3</sub> were analyzed using two well known kinetic models: Lagergren's pseudo-first order kinetic model (equation 2)<sup>95</sup> and Ho's pseudo- second order kinetic model (equation 3)<sup>96</sup> (Chapter 1, page no. 14). In this study, the kinetic data obtained for Al<sub>2</sub>O<sub>3</sub> and 15ZrO<sub>2</sub>@Al<sub>2</sub>O<sub>3</sub> using various initial F<sup>-</sup> concentrations (5, 10, 20 and 30 mg L<sup>-1</sup>) with constant adsorbent dose 3 g L<sup>-1</sup> were fitted to kinetic models.

Fig. 3.9 (i) and (ii) show the plots of pseudo-first order and pseudo-second order kinetics when experimentally obtained kinetic data for 15ZrO<sub>2</sub>@Al<sub>2</sub>O<sub>3</sub> were fitted with the kinetic model equations. Parameters obtained after fitting the kinetic data in the pseudo-first order and pseudo-second order kinetic models are listed in Table 3.2. These results indicated that, R<sup>2</sup> values of pseudo second order kinetic model were much higher than those of pseudo first order kinetic model and the adsorption capacity values (q<sub>e(cal)</sub>) calculated from pseudo second order kinetic model were much

closer to the experimental values ( $q_{e(\text{exp})}$ ). These facts indicate that,  $F^-$  adsorption on  $15ZrO_2@Al_2O_3$  follows pseudo second order kinetics. Pseudo second order kinetic model suggests that chemisorption might be responsible for the  $F^-$  adsorption on  $15ZrO_2@Al_2O_3$ .<sup>98, 145</sup>

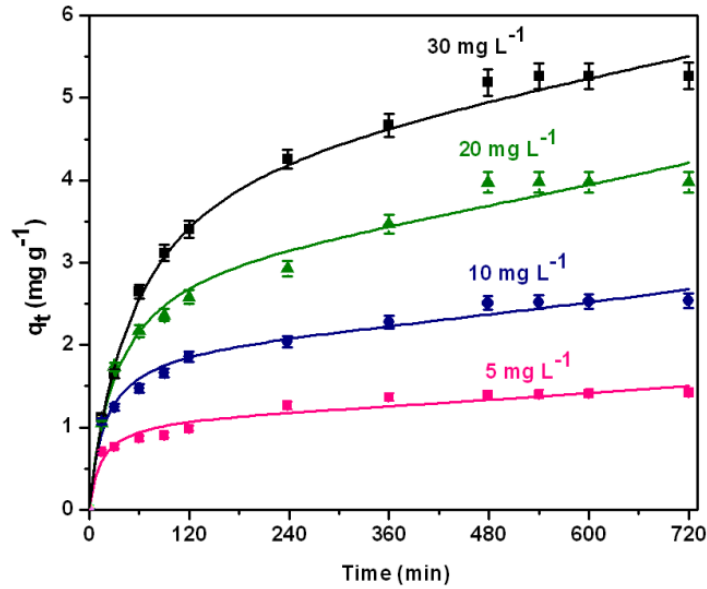


Fig. 3.8. Adsorption kinetic curves of  $F^-$  adsorption on  $15ZrO_2@Al_2O_3$  at different initial  $F^-$  concentrations ( $C_0 = 5, 10, 20$  and  $30 \text{ mg L}^{-1}$ , adsorbent dose =  $3 \text{ g L}^{-1}$ ,  $\text{pH} = 6.8 \pm 0.2$ ).

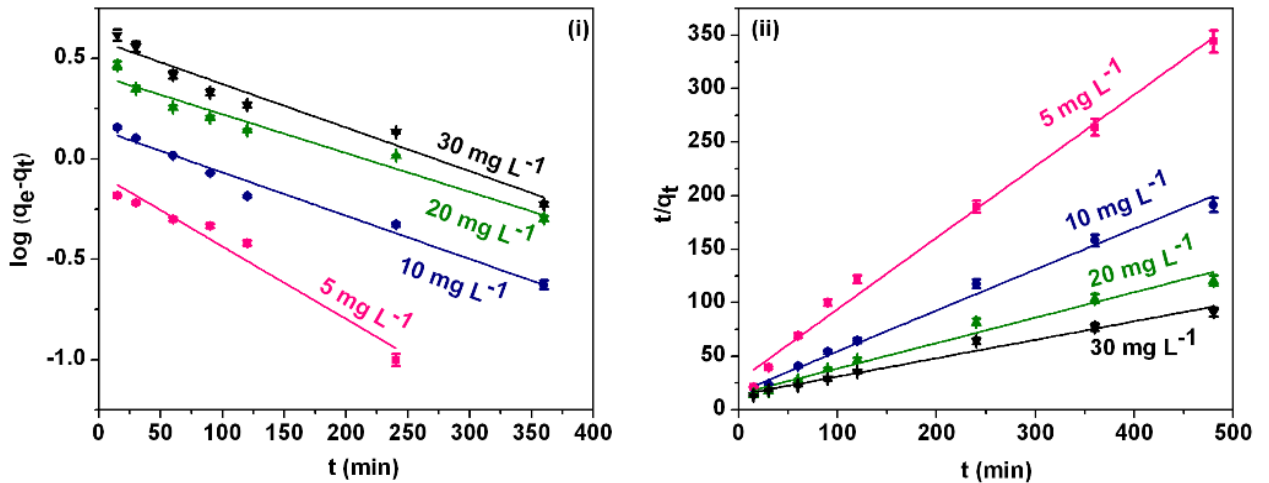


Fig. 3.9. (i) Pseudo first order and (ii) Pseudo second order adsorption kinetic model for  $F^-$  adsorption on  $15ZrO_2@Al_2O_3$  ( $C_0 = 5, 10, 20$  and  $30 \text{ mg L}^{-1}$ , adsorbent dose =  $3 \text{ g L}^{-1}$ ,  $\text{pH} = 6.8 \pm 0.2$ ).

Table 3.2. Comparison of pseudo-first order and pseudo-second order kinetic models parameters, and calculated  $q_{e(cal)}$  and experimental  $q_{e(exp)}$  values for different initial F<sup>-</sup> concentrations of Al<sub>2</sub>O<sub>3</sub> and 15ZrO<sub>2</sub>@Al<sub>2</sub>O<sub>3</sub>.

	C <sub>0</sub> (mg L <sup>-1</sup> )	q <sub>e(exp)</sub> (mg g <sup>-1</sup> )	Pseudo first order			Pseudo second order		
			q <sub>e(cal)</sub> (mg g <sup>-1</sup> )	k <sub>1</sub> (min <sup>-1</sup> )	R <sup>2</sup>	q <sub>e(cal)</sub> (mg g <sup>-1</sup> )	k <sub>2</sub> (g mg <sup>-1</sup> min <sup>-1</sup> )	R <sup>2</sup>
Al <sub>2</sub> O <sub>3</sub>	5	1.38	0.49	0.0055	0.8740	1.40	0.0315	0.9976
	10	1.80	1.12	0.0114	0.7113	1.89	0.0191	0.9943
	20	2.24	1.43	0.0094	0.8488	2.35	0.0131	0.9919
	30	2.89	1.31	0.0107	0.7336	3.00	0.0169	0.9985
15ZrO <sub>2</sub> @Al <sub>2</sub> O <sub>3</sub>	5	1.39	1.19	0.0083	0.9452	1.49	0.0164	0.9907
	10	2.51	1.41	0.0046	0.9734	2.62	0.0088	0.9889
	20	3.97	2.61	0.0044	0.9485	4.2	0.0038	0.9767
	30	5.26	3.89	0.0050	0.9291	5.81	0.0021	0.9767

### 3.2.2.5. Effect of initial fluoride concentration

The effect of initial F<sup>-</sup> concentration on F<sup>-</sup> adsorption capacity by Al<sub>2</sub>O<sub>3</sub> and 15ZrO<sub>2</sub>@Al<sub>2</sub>O<sub>3</sub> was studied by keeping all other parameters constant (adsorbent dose 3 g L<sup>-1</sup>, contact time = 8 h) and shown in Fig. 3.10. It was observed that with progressive increase in initial F<sup>-</sup> concentration, the amount of F<sup>-</sup> adsorbed increased. This should be due to more availability of F<sup>-</sup> ions at higher F<sup>-</sup> concentration (up to C<sub>0</sub> = 100 mg L<sup>-1</sup>) for adsorption. The adsorption capacity of 15ZrO<sub>2</sub>@Al<sub>2</sub>O<sub>3</sub> was found to be higher than that of Al<sub>2</sub>O<sub>3</sub>. Presence of ZrO<sub>2</sub> nanoparticles in 15ZrO<sub>2</sub>@Al<sub>2</sub>O<sub>3</sub> enhances the fluoride removal capacity of the adsorbent (for example, q<sub>e</sub> values of 15ZrO<sub>2</sub>@Al<sub>2</sub>O<sub>3</sub> was 13.6 mg g<sup>-1</sup> whereas q<sub>e</sub> for Al<sub>2</sub>O<sub>3</sub> was 4.7 mg g<sup>-1</sup> when C<sub>0</sub> value was 100 mg L<sup>-1</sup>)

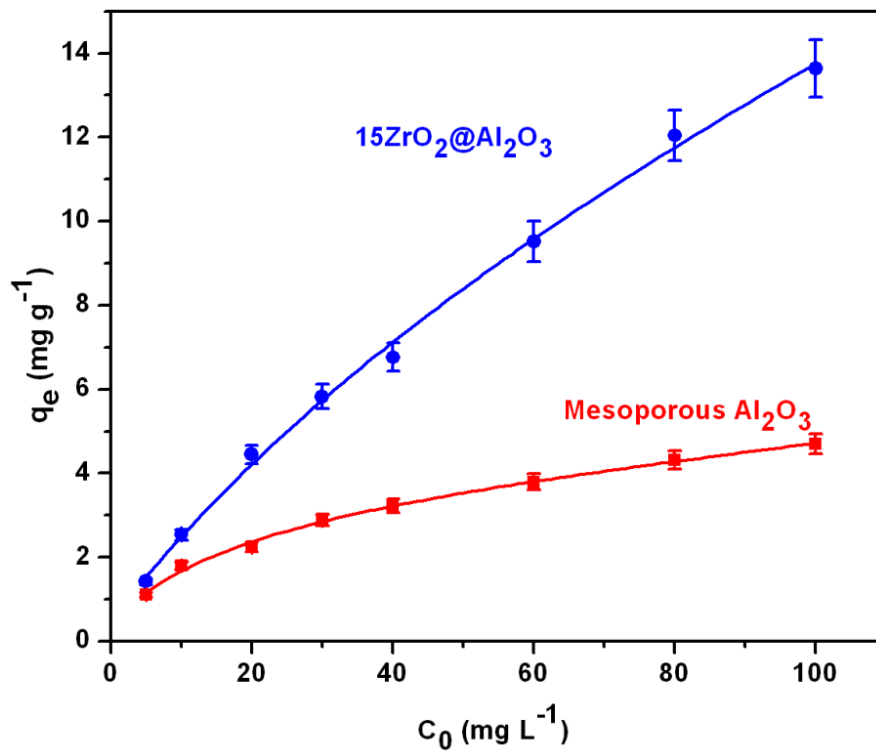


Fig. 3.10. Effect of initial F<sup>-</sup> concentration on F<sup>-</sup> adsorption capacity of Al<sub>2</sub>O<sub>3</sub> and 15ZrO<sub>2</sub>@Al<sub>2</sub>O<sub>3</sub> (adsorbent dose = 3 g L<sup>-1</sup>, contact time = 8 h, pH = 6.8 ± 0.2).

### 3.2.2.6. Adsorption Isotherms

The experimental equilibrium data of F<sup>-</sup> adsorption on Al<sub>2</sub>O<sub>3</sub> and 15ZrO<sub>2</sub>@Al<sub>2</sub>O<sub>3</sub> were fitted to standard adsorption isotherms viz. Freundlich isotherm (equation 4)<sup>99</sup> and Langmuir isotherm (equation 5)<sup>100</sup> (Chapter 1, page no.15) (Fig.3.11). Parameters obtained from Freundlich and Langmuir isotherm models are listed in Table 3.3. Comparing the correlation coefficient (R<sup>2</sup>) values for Freundlich isotherm and Langmuir isotherm models it was observed that Freundlich model fit the experimental data of Al<sub>2</sub>O<sub>3</sub> and 15ZrO<sub>2</sub>@Al<sub>2</sub>O<sub>3</sub>. Fig. 3.11(i) shows the fitting of experimental data to Freundlich isotherm equation. This indicates the heterogeneity of the adsorbent surface and considers multilayer adsorption of F<sup>-</sup> on Al<sub>2</sub>O<sub>3</sub> and 15ZrO<sub>2</sub>@Al<sub>2</sub>O<sub>3</sub>.

Another essential feature of the Langmuir model can be given in terms of dimensionless separation factor 'r', which was calculated using equation 14.<sup>231</sup> In the present case 'r' values were found to be < 1 (varies from 0.77 to 0.11 with the variation of C<sub>0</sub> from 5 to 100 mg L<sup>-1</sup>), it was assumed that favorable adsorption of F<sup>-</sup> occurred on mesoporous Al<sub>2</sub>O<sub>3</sub> and 15ZrO<sub>2</sub>@Al<sub>2</sub>O<sub>3</sub>.<sup>91</sup>

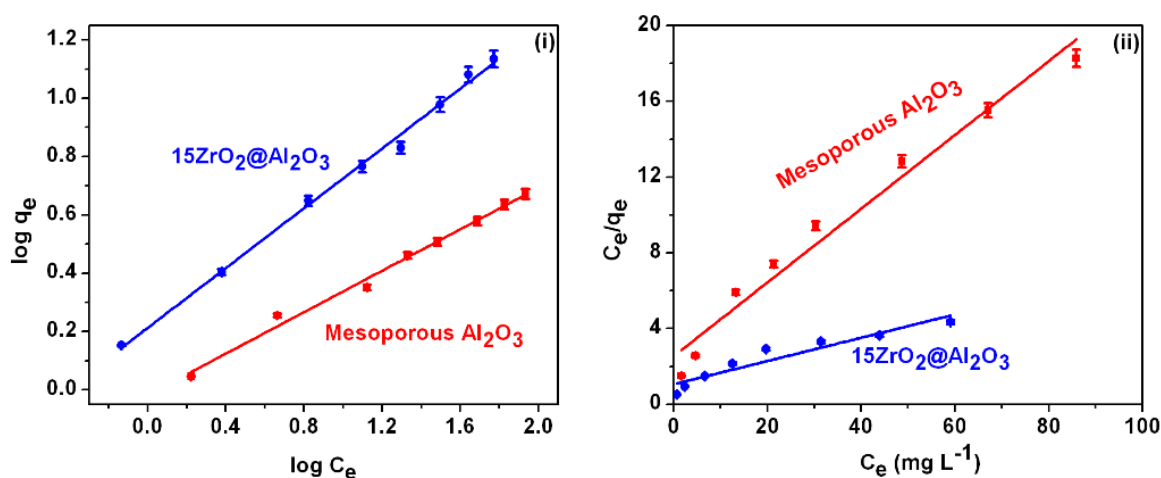


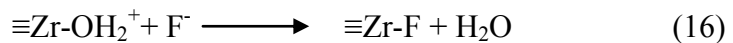
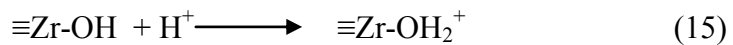
Fig. 3.11. (i) Freundlich adsorption isotherm and (ii) Langmuir adsorption isotherm fits for adsorption of F<sup>-</sup> on Al<sub>2</sub>O<sub>3</sub> and 15ZrO<sub>2</sub>@Al<sub>2</sub>O<sub>3</sub>. (C<sub>0</sub> = 5 to 100 mg L<sup>-1</sup>, adsorbent dose = 3 g L<sup>-1</sup>, contact time = 8 h, pH = 6.8 ± 0.2).

Table 3.3. Langmuir and Freundlich isotherm parameters for F<sup>-</sup> adsorption on Al<sub>2</sub>O<sub>3</sub> and 15ZrO<sub>2</sub>@Al<sub>2</sub>O<sub>3</sub> at pH of 6.8 ± 0.2.

	Langmuir isotherm			Freundlich isotherm		
	Q <sub>0</sub> (mg g <sup>-1</sup> )	b (l mg <sup>-1</sup> )	R <sup>2</sup>	K <sub>f</sub>	1/n	R <sup>2</sup>
Al <sub>2</sub> O <sub>3</sub>	5.13	0.08	0.9707	0.96	0.36	0.9918
15ZrO <sub>2</sub> @Al <sub>2</sub> O <sub>3</sub>	16.27	0.058	0.8940	1.632	0.51	0.9951

### 3.2.2.7. Effect of initial pH

To investigate the effect of initial pH of the solution on adsorption of F<sup>-</sup> ions, adsorption experiments were conducted using F<sup>-</sup> solutions having C<sub>0</sub> = 30 mg L<sup>-1</sup> and varying pH in the range of 4- 10 and adsorbent dose of 3 g L<sup>-1</sup>. The effect of initial pH on the adsorption of F<sup>-</sup> on Al<sub>2</sub>O<sub>3</sub> and 15ZrO<sub>2</sub>@Al<sub>2</sub>O<sub>3</sub> is illustrated in Fig. 3.12. The results revealed that, adsorption capacities decreased with increasing solution pH. Initially in the pH range of 4 to 6, percent of F<sup>-</sup> removal by 15ZrO<sub>2</sub>@Al<sub>2</sub>O<sub>3</sub> was decreased with increasing pH. Then in 6- 7 pH range, F<sup>-</sup> removal was not affected much. But further increase of pH (up to 10), F<sup>-</sup> removal again decreased. However in case of Al<sub>2</sub>O<sub>3</sub>, percent of F<sup>-</sup> removal did not change much with increasing pH from 4 to 7. Further increase of pH decreased percent of F<sup>-</sup> removal. This might be due to the fact that pHPZC values of Al<sub>2</sub>O<sub>3</sub> and 15ZrO<sub>2</sub>@Al<sub>2</sub>O<sub>3</sub> are 7.0 and 8.2 respectively. At lower pH, the -OH groups present on the surface of 15ZrO<sub>2</sub>@Al<sub>2</sub>O<sub>3</sub> became protonated, which facilitated to attract F<sup>-</sup> ions on the surface and eventually F<sup>-</sup> replaced H<sub>2</sub>O and attached on the surface of ZrO<sub>2</sub>. This can be represented as follows (equation 15 and 16):<sup>169</sup>



Percentage of F<sup>-</sup> removal was found to be low at higher pH values because of competition between OH<sup>-</sup> and F<sup>-</sup> ions on the adsorption sites.



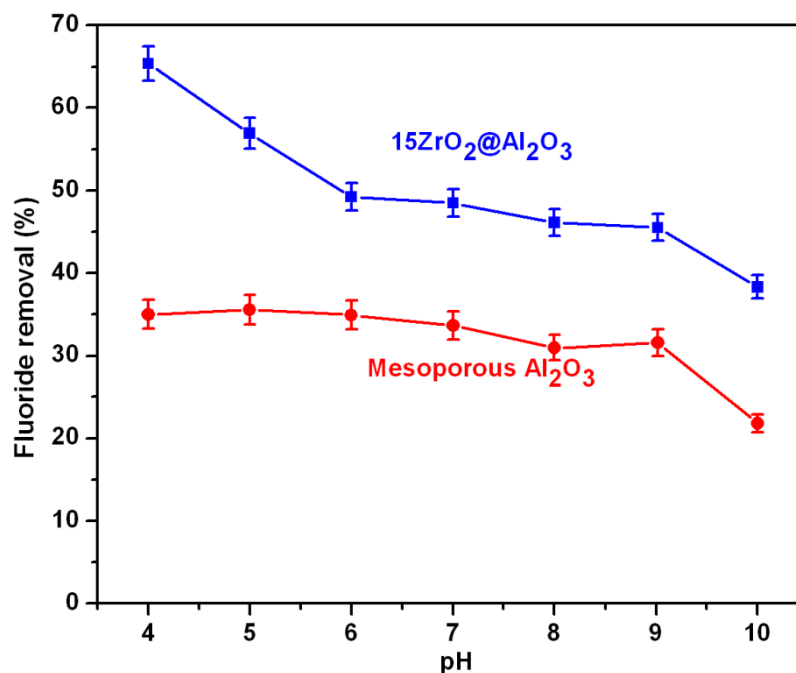


Fig. 3.12. Effect of initial pH on  $F^-$  adsorption capacity of  $Al_2O_3$  and  $15ZrO_2@Al_2O_3$  (adsorbent dose =  $3\text{ g L}^{-1}$ ,  $C_0 = 30\text{ mg L}^{-1}$ , contact time = 8 h).

### 3.2.2.8. Effect of competing anions

To study the effect of competing anions (such as chloride, nitrate, sulphate and bicarbonate) on  $F^-$  adsorption of synthesized adsorbents,  $10\text{ mg L}^{-1}$  and  $100\text{ mg L}^{-1}$  initial concentrations of  $Cl^-$ ,  $NO_3^-$ ,  $SO_4^{2-}$  and  $HCO_3^-$  were used while keeping the initial  $F^-$  concentration as  $10\text{ mg L}^{-1}$  and adsorbent dose  $3\text{ g L}^{-1}$  at  $30\text{ }^\circ\text{C}$ . The effect of competing anions (such as  $Cl^-$ ,  $NO_3^-$ ,  $SO_4^{2-}$ , and  $HCO_3^-$ ) on  $F^-$  adsorption of  $Al_2O_3$  and  $15ZrO_2@Al_2O_3$  adsorbents is shown in Fig. 3.13. In case of  $Al_2O_3$ , presence of  $Cl^-$ ,  $NO_3^-$ ,  $SO_4^{2-}$ , and  $HCO_3^-$  ( $10\text{ mg L}^{-1}$  and  $100\text{ mg L}^{-1}$ ) no significant decrease in percent of  $F^-$  adsorbed was observed. Due to the presence of  $Cl^-$ ,  $NO_3^-$  ( $10\text{ mg L}^{-1}$  and  $100\text{ mg L}^{-1}$ )  $\sim 5\%$ ,  $SO_4^{2-}$  ( $10\text{ mg L}^{-1}$  and  $100\text{ mg L}^{-1}$ )  $\sim 8\%$  and  $HCO_3^-$  ( $100\text{ mg L}^{-1}$ )  $\sim 10\text{-}12\%$  reduction of percent of  $F^-$  removal efficiency was observed for  $15ZrO_2@Al_2O_3$ . Presence of  $HCO_3^-$  ion significantly reduce the  $F^-$  removal which might be due to the competition of  $F^-$  ions with  $HCO_3^-$  ions for the adsorption on active sites of the adsorbent.

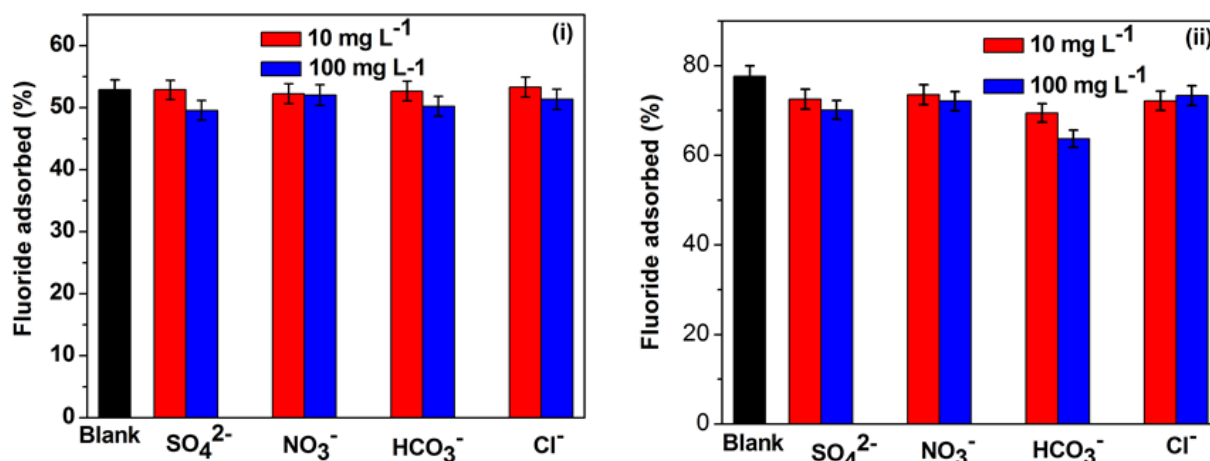


Fig. 3.13. Effect of co-existing anions on F<sup>-</sup> adsorption capacity of Al<sub>2</sub>O<sub>3</sub> and 15ZrO<sub>2</sub>@Al<sub>2</sub>O<sub>3</sub> (adsorbent dose = 3 g L<sup>-1</sup>, C<sub>0</sub> = 10 mg L<sup>-1</sup>, contact time = 8 h).

### 3.3. Summary of results

- i. ZrO<sub>2</sub> nanoparticles loaded mesoporous Al<sub>2</sub>O<sub>3</sub> adsorbents were prepared by wet impregnation method.
- ii. The synthesized materials were mesoporous in nature with high surface area.
- iii. It has been demonstrated that loading of ZrO<sub>2</sub> nanoparticles significantly enhances F<sup>-</sup> removal capacity of mesoporous Al<sub>2</sub>O<sub>3</sub>.
- iv. Kinetics of F<sup>-</sup> adsorption on Al<sub>2</sub>O<sub>3</sub> and 15ZrO<sub>2</sub>@Al<sub>2</sub>O<sub>3</sub> was explained by pseudo second order model.
- v. F<sup>-</sup> adsorption on Al<sub>2</sub>O<sub>3</sub> and 15ZrO<sub>2</sub>@Al<sub>2</sub>O<sub>3</sub> followed Freundlich model which indicates multilayer adsorption with heterogeneity of the adsorbent surface.
- vi. 15 wt% ZrO<sub>2</sub> nanoparticle loaded mesoporous  $\gamma$ -Al<sub>2</sub>O<sub>3</sub> removes greater percentage of F<sup>-</sup> (52%) than that of mesoporous Al<sub>2</sub>O<sub>3</sub> (28%).
- vii. ZrO<sub>2</sub> nanoparticles loaded mesoporous Al<sub>2</sub>O<sub>3</sub> exhibited higher F<sup>-</sup> removal capacity than that of pure Al<sub>2</sub>O<sub>3</sub>.
- viii. 15ZrO<sub>2</sub>@Al<sub>2</sub>O<sub>3</sub> exhibited good F<sup>-</sup> removal efficiency over a wide range of pH.

## CHAPTER 4

### **Preparation of MgO nanoparticle loaded mesoporous Al<sub>2</sub>O<sub>3</sub> based adsorbents and their fluoride removal performance from water**

#### **4.1. Experimental procedure for materials synthesis**

##### **4.1.1. Materials used**

Aluminium nitrate nonahydrate, sodium hydroxide, sodium sulphate were procured from Fisher Scientific, India; triethanol amine (TEA), sodium hydrogen carbonate, sodium chloride, sodium nitrate and sodium fluoride were procured from Merck, India; magnesium nitrate hexahydrate, stearic acid, and hydrochloric acid from S.d fine-chem. limited, India. All these chemicals were used as received.

##### **4.1.2. Synthesis of mesoporous Al<sub>2</sub>O<sub>3</sub>**

Mesoporous Al<sub>2</sub>O<sub>3</sub> was synthesized as per the procedure described in Chapter 2, section 2.1.2.

##### **4.1.3. Preparation of MgO nanoparticle loaded mesoporous Al<sub>2</sub>O<sub>3</sub><sup>234</sup>**

MgO nanoparticle loaded mesoporous aluminas were synthesized using a wet impregnation technique. MgO nanoparticle loaded mesoporous aluminas were synthesized with different loading percentages (5, 10, 20, 30, 40 and 50 wt.%) of MgO on mesoporous Al<sub>2</sub>O<sub>3</sub>. In a typical synthesis, in a beaker calculated amount of aqueous solution of magnesium nitrate hexahydrate was mixed with desired amount of mesoporous Al<sub>2</sub>O<sub>3</sub> powder and stirred for 12 h. The mixture was dried at 150 °C for 5 h and then calcined at 550 °C for 4 h in air atmosphere to obtain MgO loaded mesoporous Al<sub>2</sub>O<sub>3</sub> adsorbent. The 5, 10, 20, 30, 40 and 50 wt.% MgO loaded mesoporous Al<sub>2</sub>O<sub>3</sub> are now onwards will be referred as 5MgO@Al<sub>2</sub>O<sub>3</sub>,

10MgO@Al<sub>2</sub>O<sub>3</sub>, 20MgO@Al<sub>2</sub>O<sub>3</sub>, 30MgO@Al<sub>2</sub>O<sub>3</sub>, 40MgO@Al<sub>2</sub>O<sub>3</sub> and 50MgO@Al<sub>2</sub>O<sub>3</sub> respectively.

## 4.2. Results and Discussion

### 4.2.1. Characterization of the synthesized materials

#### 4.2.1.1. X-ray diffraction analysis<sup>234</sup>

The XRD patterns of MgO loaded Al<sub>2</sub>O<sub>3</sub> samples are shown in Fig. 4.1. Fig. 4.1(a) shows almost amorphous nature of  $\gamma$ -Al<sub>2</sub>O<sub>3</sub> with broad X-ray diffraction peaks at  $2\theta = 19.41^\circ$ ,  $45.45^\circ$  and  $67.14^\circ$  corresponding to (111), (400) and (440) diffraction planes (ICDD card no. 10-0425). The peak intensities corresponding to  $\gamma$ -Al<sub>2</sub>O<sub>3</sub> phase were found to be decreased with increasing MgO loading in the sample. The samples containing MgO loading up to 20 wt.% did not show any characteristic peaks of MgO. However, further increase of MgO loading on Al<sub>2</sub>O<sub>3</sub>, characteristic peaks of cubic MgO at  $2\theta = 37.01^\circ$ ,  $42.86^\circ$ ,  $62.44^\circ$ ,  $74.86^\circ$  and  $78.82^\circ$  corresponding to (111), (200), (220), (311) and (222) planes were observed (ICDD card no: 65-0476).

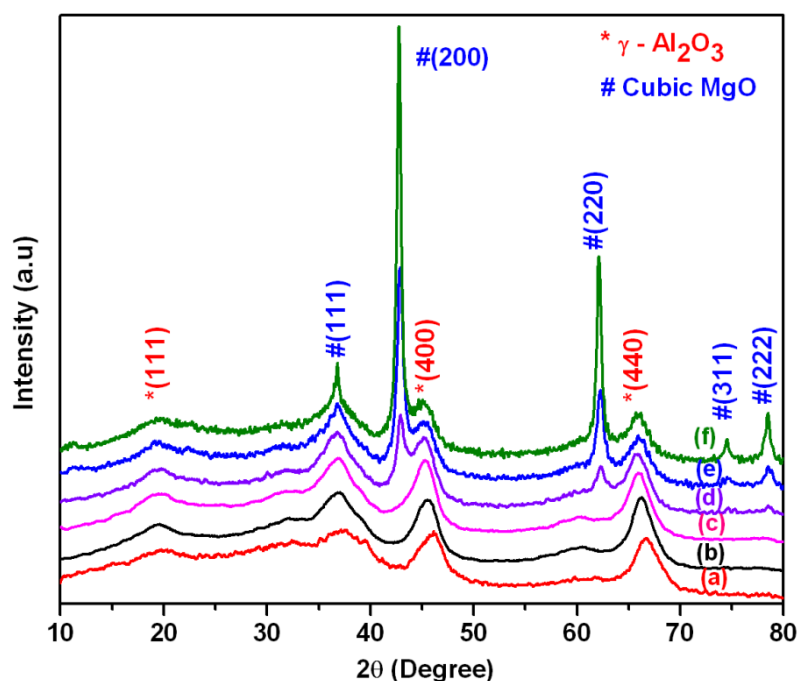


Fig. 4.1. XRD pattern of (a) Al<sub>2</sub>O<sub>3</sub>, (b) 10MgO@Al<sub>2</sub>O<sub>3</sub>, (c) 20MgO@Al<sub>2</sub>O<sub>3</sub>, (d) 30MgO @Al<sub>2</sub>O<sub>3</sub>, (e) 40MgO@Al<sub>2</sub>O<sub>3</sub>, (f) 50MgO@Al<sub>2</sub>O<sub>3</sub>.

#### 4.2.1.2. N<sub>2</sub> adsorption-desorption analysis<sup>234</sup>

N<sub>2</sub> adsorption- desorption isotherms and pore size distributions of MgO nanoparticle loaded mesoporous Al<sub>2</sub>O<sub>3</sub> are shown in Fig. 4.2. N<sub>2</sub> adsorption- desorption isotherms for pure Al<sub>2</sub>O<sub>3</sub> and MgO nanoparticle loaded adsorbents (up to 30 wt%, i.e. 5MgO@Al<sub>2</sub>O<sub>3</sub>, 10MgO@Al<sub>2</sub>O<sub>3</sub>, 20MgO@Al<sub>2</sub>O<sub>3</sub> and 30MgO@Al<sub>2</sub>O<sub>3</sub>) are typical type IV isotherms with H2 hysteresis loop. This indicates that these adsorbents possess mesoporous structure with pores having narrow necks and with wide bodies (often referred to as ink bottle pores).<sup>229</sup> However, when more than 30 wt.% MgO was impregnated within mesoporous Al<sub>2</sub>O<sub>3</sub> matrix (i.e. 40MgO@Al<sub>2</sub>O<sub>3</sub> and 50MgO@Al<sub>2</sub>O<sub>3</sub>), the nature of the isotherms has changed to H3 type hysteresis loop, indicating the formation of aggregated slit-shaped porous structure. The change in pore size of the MgO loaded Al<sub>2</sub>O<sub>3</sub> adsorbents (Fig. 2(ii)) was found to be minor (from 6.5 to 7.0 nm) when MgO nanoparticle loading was increased from 0 to 30%. Then, further increase of MgO loading led to dramatic decrease in pore size (from 6.5 to 3.8 nm). This might be due to the fact that pores have collapsed to some extent and formed aggregates of nanoparticles.<sup>229, 235</sup> Moreover, when MgO loading is high then MgO may be deposited on the walls of pore and caused reduction of pore size. The BJH pore volumes of the samples were found to be decreased with increasing MgO loading. The physical parameters obtained by means of N<sub>2</sub> adsorption- desorption study are summarized in Table 4.1. The BET surface area and pore volume of the adsorbents also found to be decreased with increasing MgO nanoparticle loading.

#### 4.2.1.3. HRTEM analysis<sup>234</sup>

HRTEM micrographs of the synthesized adsorbents Al<sub>2</sub>O<sub>3</sub> and 40MgO@Al<sub>2</sub>O<sub>3</sub> are shown in Fig. 4.3(a) and (b). Morphological aspects of the samples showed wormhole-like highly connected porous structure of mesoporous Al<sub>2</sub>O<sub>3</sub> matrix and MgO nanoparticles (size < ~8 nm) are within the porous structure (Fig. 4.3b).

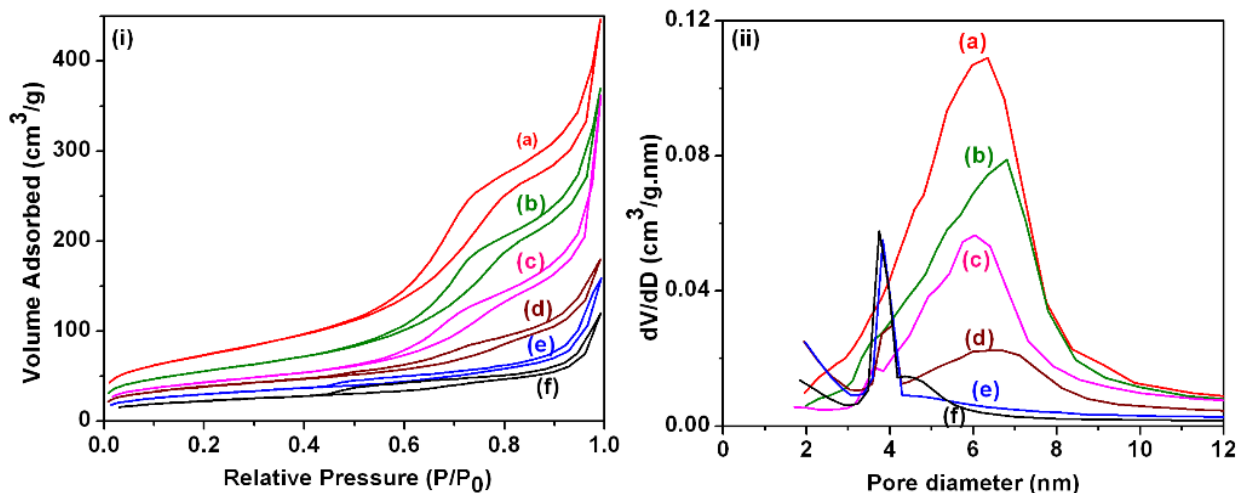


Fig. 4.2. (i) N<sub>2</sub>-adsorption-desorption isotherms and (ii) Pore size distributions of (a) Al<sub>2</sub>O<sub>3</sub>, (b) 10MgO@Al<sub>2</sub>O<sub>3</sub>, (c) 20MgO@Al<sub>2</sub>O<sub>3</sub>, (d) 30MgO@Al<sub>2</sub>O<sub>3</sub>, (e) 40MgO@Al<sub>2</sub>O<sub>3</sub>, (f) 50MgO@Al<sub>2</sub>O<sub>3</sub>.

Table 4.1. Surface area and pore size parameters of the synthesized adsorbents obtained by means of N<sub>2</sub> adsorption-desorption study.

Sample	BET Surface area (m <sup>2</sup> /g)	BJH average pore size (nm)	BJH pore volume (cm <sup>3</sup> /g)
Al <sub>2</sub> O <sub>3</sub>	264	6.5	0.62
5MgO@Al <sub>2</sub> O <sub>3</sub>	216	6.6	0.55
10MgO@Al <sub>2</sub> O <sub>3</sub>	198	6.7	0.51
20MgO@Al <sub>2</sub> O <sub>3</sub>	152	6.6	0.41
30MgO@Al <sub>2</sub> O <sub>3</sub>	134	6.9	0.26
40MgO@Al <sub>2</sub> O <sub>3</sub>	105	3.8	0.23
50MgO@Al <sub>2</sub> O <sub>3</sub>	80	3.7	0.16

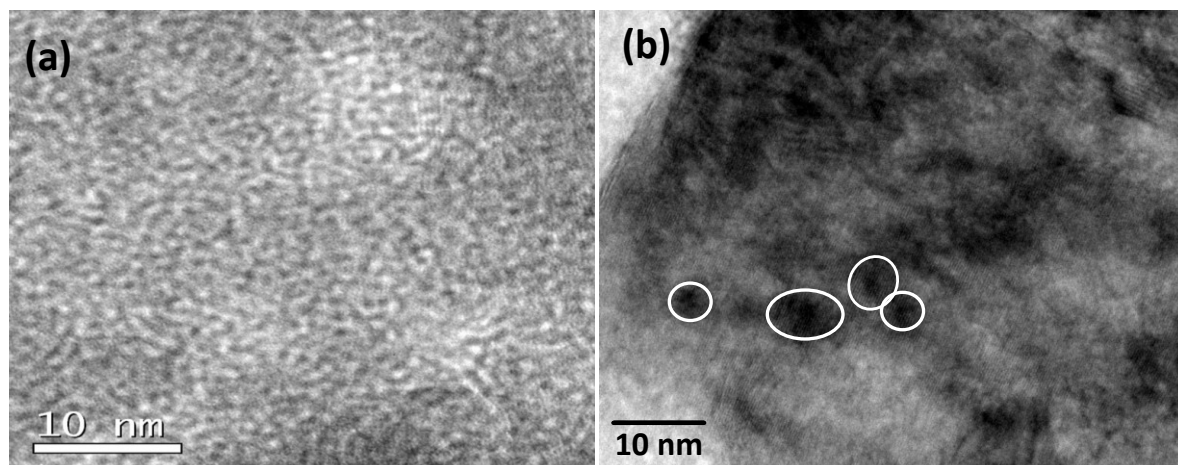


Fig. 4.3. HRTEM images of (a) Al<sub>2</sub>O<sub>3</sub>, (b) 40MgO@Al<sub>2</sub>O<sub>3</sub> (MgO nanoparticles are shown within the circle).

#### 4.2.1.4. Analysis of pHPZC of the adsorbents<sup>234</sup>

The pHPZC values for pure mesoporous Al<sub>2</sub>O<sub>3</sub> and 40MgO@Al<sub>2</sub>O<sub>3</sub> were found to be 8.2 and 11.2 respectively (Fig. 4.4). Below the pHPZC value, the surface of the adsorbent is positive, which favours the adsorption of F<sup>-</sup> on the surface of adsorbent due to columbic attraction. This indicates that 40MgO@Al<sub>2</sub>O<sub>3</sub> should have better F<sup>-</sup> adsorption capacity than that of pure Al<sub>2</sub>O<sub>3</sub>.

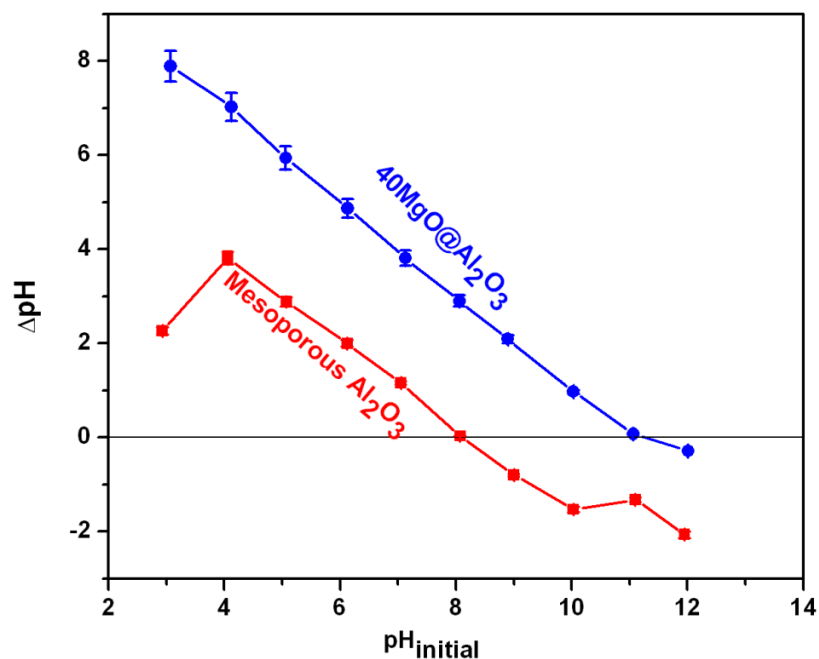


Fig. 4.4. Plot for determination of pHPZC of Al<sub>2</sub>O<sub>3</sub> and 40MgO@Al<sub>2</sub>O<sub>3</sub>.

## 4.2.2. Fluoride adsorption studies<sup>234</sup>

### 4.2.2.1. Optimization of adsorbent composition

F<sup>-</sup> adsorption analysis of different amounts of MgO loaded mesoporous aluminas are shown in Fig 4.5. The analysis was performed using a solution having initial F<sup>-</sup> concentration of 30 mg L<sup>-1</sup> and adsorbent dose of 3 g L<sup>-1</sup>. It was clearly observed that, loading of MgO nanoparticles on high surface area mesoporous Al<sub>2</sub>O<sub>3</sub> enhanced its F<sup>-</sup> adsorption capacity. For instance, pure mesoporous Al<sub>2</sub>O<sub>3</sub> adsorbed ~28% F<sup>-</sup>, whereas adsorbent having 40 wt.% MgO adsorbed ~83% F<sup>-</sup>. However, when MgO loading exceeded 40 wt.%, much enhancement in F<sup>-</sup> adsorption capacity of adsorbents was not observed. So, further studies were conducted using 40MgO@Al<sub>2</sub>O<sub>3</sub>.

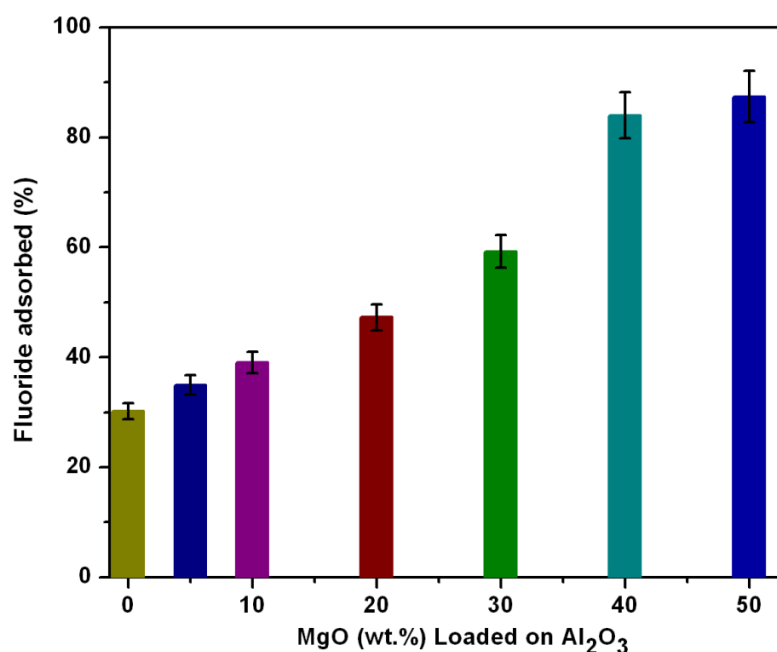


Fig. 4.5. Effect of MgO loading on mesoporous Al<sub>2</sub>O<sub>3</sub> for removal of F<sup>-</sup>. (C<sub>0</sub> = 30 mg L<sup>-1</sup>, adsorbent dose = 3 g L<sup>-1</sup>, contact time = 8 h, pH = 6.8 ± 0.2).

### 4.2.2.2. Determination of optimum adsorbent dose

The effect of adsorbent dose on F<sup>-</sup> removal at initial F<sup>-</sup> concentration of 10 mg L<sup>-1</sup> is shown in Fig. 4.6. It is evident that, the percent of F<sup>-</sup> removal was increased with increasing adsorbent dose. This is due to the fact that, a greater amount of adsorbent provides greater number of available binding sites. It was also observed that, the percent of F<sup>-</sup> adsorbed increased drastically with increasing adsorbent dose from 0.25



g L<sup>-1</sup> to 3 g L<sup>-1</sup>. However, when the adsorbent dose was more than 3 g L<sup>-1</sup>, not much increase in F<sup>-</sup> removal was observed with increasing adsorbent dose. Hence, 3 g L<sup>-1</sup> of adsorbent dose of mesoporous Al<sub>2</sub>O<sub>3</sub> and 40MgO@Al<sub>2</sub>O<sub>3</sub> was considered for further studies. Pure Al<sub>2</sub>O<sub>3</sub> removed ~ 56% F<sup>-</sup> from a solution having F<sup>-</sup> concentration of 10 mg L<sup>-1</sup> whereas, 40MgO@Al<sub>2</sub>O<sub>3</sub> exhibited its capacity of removing ~90% F<sup>-</sup> from the same solution with 3 g L<sup>-1</sup> adsorbent dose.

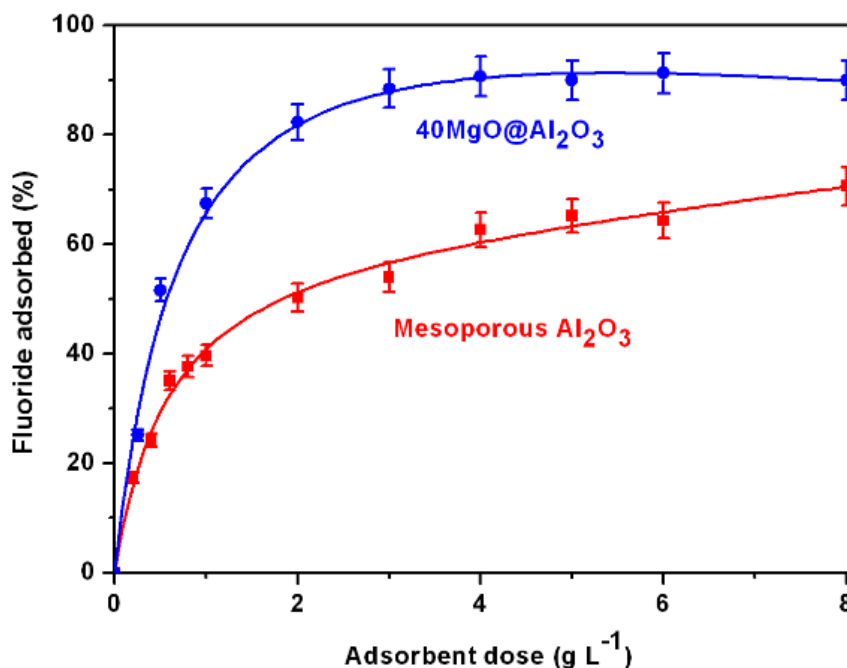


Fig. 4.6. Effect of adsorbent dose on F<sup>-</sup> adsorption capacity of adsorbents. (C<sub>0</sub> = 10 mg L<sup>-1</sup>, contact time = 8 h, pH = 6.8 ± 0.2).

#### 4.2.2.3. Effect of contact time

F<sup>-</sup> sorption on mesoporous Al<sub>2</sub>O<sub>3</sub> and 40MgO@Al<sub>2</sub>O<sub>3</sub> was investigated as a function of time using a solution having initial F<sup>-</sup> concentration 30 mg L<sup>-1</sup> and adsorbent dose was 3 g L<sup>-1</sup>. F<sup>-</sup> adsorption of 40MgO@Al<sub>2</sub>O<sub>3</sub> was found to be increased from 12% to 76% as the contact time increased from 15 min to 480 min and equilibrium was achieved at 480 min (Fig. 4.7). Pure mesoporous Al<sub>2</sub>O<sub>3</sub> adsorbed ~ 23% F<sup>-</sup> within 90 min contact time and equilibrium reached in 300 min and ~ 29 % F<sup>-</sup> was adsorbed. Hence, equilibrium time of 480 min was applied for further studies. F<sup>-</sup> adsorption was initially fast up to 120 min and then it became low. The initial rapid adsorption was presumably due to exchange of F<sup>-</sup> ions with surface hydroxyl ions of the adsorbent.

Slow adsorption in the later stage caused by the gradual uptake of F<sup>-</sup> at the inner surface of adsorbent.<sup>155, 236</sup>

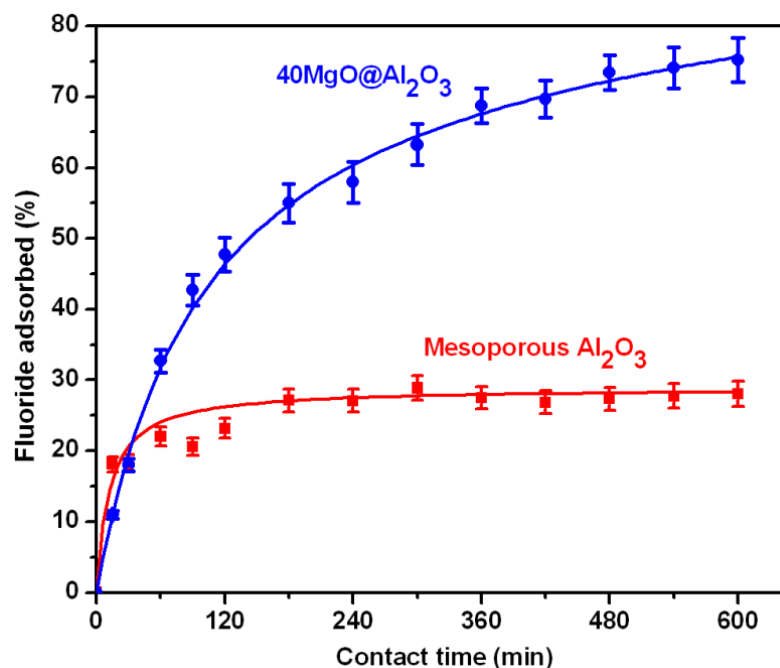


Fig. 4.7. Effect of contact time on F<sup>-</sup> adsorption capacity of adsorbents. (C<sub>0</sub> = 30 mg L<sup>-1</sup>, adsorbent dose = 3 g L<sup>-1</sup>, pH = 6.8 ± 0.2).

#### 4.2.2.4. Adsorption Kinetics

The adsorption kinetics of F<sup>-</sup> adsorption on 40MgO@Al<sub>2</sub>O<sub>3</sub> was studied using initial F<sup>-</sup> concentration (C<sub>0</sub>) of 5, 10, 20 and 30 mg L<sup>-1</sup> and adsorbent dose of 3 g L<sup>-1</sup>. The adsorption kinetics of F<sup>-</sup> on 40MgO@Al<sub>2</sub>O<sub>3</sub> are shown in Fig. 4.8. The kinetic curves show that, the sorption rate was rapid at the beginning of the processes and then became slow as equilibrium was approached towards 480 min.

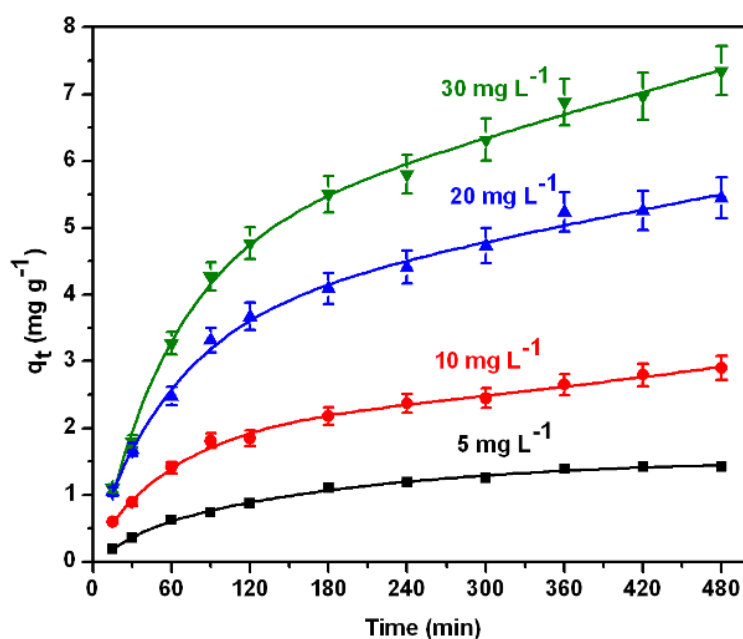


Fig. 4.8. Adsorption kinetic curves of F<sup>-</sup> adsorption on 40MgO@Al<sub>2</sub>O<sub>3</sub> at different initial F<sup>-</sup> concentrations (C<sub>0</sub> = 5, 10, 20 and 30 mg L<sup>-1</sup>, adsorbent dose = 3 g L<sup>-1</sup>, pH = 6.8 ± 0.2).

The rate of sorption depends on structural properties of the sorbent, initial F<sup>-</sup> concentration in solution, interaction between F<sup>-</sup> ions and active sites of adsorbents.<sup>233</sup> To understand the kinetics of F<sup>-</sup> adsorption onto the surface of the adsorbent, Lagergren's pseudo-first order kinetic model (equation 2)<sup>95</sup> and Ho's pseudo-second order kinetic model (equation 3)<sup>96</sup> equations were used (Chapter 1, page no.14). In this study, the kinetic data obtained for 40MgO@Al<sub>2</sub>O<sub>3</sub> using various initial F<sup>-</sup> concentrations (C<sub>0</sub> = 5, 10, 20 and 30 mg L<sup>-1</sup>) with constant adsorbent dose (3 g L<sup>-1</sup>) was fitted to kinetic models. Parameters obtained after fitting the F<sup>-</sup> adsorption kinetic data of mesoporous Al<sub>2</sub>O<sub>3</sub> and 40MgO@Al<sub>2</sub>O<sub>3</sub> in the pseudo-first order and pseudo-second order kinetic models are listed in Table 4.2. Fig. 4.9 (i) and (ii) show the representative plots of pseudo-first order and pseudo-second order kinetic models when experimentally obtained kinetic data for 40MgO@Al<sub>2</sub>O<sub>3</sub> was fitted with the kinetic model equations (equation 2 and 3). As indicated in Table 4.2, R<sup>2</sup> values of pseudo-second order kinetic model were much higher than those of pseudo-first order kinetic model and the adsorption capacity values (q<sub>e(cal)</sub>), calculated from pseudo-second order kinetic model, were much closer to the experimental values (q<sub>e(exp)</sub>). These facts indicate that F<sup>-</sup> adsorption on 40MgO@Al<sub>2</sub>O<sub>3</sub> follows pseudo-second

order kinetics. Pseudo-second order kinetic model suggests that chemisorption might be responsible for the F<sup>-</sup> adsorption on 40MgO@Al<sub>2</sub>O<sub>3</sub>.<sup>98, 173</sup>

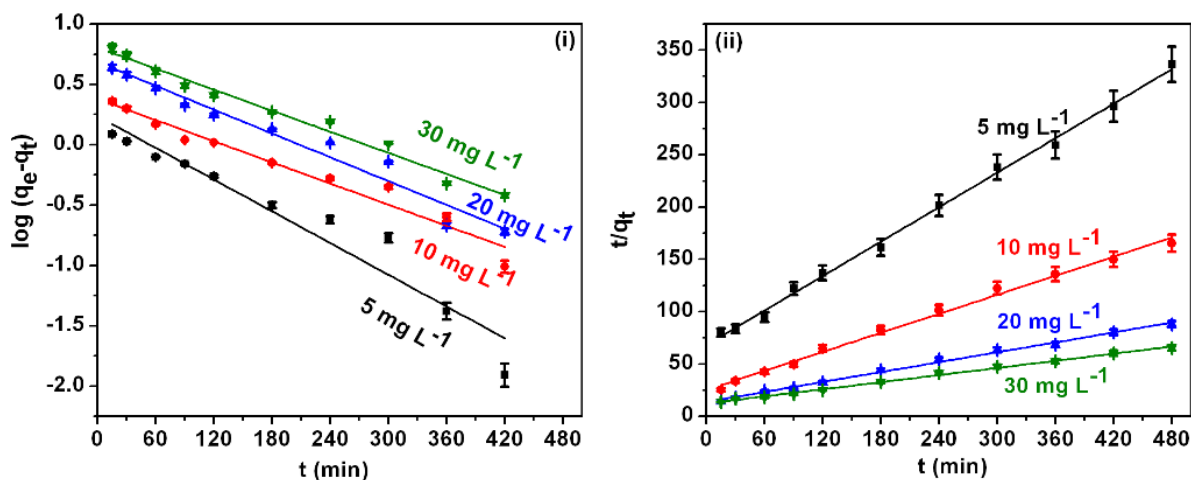


Fig. 4.9. (i) Pseudo first order and (ii) Pseudo second order adsorption kinetic model for F<sup>-</sup> adsorption on 40MgO@Al<sub>2</sub>O<sub>3</sub> ( $C_0 = 5, 10, 20$  and  $30 \text{ mg L}^{-1}$ , adsorbent dose =  $3 \text{ g L}^{-1}$ ,  $\text{pH} = 6.8 \pm 0.2$ ).

#### 4.2.2.5. Effect of initial fluoride concentration

The effect of initial F<sup>-</sup> concentration ( $5 \text{ mg L}^{-1}$  to  $1000 \text{ mg L}^{-1}$ ) on F<sup>-</sup> adsorption capacity of mesoporous Al<sub>2</sub>O<sub>3</sub> and 40MgO@Al<sub>2</sub>O<sub>3</sub> was studied by keeping all other parameters constant (adsorbent dose  $3 \text{ g L}^{-1}$ , contact time = 8 h, temperature  $30 \pm 2$  °C) (Fig. 4.10). It was observed that, with increasing initial F<sup>-</sup> concentration ( $C_0$ ), F<sup>-</sup> adsorption capacity ( $q_e$ ) of the adsorbent increased and then reached a plateau. This might be due to more availability of F<sup>-</sup> ions at higher F<sup>-</sup> concentration (up to  $C_0 = 500 \text{ mg L}^{-1}$ ) for adsorption and the plateau forms due to the saturation of active sites of the adsorbent surfaces at higher F<sup>-</sup> concentrations. The adsorption capacity of 40MgO@Al<sub>2</sub>O<sub>3</sub> was found to be higher than that of mesoporous Al<sub>2</sub>O<sub>3</sub>. The presence of MgO in 40MgO@Al<sub>2</sub>O<sub>3</sub> enhanced the F<sup>-</sup> removal capacity of the adsorbents (for example, when initial F<sup>-</sup> concentration was  $1000 \text{ mg L}^{-1}$ , the  $q_e$  values of mesoporous Al<sub>2</sub>O<sub>3</sub> and 40MgO@Al<sub>2</sub>O<sub>3</sub> were  $23 \text{ mg g}^{-1}$  and  $37 \text{ mg g}^{-1}$  respectively).

Table 4.2. Comparison of pseudo-first order and pseudo-second order kinetic models parameters, and calculated  $q_{e(cal)}$  and experimental  $q_{e(exp)}$  values for different initial F<sup>-</sup> concentrations of Al<sub>2</sub>O<sub>3</sub> and 40MgO@Al<sub>2</sub>O<sub>3</sub>.

	C <sub>0</sub> (mg L <sup>-1</sup> )	q <sub>e(exp)</sub> (mg g <sup>-1</sup> )	Pseudo first order			Pseudo second order		
			q <sub>e(cal)</sub> (mg g <sup>-1</sup> )	k <sub>1</sub> (min <sup>-1</sup> )	R <sup>2</sup>	q <sub>e(cal)</sub> (mg g <sup>-1</sup> )	k <sub>2</sub> (g mg <sup>-1</sup> min <sup>-1</sup> )	R <sup>2</sup>
Al <sub>2</sub> O <sub>3</sub>	5	1.38	0.49	0.0055	0.8740	1.40	0.0315	0.9976
	10	1.80	1.12	0.0114	0.7113	1.89	0.0191	0.9943
	20	2.24	1.43	0.0094	0.8488	2.35	0.0131	0.9919
	30	2.89	1.31	0.0107	0.7336	3.00	0.0169	0.9985
40MgO@Al <sub>2</sub> O <sub>3</sub>	5	1.43	1.73	0.0101	0.9258	1.56	0.0044	0.9970
	10	2.9	2.4	0.0067	0.9567	3.12	0.0036	0.9939
	20	5.45	4.85	0.0076	0.9573	5.72	0.0018	0.9951
	30	7.35	6.4	0.0067	0.9812	7.83	0.0010	0.9962

Moreover, higher pH<sub>PZC</sub> of 40MgO@Al<sub>2</sub>O<sub>3</sub> (pH<sub>PZC</sub> = 11.2) in comparison with pure mesoporous Al<sub>2</sub>O<sub>3</sub> (pH<sub>PZC</sub> = 8.2) may also contribute towards its higher adsorption capacity.

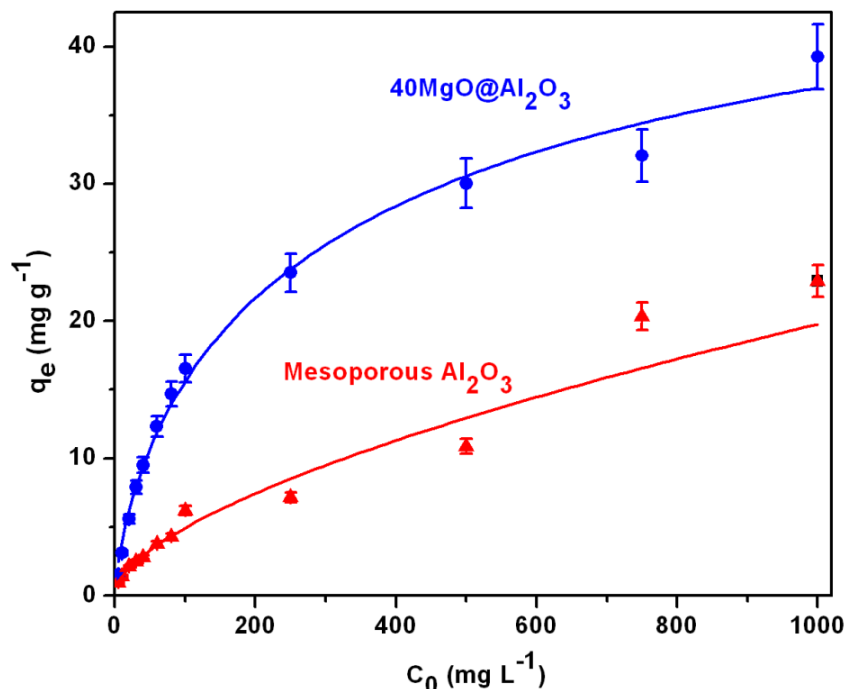


Fig. 4.10. Effect of initial F<sup>-</sup> concentration on F<sup>-</sup> adsorption capacity of Al<sub>2</sub>O<sub>3</sub> and 40MgO@Al<sub>2</sub>O<sub>3</sub> (C<sub>0</sub> = 5 to 1000 mg L<sup>-1</sup>, adsorbent dose = 3 g L<sup>-1</sup>, contact time = 8 h, pH = 6.8 ± 0.2).

#### 4.2.2.6. Adsorption Isotherms

After conducting equilibrium studies to determine the optimum conditions for maximum F<sup>-</sup> removal of mesoporous Al<sub>2</sub>O<sub>3</sub> and 40MgO@Al<sub>2</sub>O<sub>3</sub>, the obtained equilibrium data were analyzed by fitting them in linear isotherm model equations, viz. Freundlich (equation 4),<sup>99</sup> and Langmuir isotherms (equation 5)<sup>100</sup> (Chapter 1, page no. 15). The fitted parameters obtained from these models are summarized in Table 4.3. After fitting the F<sup>-</sup> adsorption data to the Freundlich and Langmuir isotherm models following important points were noted: (i) in case of mesoporous Al<sub>2</sub>O<sub>3</sub>, adsorption data for F<sup>-</sup> ion concentration range 5 to 1000 mg L<sup>-1</sup>, fitted well with Freundlich model (R<sup>2</sup><sub>(Freundlich)</sub> = 0.9690 and R<sup>2</sup><sub>(Langmuir)</sub> = 0.7391), whereas data for 40MgO@Al<sub>2</sub>O<sub>3</sub> fitted well with both Freundlich (R<sup>2</sup> = 0.9639) as well as Langmuir (R<sup>2</sup> = 0.9752) model (Fig. 4.11). When the adsorption data for low F<sup>-</sup>

concentration range (5- 100 mg L<sup>-1</sup>) were considered, the data for mesoporous Al<sub>2</sub>O<sub>3</sub> fitted well with Freundlich model ( $R^2_{\text{(Freundlich)}} = 0.9609$  whereas  $R^2_{\text{(Langmuir)}} = 0.7902$ ) and for 40MgO@Al<sub>2</sub>O<sub>3</sub>, F<sup>-</sup> adsorption data fitted well with both Freundlich ( $R^2 = 0.9627$ ) as well as Langmuir ( $R^2 = 0.9756$ ) model. So, F<sup>-</sup> adsorption on 40MgO@Al<sub>2</sub>O<sub>3</sub> can be considered to be favorable and single layered.<sup>84, 149, 151</sup> (ii)  $K_f$  value of 40MgO@Al<sub>2</sub>O<sub>3</sub> was greater than that of Al<sub>2</sub>O<sub>3</sub>. This indicates adsorption capacity of 40MgO@Al<sub>2</sub>O<sub>3</sub> is higher than that of mesoporous Al<sub>2</sub>O<sub>3</sub>. (iii) 1/n value of 40MgO@Al<sub>2</sub>O<sub>3</sub> is less than unity as well as less than the 1/n value of pure Al<sub>2</sub>O<sub>3</sub>. This fact also indicates that, favorable adsorption of F<sup>-</sup> on 40MgO@Al<sub>2</sub>O<sub>3</sub>. (iv) within the experimental conditions, maximum F<sup>-</sup> adsorption capacity of 40MgO@Al<sub>2</sub>O<sub>3</sub> is 37.45 mg g<sup>-1</sup> which is higher than that of pure mesoporous Al<sub>2</sub>O<sub>3</sub> (23.35 mg g<sup>-1</sup>).

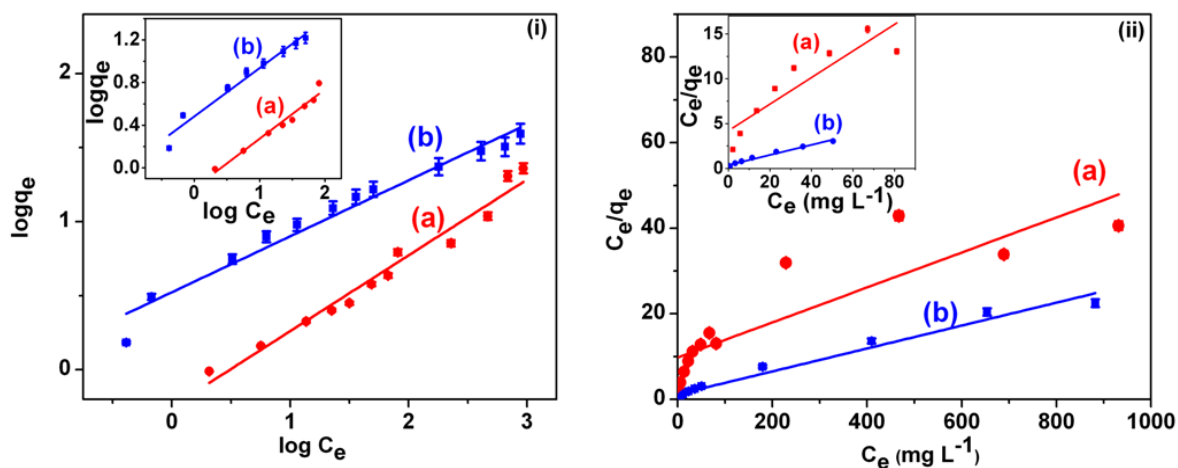


Fig. 4.11. (i) Freundlich adsorption isotherm models and (ii) Langmuir adsorption isotherm models for adsorption of F<sup>-</sup> on (a) mesoporous Al<sub>2</sub>O<sub>3</sub> and (b) 40MgO@Al<sub>2</sub>O<sub>3</sub>. (C<sub>0</sub> = 5 to 1000 mg L<sup>-1</sup>, adsorbent dose = 3 g L<sup>-1</sup>, contact time = 8 h, pH = 6.8 ± 0.2) (The inset is isotherm models at low F<sup>-</sup> concentration ranging from 5 to 100 mg L<sup>-1</sup>).

Another essential feature of the Langmuir model can be given in terms of dimensionless separation factor 'r', which was calculated using equation 14.<sup>231</sup> In the present case 'r' values were found to be < 1 (varies from 0.98 to 0.04 with the variation of C<sub>0</sub> from 5 to 1000 mg L<sup>-1</sup>), it was assumed that favorable adsorption of F<sup>-</sup> occurred on mesoporous Al<sub>2</sub>O<sub>3</sub> and 40MgO@Al<sub>2</sub>O<sub>3</sub>.<sup>91</sup>

Table 4.3. Langmuir and Freundlich isotherm parameters for F<sup>-</sup> adsorption on Al<sub>2</sub>O<sub>3</sub> and 40MgO@Al<sub>2</sub>O<sub>3</sub> at pH of 6.8 ± 0.2.

	Langmuir isotherm			Freundlich isotherm		
	Q <sub>0</sub> (mg g <sup>-1</sup> )	b (l mg <sup>-1</sup> )	R <sup>2</sup>	K <sub>f</sub>	1/n	R <sup>2</sup>
Al <sub>2</sub> O <sub>3</sub>	24.45	0.004	0.7391	0.56	0.51	0.9690
40MgO@Al <sub>2</sub> O <sub>3</sub>	37.35	0.0227	0.9752	3.33	0.38	0.9639

#### 4.2.2.7. Effect of initial pH

The effect of initial pH of the solution on F<sup>-</sup> removal by mesoporous Al<sub>2</sub>O<sub>3</sub> and 40MgO@Al<sub>2</sub>O<sub>3</sub> was investigated at different pH ranging from 4 to 10, with a constant adsorbent dose of 3 g L<sup>-1</sup>, initial F<sup>-</sup> concentration 30 mg L<sup>-1</sup>, contact time 8 h and shown in Fig. 4.12. It was observed that, F<sup>-</sup> adsorption capacity of 40MgO@Al<sub>2</sub>O<sub>3</sub> did not change much within the pH range of 4-10.

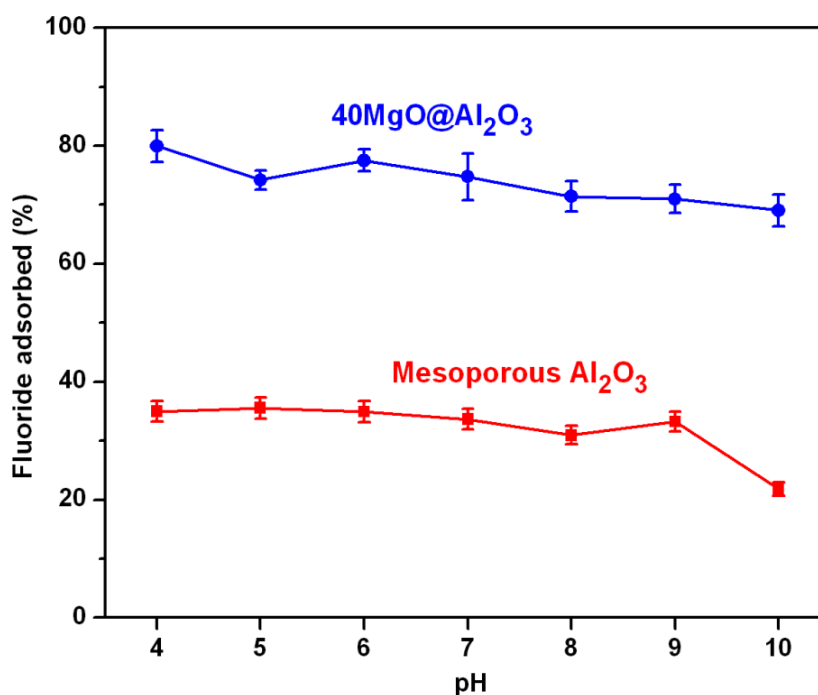


Fig. 4.12. Effect of initial pH on F<sup>-</sup> adsorption capacity of Al<sub>2</sub>O<sub>3</sub> and 40MgO@Al<sub>2</sub>O<sub>3</sub> (adsorbent dose = 3 g L<sup>-1</sup>, C<sub>0</sub> = 30 mg L<sup>-1</sup>, contact time = 8 h).



#### 4.2.2.8. Effect of co-existing anions

To study the effect of co-existing anions on F<sup>-</sup> adsorption of synthesized adsorbents, 10 mg L<sup>-1</sup> and 100 mg L<sup>-1</sup> initial concentrations of Cl<sup>-</sup>, NO<sub>3</sub><sup>-</sup>, SO<sub>4</sub><sup>2-</sup> and HCO<sub>3</sub><sup>-</sup> were used while keeping the initial fluoride concentration as 10 mg L<sup>-1</sup> and adsorbent dose 3 g L<sup>-1</sup>. The effect of competing anions (such as Cl<sup>-</sup>, NO<sub>3</sub><sup>-</sup>, SO<sub>4</sub><sup>2-</sup>, and HCO<sub>3</sub><sup>-</sup>) on F<sup>-</sup> adsorption of mesoporous Al<sub>2</sub>O<sub>3</sub> and 40MgO@Al<sub>2</sub>O<sub>3</sub> adsorbents is shown in Fig. 4.13. It was observed that, within the experimental condition presence of Cl<sup>-</sup>, NO<sub>3</sub><sup>-</sup>, SO<sub>4</sub><sup>2-</sup>, and HCO<sub>3</sub><sup>-</sup> ions did not affect much (< 7 %) the F<sup>-</sup> removal capacity of 40MgO@Al<sub>2</sub>O<sub>3</sub> as well as Al<sub>2</sub>O<sub>3</sub>.

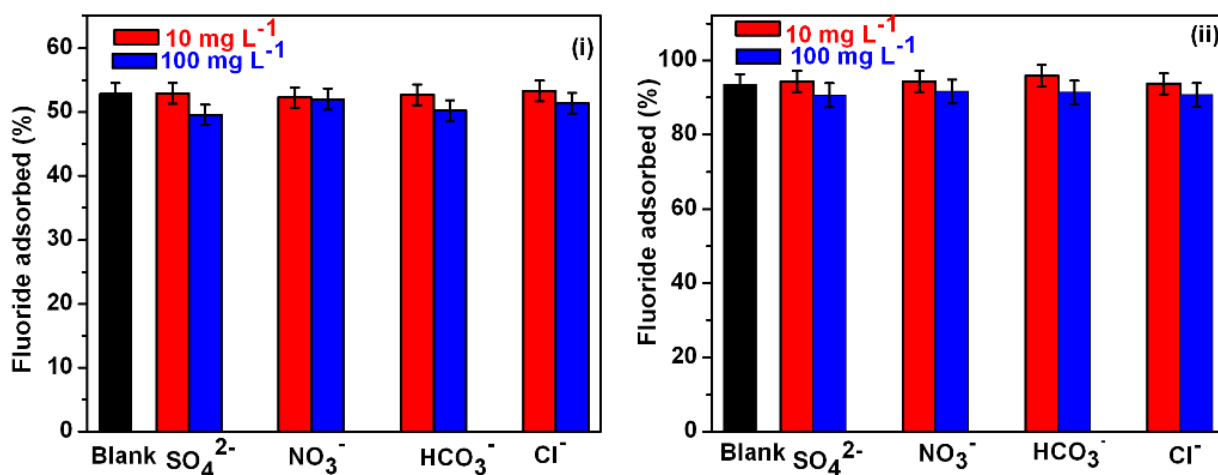


Fig. 4.13. Effect of co-existing anions on fluoride adsorption capacity of Al<sub>2</sub>O<sub>3</sub> and 40MgO@Al<sub>2</sub>O<sub>3</sub> (adsorbent dose = 3 g L<sup>-1</sup>, C<sub>0</sub> = 10 mg L<sup>-1</sup>, contact time = 8 h).

#### 4.3. Summary of results

- i. MgO nanoparticle loaded mesoporous Al<sub>2</sub>O<sub>3</sub> adsorbents were successfully synthesized.
- ii. It was observed that, loading of 40 wt% MgO nanoparticle within the porous matrix of mesoporous Al<sub>2</sub>O<sub>3</sub> significantly enhanced the F<sup>-</sup> removal capacity of the adsorbent (40MgO@Al<sub>2</sub>O<sub>3</sub>) in comparison with pure mesoporous Al<sub>2</sub>O<sub>3</sub>, commercial Al<sub>2</sub>O<sub>3</sub> as well as pure MgO nanoparticle.<sup>122</sup>
- iii. 40MgO@Al<sub>2</sub>O<sub>3</sub> exhibited its capability to remove ~90% F<sup>-</sup> from an aqueous F<sup>-</sup> solution having initial F<sup>-</sup> concentration 10 mg L<sup>-1</sup>.

## CHAPTER 5

### Preparation of CaO nanoparticle loaded mesoporous Al<sub>2</sub>O<sub>3</sub> based adsorbents and their fluoride removal performance from water

#### 5.1. Experimental procedure for materials synthesis

##### 5.1.1. Materials used

Aluminium nitrate nonahydrate, sodium hydroxide, sodium sulphate were procured from Fisher Scientific, India; triethanol amine, sodium hydrogen carbonate, sodium chloride, sodium nitrate and sodium fluoride were procured from Merck, India; calcium nitrate tetrahydrate, stearic acid, and hydrochloric acid from S.d fine-chem. limited, India. All these chemicals were used as received.

##### 5.1.2. Synthesis of mesoporous Al<sub>2</sub>O<sub>3</sub>

Mesoporous Al<sub>2</sub>O<sub>3</sub> was synthesized as per the procedure described in Chapter 2, section 2.1.2.

##### 5.1.3. Preparation of CaO nanoparticle loaded mesoporous Al<sub>2</sub>O<sub>3</sub><sup>230</sup>

CaO nanoparticle loaded mesoporous aluminas were synthesized using a wet impregnation technique. CaO loaded mesoporous aluminas were synthesized with different loading percentages (5, 10, 15, 20 and 30 wt.%) of CaO on mesoporous Al<sub>2</sub>O<sub>3</sub>. In a typical synthesis, in a beaker calculated amount of aqueous solution of calcium nitrate tetrahydrate was mixed with desired amount of mesoporous Al<sub>2</sub>O<sub>3</sub> powder and stirred for 12 h. The mixture was then dried on a hot plate at 90 °C. The dried material was calcined at 550 °C for 4 h in air atmosphere to obtain CaO loaded mesoporous Al<sub>2</sub>O<sub>3</sub> adsorbent. The 5, 10, 15, 20, 25 and 30 wt.% CaO loaded mesoporous Al<sub>2</sub>O<sub>3</sub> are now onwards will be referred as 5CaO@Al<sub>2</sub>O<sub>3</sub>,

10CaO@Al<sub>2</sub>O<sub>3</sub>, 15CaO@Al<sub>2</sub>O<sub>3</sub>, 20CaO@Al<sub>2</sub>O<sub>3</sub>, 25CaO@Al<sub>2</sub>O<sub>3</sub> and 30CaO@Al<sub>2</sub>O<sub>3</sub> respectively.

## 5.2. Results and discussions

### 5.2.1. Characterization

#### 5.2.1.1. X-ray diffraction analysis<sup>230</sup>

Wide angle powder XRD analysis was carried out for the synthesized materials to identify their crystalline phase and shown in Fig. 5.1. Though the XRD patterns of the materials showed poor crystalline structure with broad diffraction peaks, characteristic peaks of  $\gamma$ - Al<sub>2</sub>O<sub>3</sub> were identified (ICDD card no. 10-0425). The peak intensities corresponding to  $\gamma$ - Al<sub>2</sub>O<sub>3</sub> phase were found to be decreased with increasing CaO loading in the sample. For the samples having higher loading of CaO (e.g. 20CaO@ Al<sub>2</sub>O<sub>3</sub>, 30CaO@ Al<sub>2</sub>O<sub>3</sub>) a broad peak in the region of  $2\theta = 26$ - 35° was observed which can be assigned for amorphous CaO (ICDD card no. 28-0775). This fact indicates the amorphous nature of CaO in CaO loaded mesoporous Al<sub>2</sub>O<sub>3</sub> samples.

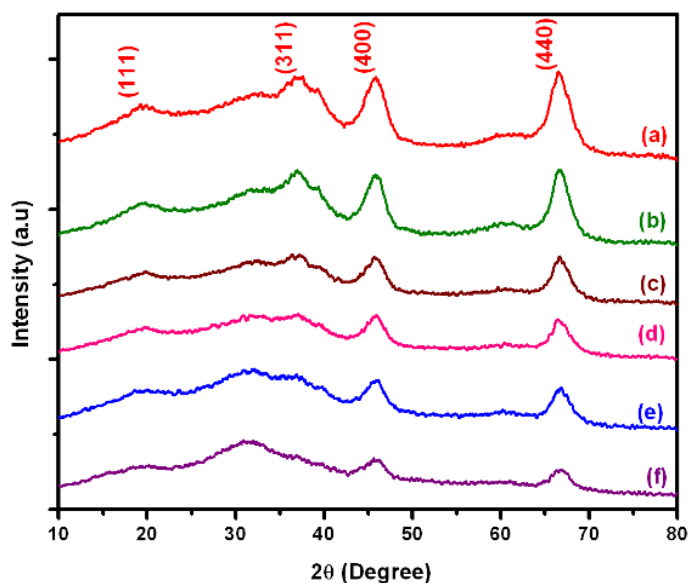


Fig. 5.1. XRD pattern of (a) mesoporous Al<sub>2</sub>O<sub>3</sub>, (b) 5CaO@Al<sub>2</sub>O<sub>3</sub>, (c) 10CaO@Al<sub>2</sub>O<sub>3</sub>, (d) 15CaO@Al<sub>2</sub>O<sub>3</sub>, (e) 20CaO@Al<sub>2</sub>O<sub>3</sub> and (f) 30CaO@Al<sub>2</sub>O<sub>3</sub>.

### 5.2.1.2. N<sub>2</sub> adsorption-desorption analysis<sup>230</sup>

N<sub>2</sub> adsorption - desorption isotherm analysis were conducted to evaluate the surface area and pore structure of the synthesized Al<sub>2</sub>O<sub>3</sub> and CaO loaded aluminas. Isotherms for all the samples (Fig. 5.2(i)) are typical type IV isotherms with H2 hysteresis loop, which indicates the mesoporous nature of synthesized materials. H2 hysteresis loops for these isotherms suggest the presence of pores with narrow necks with wide bodies (often referred to as ink bottle pores).<sup>229</sup> Large hysteresis loop for pure mesoporous Al<sub>2</sub>O<sub>3</sub> can be attributed to its large pores.<sup>199</sup> However, loading of CaO on mesoporous Al<sub>2</sub>O<sub>3</sub> does not change the shape of the isotherms. The pore size distribution of all the synthesized samples also confirmed the mesoporosity of the materials (Fig. 5.2 (ii)). Surface area and pore size parameters of the synthesized adsorbents are summarized in Table 5.1. It was observed that BET surface area and pore volume of CaO loaded aluminas decreased with increasing CaO loading on mesoporous Al<sub>2</sub>O<sub>3</sub>. Decrease of pore volume indicated that CaO particles are incorporated into the pores of Al<sub>2</sub>O<sub>3</sub>.

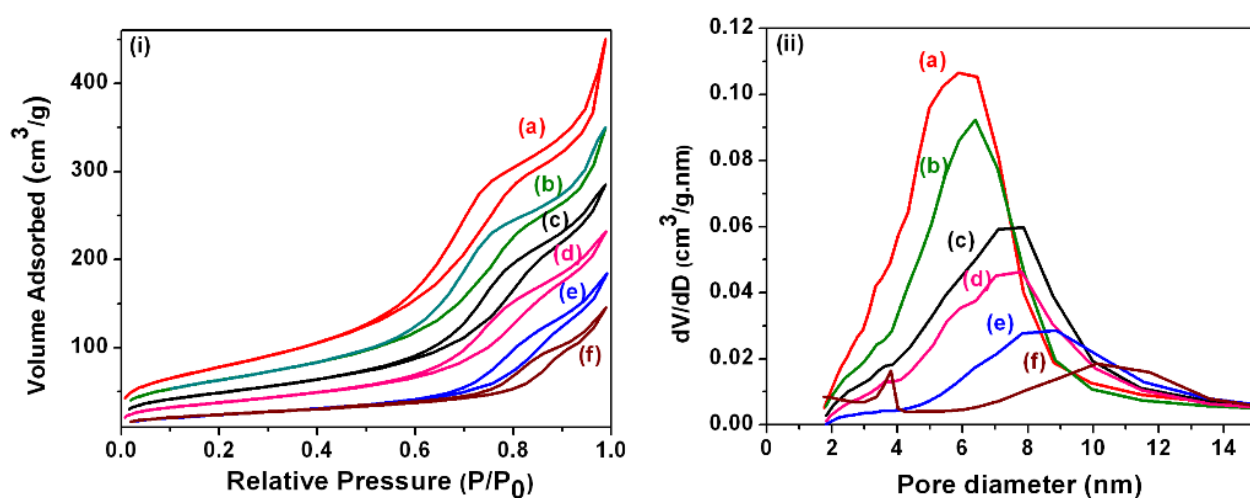


Fig. 5.2. (i) N<sub>2</sub>-adsorption-desorption isotherms and (ii) Pore size distributions of (a) mesoporous Al<sub>2</sub>O<sub>3</sub>, (b) 5CaO@Al<sub>2</sub>O<sub>3</sub>, (c) 10CaO@Al<sub>2</sub>O<sub>3</sub>, (d) 15CaO@Al<sub>2</sub>O<sub>3</sub>, (e) 20CaO@Al<sub>2</sub>O<sub>3</sub> and (f) 30CaO@Al<sub>2</sub>O<sub>3</sub>.

Table 5.1. Surface area and pore size parameters of the synthesized adsorbents obtained by means of N<sub>2</sub> adsorption-desorption study.

Sample description	BET surface area (m <sup>2</sup> /g)	BJH average pore size (nm)	BJH pore volume (cm <sup>3</sup> /g)
Al <sub>2</sub> O <sub>3</sub>	284	7.4	0.70
5CaO@Al <sub>2</sub> O <sub>3</sub>	228	7.5	0.55
10CaO@Al <sub>2</sub> O <sub>3</sub>	175	8.2	0.45
15CaO@Al <sub>2</sub> O <sub>3</sub>	135	8.6	0.36
20CaO@Al <sub>2</sub> O <sub>3</sub>	93	10.1	0.29
30CaO@Al <sub>2</sub> O <sub>3</sub>	86	10.9	0.23

#### 5.2.1.3. HRTEM analysis<sup>230</sup>

In order to study the surface morphology of the synthesized materials HRTEM images of the samples were recorded and shown in Fig. 5.3. The morphological aspects of the samples show wormhole-like, highly connected porous structure of the materials. However, the pores are disordered in nature. In Fig. 5.3(b) it was observed that, presence of CaO nanoparticles (5- 8 nm) on mesoporous Al<sub>2</sub>O<sub>3</sub> matrix in the CaO loaded sample.

#### 5.2.1.4. Analysis of pH<sub>PZC</sub> of the adsorbents<sup>230</sup>

The pH<sub>PZC</sub> values for pure Al<sub>2</sub>O<sub>3</sub> and 20CaO@Al<sub>2</sub>O<sub>3</sub> were found to be 8.2 and 11.91 respectively (Fig. 5.4). This indicates that CaO loaded Al<sub>2</sub>O<sub>3</sub> should have better F<sup>-</sup> adsorption capacity than that of pure Al<sub>2</sub>O<sub>3</sub>.

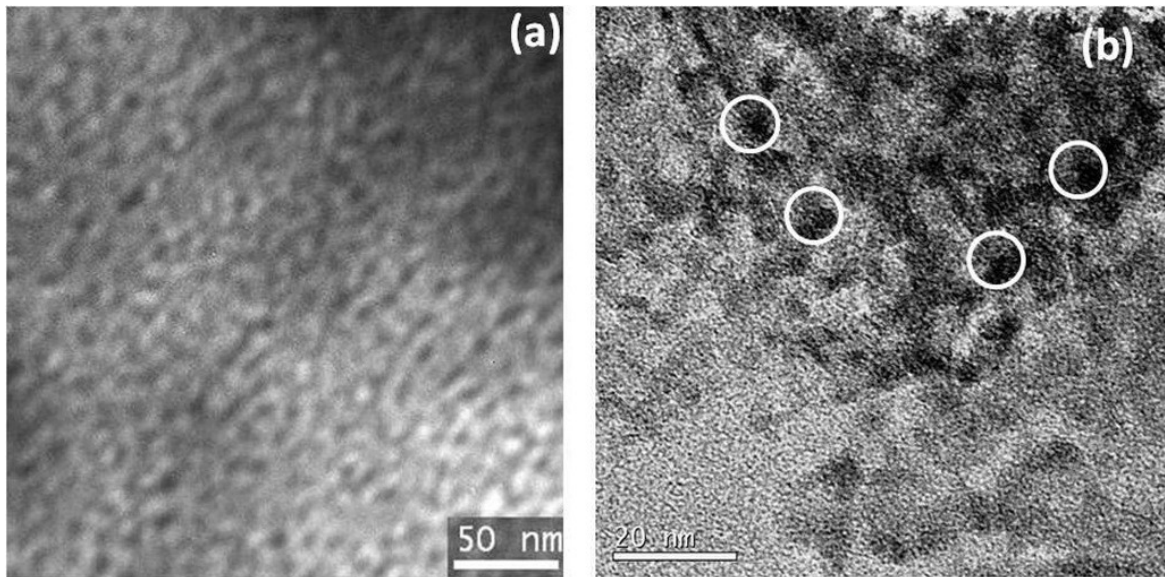


Fig. 5.3. HRTEM images of (a) Al<sub>2</sub>O<sub>3</sub> and (b) 20CaO@Al<sub>2</sub>O<sub>3</sub>. CaO nanoparticles are shown within the circle.

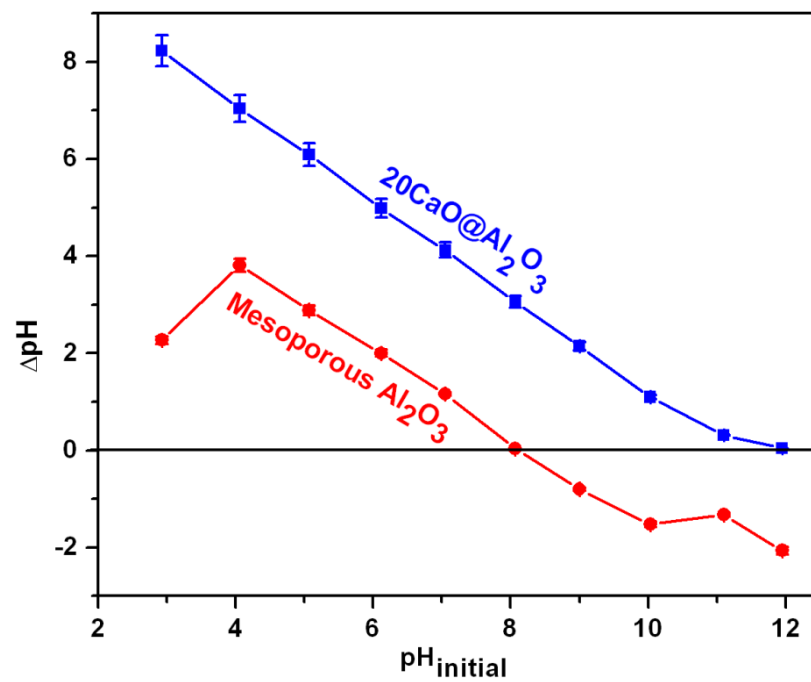
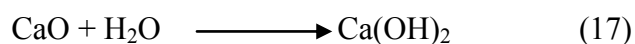


Fig. 5.4. Plot for determination of pHPZC of Al<sub>2</sub>O<sub>3</sub> and 20CaO@Al<sub>2</sub>O<sub>3</sub> adsorbent.

## 5.2.2. Fluoride adsorption studies<sup>230</sup>

### 5.2.2.1. Optimization of adsorbent composition

Fluoride adsorption studies of various amount of CaO loaded aluminas were performed using a solution having initial F<sup>-</sup> concentration 30 mg L<sup>-1</sup> and adsorbent dose of 3 g L<sup>-1</sup>. It was observed that pure mesoporous Al<sub>2</sub>O<sub>3</sub> adsorbed ~28% F<sup>-</sup> whereas 20CaO@Al<sub>2</sub>O<sub>3</sub> adsorbed ~ 90% F<sup>-</sup>. However, it was also observed that, due to 5 wt.% CaO loading BET surface area of Al<sub>2</sub>O<sub>3</sub> has decreased from 284 m<sup>2</sup>/g to 228 m<sup>2</sup>/g and percentage of F<sup>-</sup> adsorption has also decreased from ~28 to ~13% in comparison with pure mesoporous Al<sub>2</sub>O<sub>3</sub> (Fig. 5.5). But, further increase of CaO loading (up to 20 wt.%) resulted in increase of percentage of F<sup>-</sup> adsorption (up to 90%) though the surface area of the adsorbents was decreased with increasing CaO loading (Table 5.1). This is because of the fact that, surface area of the adsorbent is not the only factor which dictates the F<sup>-</sup> adsorption capacity of CaO loaded Al<sub>2</sub>O<sub>3</sub> adsorbents. Presence of CaO also plays an important role. According to Patel et al.<sup>125</sup>, in presence of water CaO forms calcium hydroxide and adsorption of F<sup>-</sup> occurs by surface chemical reaction, in which -OH groups of Ca(OH)<sub>2</sub> are replaced by F<sup>-</sup> resulting in formation of CaF<sub>2</sub>. This process can be represented by the following equations:



When less amount of CaO (5 wt.%) was present in the adsorbent, CaO nanoparticles were deposited within some pores of mesoporous Al<sub>2</sub>O<sub>3</sub> matrix which caused the reduction of the surface area of the adsorbent but these CaO particles might not get chance to come in contact with F<sup>-</sup> ions. So, the fluoride adsorption on 5CaO@Al<sub>2</sub>O<sub>3</sub> was found to be lower than that of Al<sub>2</sub>O<sub>3</sub>. But when CaO loading was further increased, some CaO particles were also deposited on the surface of Al<sub>2</sub>O<sub>3</sub> matrix. These CaO particles reacted with F<sup>-</sup> and formed CaF<sub>2</sub>. Due to this reason, adsorbents having higher CaO loading exhibited their higher F<sup>-</sup> adsorption capacities than that of pure Al<sub>2</sub>O<sub>3</sub>. 20 wt.% CaO loaded Al<sub>2</sub>O<sub>3</sub> sample exhibited its capacity to absorb ~90% F<sup>-</sup> from solution with a very fast rate (detailed discussion is in section

5.2.2.4), further increase of CaO loading did not show much enhancement in F<sup>-</sup> adsorption capacity of the adsorbents. So, further studies were performed by using 20CaO@Al<sub>2</sub>O<sub>3</sub>.

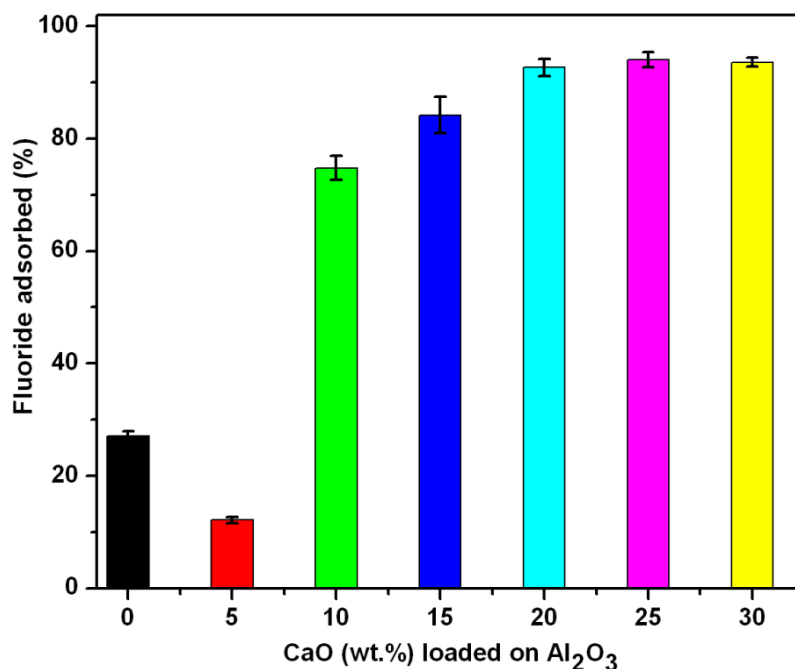


Fig. 5.5. Effect of CaO loading on mesoporous Al<sub>2</sub>O<sub>3</sub> for removal of F<sup>-</sup>. (C<sub>0</sub> = 30 mg L<sup>-1</sup>, adsorbent dose = 3 g L<sup>-1</sup>, contact time = 8 h, pH = 6.8 ± 0.2)

#### 5.2.2.2. Effect of adsorbent dose

The effect of adsorption dose on removal of F<sup>-</sup> using pure Al<sub>2</sub>O<sub>3</sub> and 20CaO@Al<sub>2</sub>O<sub>3</sub> is shown in Fig. 5.6, in which percent of F<sup>-</sup> removal is plotted against adsorption dose. It was observed that, initially the percent of F<sup>-</sup> removal increased rapidly with the increase of adsorbent dose and maximum F<sup>-</sup> removal occurred when adsorbent was 3 g L<sup>-1</sup>. The percentage of F<sup>-</sup> removal increased from 20 to 90% with increase in 20CaO@Al<sub>2</sub>O<sub>3</sub> dose from 0.25 to 7.5 g L<sup>-1</sup> at C<sub>0</sub> 10 mg L<sup>-1</sup>. However, when the adsorbent dose was more than 3 g L<sup>-1</sup>, not much increase in F<sup>-</sup> removal was observed with increasing adsorbent dose. Hence, 3 g L<sup>-1</sup> of adsorbent dose of Al<sub>2</sub>O<sub>3</sub> and 20CaO@Al<sub>2</sub>O<sub>3</sub> was considered for further studies. It was observed that 3 g L<sup>-1</sup> of pure Al<sub>2</sub>O<sub>3</sub> removed ~56% fluoride from a solution having fluoride concentration of 10 mg L<sup>-1</sup> whereas, 20CaO@Al<sub>2</sub>O<sub>3</sub> removed ~90% fluoride from the same solution.



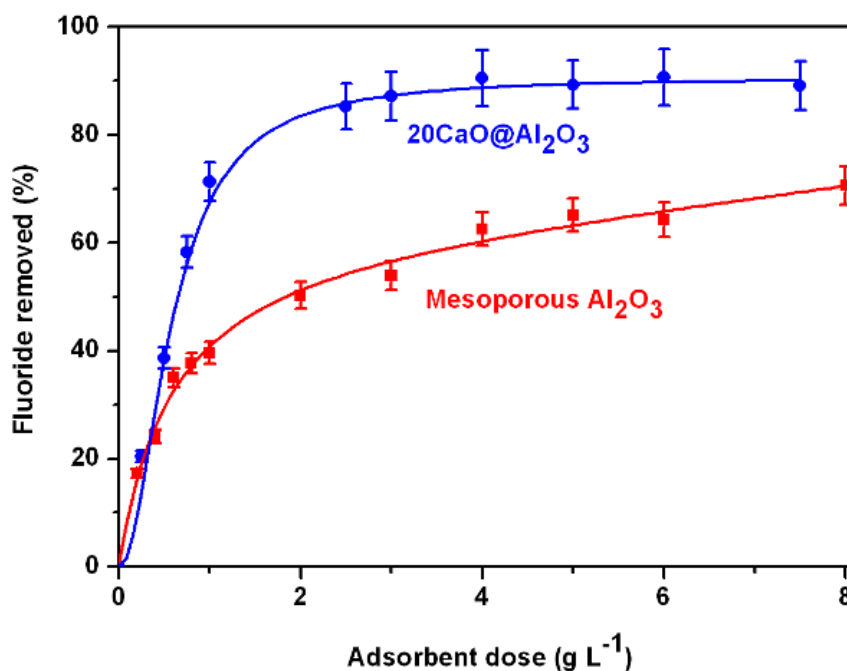


Fig. 5.6. Effect of adsorbent dose on F<sup>-</sup> adsorption capacity of adsorbents. (C<sub>0</sub> = 10 mg L<sup>-1</sup>, contact time = 8 h, pH = 6.8 ± 0.2).

### 5.2.2.3. Effect of contact time

The fluoride sorption on Al<sub>2</sub>O<sub>3</sub> and 20CaO@Al<sub>2</sub>O<sub>3</sub> was investigated as a function of time using a solution having initial F<sup>-</sup> concentration 30 mg L<sup>-1</sup> and adsorbent dose was 3 g L<sup>-1</sup>. It was observed that, F<sup>-</sup> adsorption by Al<sub>2</sub>O<sub>3</sub> and 20CaO@Al<sub>2</sub>O<sub>3</sub> was increased with time (Fig. 5.7). Initially, F<sup>-</sup> adsorption on adsorbents occurred fast, followed by slower adsorption till the equilibrium was reached. In case of Al<sub>2</sub>O<sub>3</sub>, ~ 22% F<sup>-</sup> sorption occurred within 1 h contact time and equilibrium reached in 5 h and ~ 29% F<sup>-</sup> was adsorbed. In case of 20CaO@Al<sub>2</sub>O<sub>3</sub>, ~ 82% F<sup>-</sup> was adsorbed within 15 min and the equilibrium was reached in 30 min with ~ 92% F<sup>-</sup> adsorption.

### 5.2.2.4. Adsorption Kinetics

The adsorption kinetics of F<sup>-</sup> onto 20CaO@Al<sub>2</sub>O<sub>3</sub> is shown in Fig. 5.8. It was observed that, within 15 min 90% F<sup>-</sup> adsorption was observed and equilibrium was reached in 30 min.

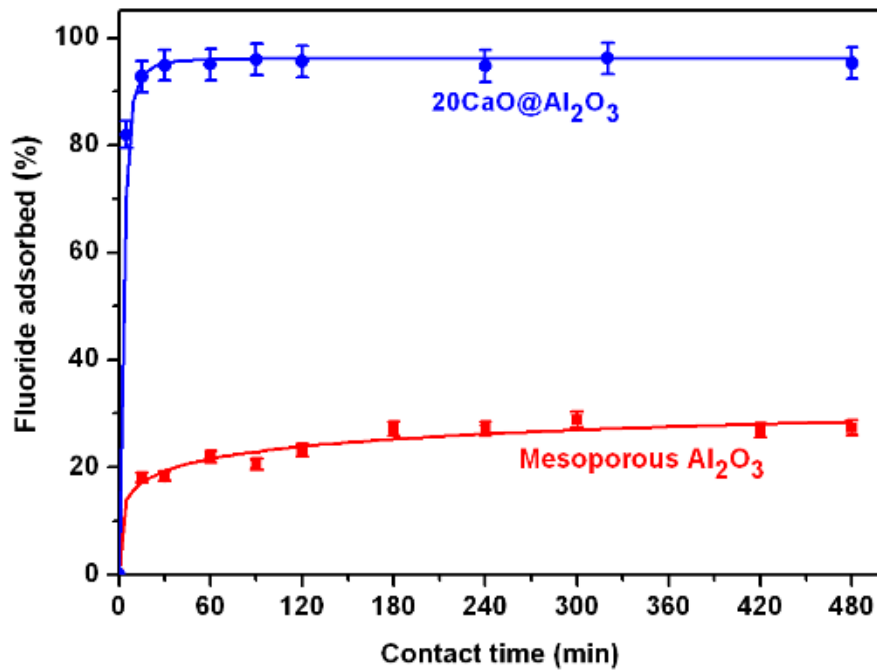


Fig. 5.7. Effect of contact time on F<sup>-</sup> adsorption capacity of adsorbents. (C<sub>0</sub> = 30 mg L<sup>-1</sup>, adsorbent dose = 3 g L<sup>-1</sup>, pH = 6.8 ± 0.2).

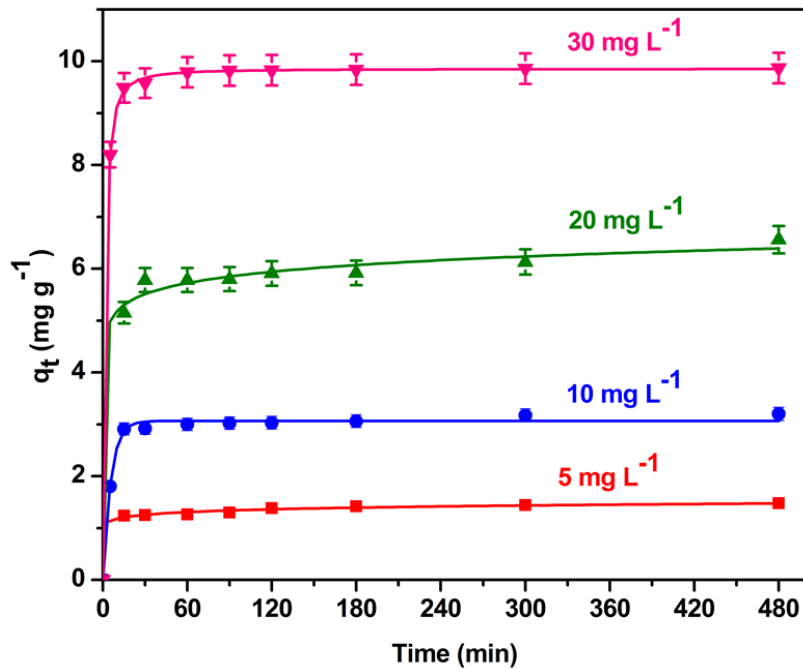


Fig. 5.8. Adsorption kinetic curves of F<sup>-</sup> adsorption on 20CaO@Al<sub>2</sub>O<sub>3</sub> at different initial F<sup>-</sup> concentrations (C<sub>0</sub> = 5, 10, 20 and 30 mg L<sup>-1</sup>, adsorbent dose = 3 g L<sup>-1</sup>, pH = 6.8 ± 0.2).

The kinetics of F<sup>-</sup> adsorption on 20CaO@Al<sub>2</sub>O<sub>3</sub> was analyzed using Lagergren's pseudo-first order kinetic model (equation 2)<sup>95</sup> and Ho's pseudo-second order kinetic model<sup>96</sup> (equation 3) (chapter 1, page no. 14) to identify the dynamics of the F<sup>-</sup> adsorption process. The plots  $\log(q_e - q_t)$  vs  $t$  according to pseudo-first order kinetics are shown in Fig.5.9(i). For pseudo-second order kinetics model, the kinetics data were plotted  $t/q_t$  vs  $t$  and  $k_2$  values were calculated from the intercept and slope of the plot (Fig. 5.9(ii)). Parameters obtained after fitting the experimental data in the pseudo-first order and pseudo-second order kinetic models are shown in Table 5.2. As indicated in Table 5.2, the R<sup>2</sup> values of pseudo-second order kinetic model (> 0.99) were much higher than those of pseudo-first order kinetic model (< 0.94) and the adsorption capacity values ( $q_{e(cal)}$ ) calculated from pseudo-second order kinetic model were much closer to the experimental values ( $q_{e(exp)}$ ). These facts indicate the applicability of the pseudo-second order kinetic model for F<sup>-</sup> adsorption on 20CaO@Al<sub>2</sub>O<sub>3</sub>. Similar trend was also reported by Camacho et al.<sup>98</sup> and Jagtap et al.<sup>91</sup> Pseudo-second order fitting suggests that chemisorption might be responsible for the F<sup>-</sup> adsorption on 20CaO@Al<sub>2</sub>O<sub>3</sub>. Aluminium fluoride complexes and CaF<sub>2</sub> are the main components forming on the surface of the adsorbents during F<sup>-</sup> adsorption process.<sup>98, 173</sup>

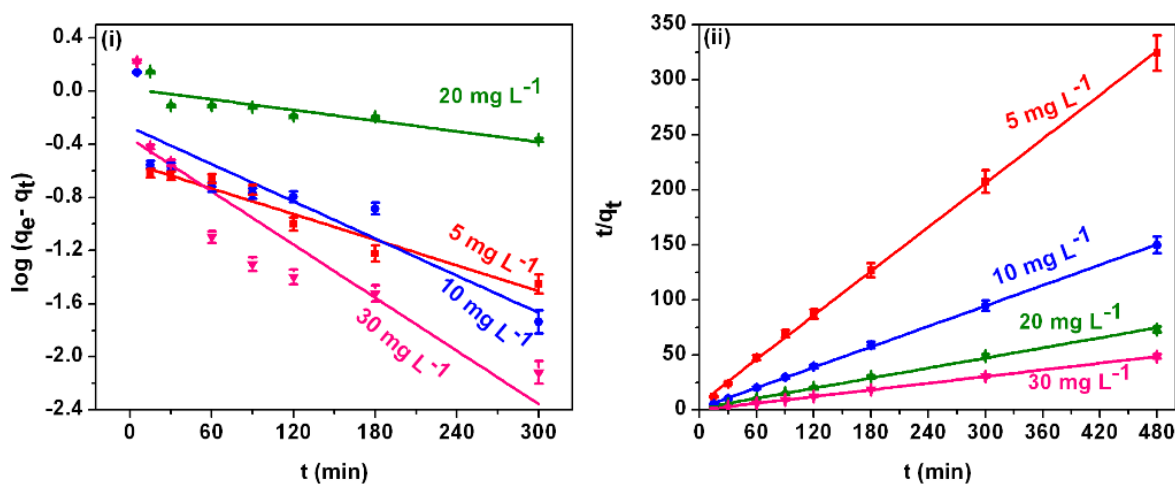


Fig. 5.9. (i) Pseudo first order adsorption kinetic model and (ii) Pseudo second order adsorption kinetic model for F<sup>-</sup> adsorption on 20CaO@Al<sub>2</sub>O<sub>3</sub> ( $C_0 = 5, 10, 20$  and  $30 \text{ mg L}^{-1}$ , adsorbent dose =  $3 \text{ g L}^{-1}$ , pH=  $6.8 \pm 0.2$ ).

Table 5.2. Comparison of pseudo-first order and pseudo-second order kinetic models parameters, and calculated  $q_{e(cal)}$  and experimental  $q_{e(exp)}$  values for different initial F<sup>-</sup> concentrations of Al<sub>2</sub>O<sub>3</sub> and 20CaO@Al<sub>2</sub>O<sub>3</sub>.

	Pseudo first order					Pseudo second order		
	C <sub>0</sub> (mg L <sup>-1</sup> )	q <sub>e(exp)</sub> (mg g <sup>-1</sup> )	q <sub>e(cal)</sub> (mg g <sup>-1</sup> )	k <sub>1</sub> (min <sup>-1</sup> )	R <sup>2</sup>	q <sub>e(cal)</sub> (mg g <sup>-1</sup> )	k <sub>2</sub> (g mg <sup>-1</sup> min <sup>-1</sup> )	R <sup>2</sup>
Al <sub>2</sub> O <sub>3</sub>	5	1.38	0.49	0.0055	0.8740	1.40	0.0315	0.9976
	10	1.80	1.12	0.0114	0.7113	1.89	0.0191	0.9943
	20	2.24	1.43	0.0094	0.8488	2.35	0.0131	0.9919
	30	2.89	1.31	0.0107	0.7336	3.00	0.0169	0.9985
20CaO@Al <sub>2</sub> O <sub>3</sub>	5	1.48	0.29	0.0074	0.9392	1.49	0.0753	0.9994
	10	3.20	0.54	0.0107	0.7797	3.22	0.0649	0.9994
	20	6.56	1.04	0.0031	0.6980	6.55	0.0151	0.9974
	30	9.87	0.44	0.0154	0.7781	9.88	0.1315	1

### 5.2.2.5. Effect of initial fluoride concentration

The effect of initial F<sup>-</sup> concentration (5 mg L<sup>-1</sup>- 1000 mg L<sup>-1</sup>) on F<sup>-</sup> adsorption capacity by Al<sub>2</sub>O<sub>3</sub> and 20CaO@Al<sub>2</sub>O<sub>3</sub> was studied by keeping all other parameters constant (adsorbent dose 3 g L<sup>-1</sup>, contact time = 8 h) as shown in Fig. 5.10. It was observed that, with increase in F<sup>-</sup> concentration, F<sup>-</sup> adsorption capacity (q<sub>e</sub>) of the adsorbent increases and then reaches a plateau. This should be due to more availability of F<sup>-</sup> ions at higher F<sup>-</sup> concentration (up to C<sub>0</sub> = 750 mg L<sup>-1</sup>) for adsorption and the plateau forms due to the saturation of active sites of the adsorbent surfaces. The F<sup>-</sup> adsorption capacity of 20CaO@Al<sub>2</sub>O<sub>3</sub> is higher than that of Al<sub>2</sub>O<sub>3</sub>. The presence of CaO in 20CaO@Al<sub>2</sub>O<sub>3</sub> enhances the F<sup>-</sup> removal capacity of the adsorbents by forming insoluble CaF<sub>2</sub>. Moreover, the higher pH<sub>PZC</sub> of 20CaO@Al<sub>2</sub>O<sub>3</sub> may also contribute towards its higher adsorption capacity. A closer look of these results infers that the increase in q<sub>e</sub> is very significant as 135 mg g<sup>-1</sup> of q<sub>e</sub> could be achieved at higher fluoride concentration.

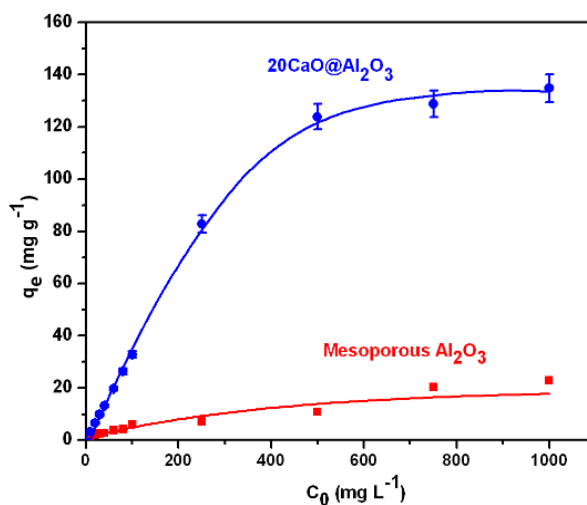


Fig. 5.10. Effect of initial F<sup>-</sup> concentration on F<sup>-</sup> adsorption capacity of Al<sub>2</sub>O<sub>3</sub> and 20CaO@Al<sub>2</sub>O<sub>3</sub> (adsorbent dose = 3 g L<sup>-1</sup>, contact time = 8 h, pH = 6.8 ± 0.2).

### 5.2.2.6. Adsorption Isotherms

In the present study two well known isotherm models, viz, Freundlich isotherm<sup>99</sup> (equation 4) and Langmuir isotherm<sup>100</sup> (equation 5) (Chapter 1, page no. 15) were used. The values of Freundlich parameters K<sub>f</sub> and 1/n were obtained from the slope and intercept of the linear Freundlich plot of log q<sub>e</sub> vs log C<sub>e</sub> shown in Fig. 5.11 (i). The values of Langmuir parameters Q<sub>0</sub> and b were calculated from the slope and

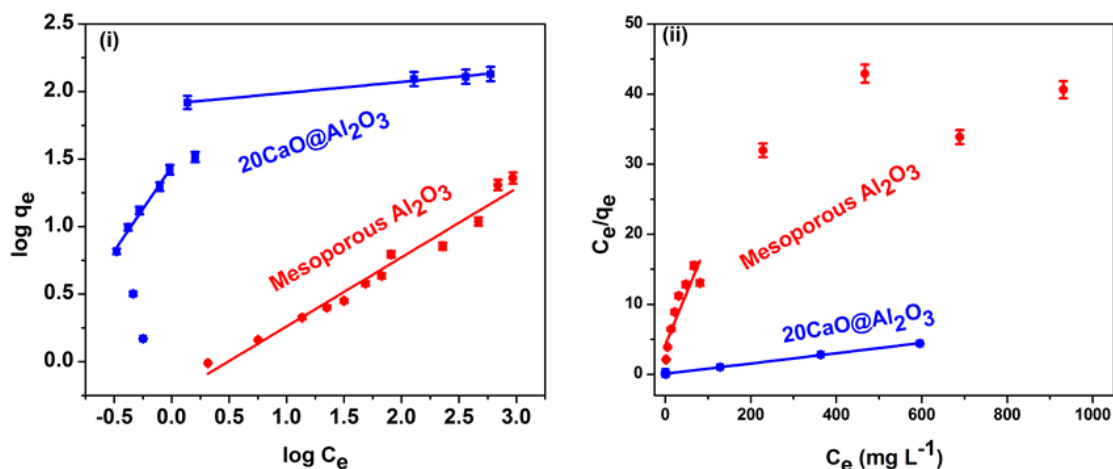
intercept of the linear Langmuir plot of  $C_e/q_e$  vs  $C_e$  (Fig. 5.11(ii)). Parameters obtained from Freundlich and Langmuir isotherms are listed in Table 5.3. Freundlich adsorption isotherm model fitted well for pure Al<sub>2</sub>O<sub>3</sub> ( $R^2 = 0.9690$ ) (Fig. 5.11(i)) whereas, Langmuir adsorption isotherm model fitted well for 20CaO@Al<sub>2</sub>O<sub>3</sub> ( $R^2 = 0.9942$ ) (Fig. 5.11(ii)) in the F<sup>-</sup> concentration range of 5 to 1000 mg L<sup>-1</sup>. However, at lower F<sup>-</sup> concentrations (5 to 100 mg L<sup>-1</sup>) ( $R^2 = 0.9852$ ) as well as at higher F<sup>-</sup> concentrations (250 to 1000 mg L<sup>-1</sup>) ( $R^2 = 0.9878$ ) the adsorption of F<sup>-</sup> on 20CaO@Al<sub>2</sub>O<sub>3</sub> follows the Freundlich isotherm model (Fig. 5.11(i)). It was observed that, at lower F<sup>-</sup> concentrations, adsorption of F<sup>-</sup> on 20CaO@Al<sub>2</sub>O<sub>3</sub> occurred very fast whereas at higher F<sup>-</sup> concentrations the F<sup>-</sup> adsorption increased slowly and reached saturation. This may be due to the multilayer adsorption of F<sup>-</sup> ions inside the pores of 20CaO@Al<sub>2</sub>O<sub>3</sub>. The maximum F<sup>-</sup> adsorption capacities of Al<sub>2</sub>O<sub>3</sub> and 20CaO@Al<sub>2</sub>O<sub>3</sub> obtained from Langmuir isotherm were found to be 24.45 mg g<sup>-1</sup> and 136.99 mg g<sup>-1</sup> respectively. Theoretically calculated Q<sub>0</sub> value of 20CaO@Al<sub>2</sub>O<sub>3</sub> is 155 mg g<sup>-1</sup> (considering Q<sub>0</sub> of pure Al<sub>2</sub>O<sub>3</sub> 24.45 mg g<sup>-1</sup> and assuming all CaO, present in 20CaO@Al<sub>2</sub>O<sub>3</sub>, reacted with F<sup>-</sup> and formed CaF<sub>2</sub>). But Q<sub>0</sub> value of 20CaO@Al<sub>2</sub>O<sub>3</sub> obtained from experiments is 136.99 mg g<sup>-1</sup>, which is 88% of the theoretical value. This is because of the fact that, certain amount of CaO nanoparticles were deposited within the pores of mesoporous Al<sub>2</sub>O<sub>3</sub> and these CaO particles might not get a chance to come in contact with F<sup>-</sup> ions and so did not participate in F<sup>-</sup> adsorption process.

Table 5.3. Langmuir and Freundlich isotherm parameters for F<sup>-</sup> adsorption on Al<sub>2</sub>O<sub>3</sub> and 20CaO@Al<sub>2</sub>O<sub>3</sub> at pH of 6.8 ± 0.2.

	Langmuir isotherm			Freundlich isotherm		
	Q <sub>0</sub> (mg g <sup>-1</sup> )	b (l mg <sup>-1</sup> )	R <sup>2</sup>	K <sub>f</sub>	1/n	R <sup>2</sup>
Al <sub>2</sub> O <sub>3</sub>	24.45	0.004	0.7391	0.56	0.5115	0.9690
20CaO@Al <sub>2</sub> O <sub>3</sub>	136.99	0.084	0.9942	13.59	0.4182	0.5779

To predict the adsorption efficiency, the dimensionless quantity ‘r’ was calculated using equation 14.<sup>231</sup> In the present case ‘r’ values were found to be < 1

(varies from 0.98 to 0.01 with the variation of C<sub>0</sub> from 5 to 1000 mg L<sup>-1</sup>), it was



assumed that favorable adsorption of F<sup>-</sup> occurred on Al<sub>2</sub>O<sub>3</sub> and CaO20@Al<sub>2</sub>O<sub>3</sub>.

Fig. 5.11. (i) Freundlich adsorption isotherm and (ii) Langmuir adsorption isotherm for adsorption of F<sup>-</sup> on Al<sub>2</sub>O<sub>3</sub> and 20CaO@Al<sub>2</sub>O<sub>3</sub>. (C<sub>0</sub> = 5 mg L<sup>-1</sup> to 1000 mg L<sup>-1</sup>, adsorbent dose = 3 g L<sup>-1</sup>, contact time = 8 h, pH = 6.8 ± 0.2).

### 5.2.2.7. Effect of initial pH

The effect of initial pH of the solution on F<sup>-</sup> removal by Al<sub>2</sub>O<sub>3</sub> and 20CaO@Al<sub>2</sub>O<sub>3</sub> was investigated at different pH ranging from 4 to 10, with a constant adsorbent dose of 3 g L<sup>-1</sup>, initial F<sup>-</sup> concentration 30 mg L<sup>-1</sup>, contact time 8 h, temperature (30 ± 2) °C and shown in Fig. 5.12. The adsorption of F<sup>-</sup> on Al<sub>2</sub>O<sub>3</sub> does not change much within the pH range of 4 to 9. However, when initial pH was 10, the fluoride adsorption capacity of pure Al<sub>2</sub>O<sub>3</sub> was decreased. This might be due to the fact that pH<sub>PZC</sub> value of Al<sub>2</sub>O<sub>3</sub> 8.2 which is < 10. F<sup>-</sup> adsorption capacity of 20CaO@Al<sub>2</sub>O<sub>3</sub> does not affect much within the pH range of 4- 10.

### 5.2.2.8. Effect of co-existing anions

To study the effect of co-existing anions on F<sup>-</sup> adsorption on synthesized adsorbents, 10 mg L<sup>-1</sup> and 100 mg L<sup>-1</sup> initial concentrations of Cl<sup>-</sup>, NO<sub>3</sub><sup>-</sup>, SO<sub>4</sub><sup>2-</sup> and HCO<sub>3</sub><sup>-</sup> were used while keeping the initial F<sup>-</sup> concentration as 10 mg L<sup>-1</sup>. The effect of co-ions on the F<sup>-</sup> removal efficiency of Al<sub>2</sub>O<sub>3</sub> and 20CaO@Al<sub>2</sub>O<sub>3</sub> is shown in Fig. 5.13. It was observed that the presence of Cl<sup>-</sup> did not affect F<sup>-</sup> removal capacity of the adsorbents.

Presence of NO<sub>3</sub><sup>-</sup> (10 and 100 mg L<sup>-1</sup>) and SO<sub>4</sub><sup>2-</sup> (10 mg L<sup>-1</sup>) ions slightly decreased (~ 2- 3%) the F<sup>-</sup> removal capacity of the adsorbent, whereas ~8- 9% decrease was observed when HCO<sub>3</sub><sup>-</sup> was present. This is due to the competition between HCO<sub>3</sub><sup>-</sup> and F<sup>-</sup> for the adsorption on active sites of the adsorbent.

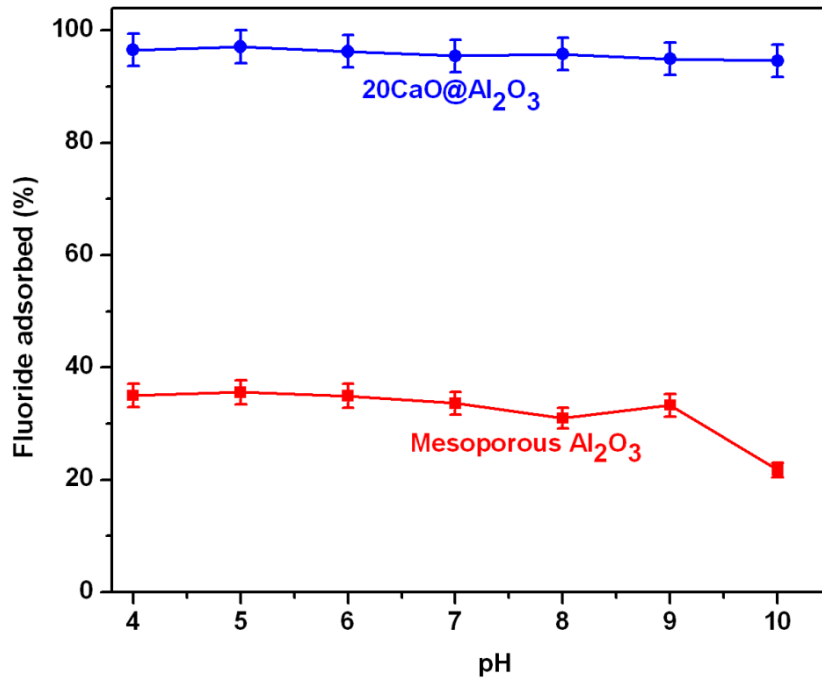


Fig. 5.12. Effect of initial pH on F<sup>-</sup> adsorption capacity of Al<sub>2</sub>O<sub>3</sub> and 20CaO@Al<sub>2</sub>O<sub>3</sub> (adsorbent dose = 3 g L<sup>-1</sup>, C<sub>0</sub> = 30 mg L<sup>-1</sup>, contact time = 8 h).

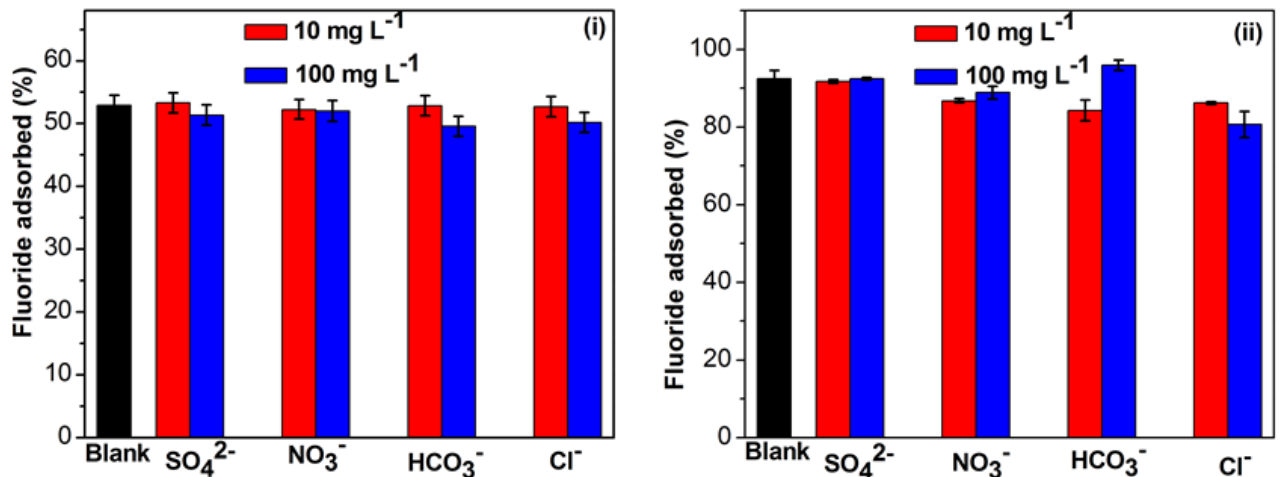


Fig. 5.13. Effect of co-existing anions on F<sup>-</sup> adsorption capacity of Al<sub>2</sub>O<sub>3</sub> and 20CaO@Al<sub>2</sub>O<sub>3</sub> (adsorbent dose = 3 g L<sup>-1</sup>, C<sub>0</sub> = 10 mg L<sup>-1</sup>, contact time = 8 h).



### 5.3. Summary of results

- i. CaO nanoparticle loaded mesoporous Al<sub>2</sub>O<sub>3</sub> adsorbents, were successfully synthesized.
- ii. It has been demonstrated that loading of 20 wt.% CaO significantly enhances the F<sup>-</sup> removal capacity of mesoporous Al<sub>2</sub>O<sub>3</sub>.
- iii. 20CaO@Al<sub>2</sub>O<sub>3</sub> is capable of removing ~90% F<sup>-</sup> within 15 min using a moderate adsorbent dose of 3 g L<sup>-1</sup> whereas, pure Al<sub>2</sub>O<sub>3</sub> removes only ~22% after 1 h.
- iv. The maximum F<sup>-</sup> adsorption capacities of Al<sub>2</sub>O<sub>3</sub> and 20CaO@Al<sub>2</sub>O<sub>3</sub> were found to be 24.45 mg g<sup>-1</sup> and 136.99 mg g<sup>-1</sup> respectively.
- v. The CaO loaded mesoporous Al<sub>2</sub>O<sub>3</sub> exhibited higher F<sup>-</sup> removal capacity than that of pure mesoporous Al<sub>2</sub>O<sub>3</sub> and commercial Al<sub>2</sub>O<sub>3</sub> (ca. 7 mg g<sup>-1</sup>),<sup>84</sup> because of Ca may react with F<sup>-</sup> ions to form CaF<sub>2</sub> precipitates and high value of pH<sub>PZC</sub> of 20CaO@Al<sub>2</sub>O<sub>3</sub>.
- vi. 20CaO@Al<sub>2</sub>O<sub>3</sub> exhibited good F<sup>-</sup> removal efficiency over a wide range of pH (4- 10).

## Chapter 6

### Conclusions and future scope of work

#### 6.1. Conclusions

Based on the results obtained (which have been discussed in Chapter 2 to Chapter 5) following conclusions have been drawn:

- (i) An aqueous solution based cost effective chemical method has been developed for preparation of mesoporous  $\text{Al}_2\text{O}_3$  and  $\text{ZrO}_2$ ,  $\text{MgO}$  and  $\text{CaO}$  nanoparticle loaded mesoporous  $\text{Al}_2\text{O}_3$ .
- (ii) Synthesized mesoporous  $\text{Al}_2\text{O}_3$  showed more  $\text{F}^-$  adsorption capacity than commercial  $\text{Al}_2\text{O}_3$ .
- (iii) Incorporation of metal oxide nanoparticle ( $\text{ZrO}_2$ ,  $\text{MgO}$  and  $\text{CaO}$ ) enhances the  $\text{F}^-$  adsorption capacity of mesoporous  $\text{Al}_2\text{O}_3$ .
- (iv) The decreasing order of  $\text{F}^-$  removal performance of the synthesized adsorbents is as follows:  
 $\text{CaO@Al}_2\text{O}_3 > \text{MgO@Al}_2\text{O}_3 > \text{ZrO}_2\text{@Al}_2\text{O}_3 > \text{Synthesized Al}_2\text{O}_3 > \text{Commercial Al}_2\text{O}_3$ .
- (v)  $\text{CaO}$  nanoparticle loaded mesoporous  $\text{Al}_2\text{O}_3$  showed faster kinetics as well as higher  $\text{F}^-$  adsorption capacity. The maximum  $\text{F}^-$  adsorption capacity of  $20\text{CaO@Al}_2\text{O}_3$  was found to be  $137 \text{ mg g}^{-1}$ .  $20\text{CaO@Al}_2\text{O}_3$  exhibited good  $\text{F}^-$  removal efficiency over a wide range of pH (4- 10).

Table 6.1. Comparison of F<sup>-</sup> adsorption performance of synthesized adsorbents.

Adsorbent	Maximum adsorption capacity (mg g <sup>-1</sup> )	F <sup>-</sup> adsorbed (%) (time=8 h, C <sub>0</sub> =30 mg L <sup>-1</sup> , Adsorbent dose = 3 g L <sup>-1</sup> )
20CaO@Al <sub>2</sub> O <sub>3</sub>	137	90
40MgO@Al <sub>2</sub> O <sub>3</sub>	37.35	83
15ZrO <sub>2</sub> @Al <sub>2</sub> O <sub>3</sub>	16.27	48
Synthesized Al <sub>2</sub> O <sub>3</sub>	5.13	28
Commercial Al <sub>2</sub> O <sub>3</sub>	2.08	12

(vi) Generally, the fluoride concentration in contaminated ground water is ~ 5- 10 mg L<sup>-1</sup>. It was observed that, when the solutions having F<sup>-</sup> concentration of 5 mg L<sup>-1</sup> and 10 mg L<sup>-1</sup> was treated with 20CaO@Al<sub>2</sub>O<sub>3</sub> with adsorbent dose of 3 g L<sup>-1</sup>, the F<sup>-</sup> concentration of treated water became < 1 mg L<sup>-1</sup>, which is well below the recommendation of WHO.

Overall, the simplicity and cost-effectiveness of the developed method and high F<sup>-</sup> adsorption capacity as well as fast rate of adsorption makes 20CaO@Al<sub>2</sub>O<sub>3</sub> a potential candidate as an adsorbent in F<sup>-</sup> removal devices.

## 6.2. Future scope of work

1. Detailed investigations on recycling the adsorbents and fluoride removal capacity of recycled adsorbent.
2. Detailed investigations on the mechanism of F<sup>-</sup> ion adsorption process which dictates the selectivity of ion adsorption of the adsorbents in presence of different ions.
3. Detailed investigations on defluoridation of drinking water using synthesized mesoporous alumina based adsorbents.
4. Coating of synthesized adsorbents on solid matrix (like honeycomb) and use this honeycomb to construct F<sup>-</sup> removal device/kit.
5. Synthesized mesoporous materials can also be used for adsorption of arsenic ions present in water.

**References**

1. D. Dayananda and N. N. Ghosh, Applications of Nanomaterials for removal of fluoride from Water, *Encyclopedia of Nanoscience and Nanotechnology*, H. S. Nalwa (ed.), American Scientific Publishers, USA, **(2015)** (Accepted).
2. A. Bhatnagar, E. Kumar and M. Sillanpää, *Chem. Eng. J.* 171, 811-840 **(2011)**.
3. K. B. J. Fawell, J. Chilton, E. Dahi, L. Fewtrell and Y. Magara, *Fluoride in Drinking-water*, IWA Publishing, London **(2006)**.
4. D. Ozsvath, *Rev Environ Sci Biotechnol* 8, 59-79 **(2009)**.
5. P. T. C. Harrison, *J. Fluorine Chem.* 126, 1448-1456 **(2005)**.
6. World Health Organization, Guidelines for Drinking-Water Quality [Electronic Resource]: Incorporating First Addendum (vol. I) Recommendations, 375-377 **(2006)**.
7. X. Fan, D. J. Parker and M. D. Smith, *Water Res.* 37, 4929-4937 **(2003)**.
8. D. P. Das, J. Das and K. Parida, *J. Colloid Interface Sci.* 261, 213-220 **(2003)**.
9. I. Abe, S. Iwasaki, T. Tokimoto, N. Kawasaki, T. Nakamura and S. Tanada, *J. Colloid Interface Sci.* 275, 35-39 **(2004)**.
10. E. J. Reardon and Y. Wang, *Environ. Sci. Technol.* 34, 3247-3253 **(2000)**.
11. D. Banks, C. Reimann, O. Røyset, H. Skarphagen and O. M. Sæther, *Appl. Geochem.* 10, 1-16 **(1995)**.
12. W. B. Apambire, D. R. Boyle and F. A. Michel, *Environ. Geol.* 33, 13-24 **(1997)**.
13. A. M. Raichur and M. Jyoti Basu, *Sep. Purif. Technol.* 24, 121-127 **(2001)**.
14. F. Shen, X. Chen, P. Gao and G. Chen, *Chem. Eng. Sci.* 58, 987-993 **(2003)**.
15. Y.-H. Li, S. Wang, X. Zhang, J. Wei, C. Xu, Z. Luan and D. Wu, *Mater. Res. Bull.* 38, 469-476 **(2003)**.

16. G. de la Puente, J. J. Pis, J. A. Menéndez and P. Grange, *J. Anal. Appl. Pyrolysis* 43, 125-138 (1997).
17. M. Amini, K. Mueller, K. C. Abbaspour, T. Rosenberg, M. Afyuni, K. N. Møller, M. Sarr and C. A. Johnson, *Environ. Sci. Technol.* 42, 3662-3668 (2008).
18. W. Czarnowski, K. Wrzeźniowska and J. Krechniak, *Sci. Total Environ.* 191, 177-184 (1996).
19. S. Ayoob, A. K. Gupta and V. T. Bhat, *Crit. Rev. Environ. Sci. Technol.* 38, 401-470 (2008).
20. T. Chernet, Y. Trafi and V. Valles, *Water Res.* 35, 2819 (2002).
21. W. K. N. Moturi, M. P. Tole and T. C. Davies, *Environ. Geochem. Health* 24, 123 (2002).
22. S. Ayoob and A. K. Gupta, *Crit. Rev. Environ. Sci. Technol.* 36, 433-487 (2006).
23. N. Azbar and A. Turkman, *Water Sci. Technol.* 42, 403-407 (2000).
24. W. Wang, R. Li, J. Tan, K. Luo, L. Yang, H. Li and Y. Li, *Fluoride* 35, 122-129 (2002).
25. M. Agarwal, K. Rai, R. Shrivastav and S. Dass, *J. Clean Prod.* 11, 439-444 (2003).
26. C. B. Dissanayake, *Int. J. Environ. Stud.* 19, 137-156 (1991).
27. S. P. S. Teotia, M. Teotia and R. K. Singh, *Fluoride* 14, 69-74 (1981).
28. A. K. Susheela, *Curr. Sci.* 77, 1250-1255 (1999).
29. S. Jagtap, M. K. Yenkie, N. Labhsetwar and S. Rayalu, *Chem. Rev.* 112, 2454-2466 (2012).

30. M. Mohapatra, S. Anand, B. K. Mishra, D. E. Giles and P. Singh, *J. Environ. Manage.* 91, 67-77 (2009).
31. P. Loganathan, S. Vigneswaran, J. Kandasamy and R. Naidu, *J. Hazard. Mater.* 248-249, 1-19 (2013).
32. E. Kumar, A. Bhatnagar, W. Hogland, M. Marques and M. Sillanpää, *Chem. Eng. J.* 241, 443-456 (2014).
33. M. J. Larsen and E. I. F. Pearce, *Caries Res.* 36, 341-346 (2002).
34. Z. Qafas, K. E. Kacemi, E. Ennaassia and M. C. Edelahi, *Sci. Lett.* 3, 1 (2002).
35. J. H. Potgeiter, *ChemSA* 317-318 (1990).
36. W. G. Nawlakhe, D. N. Kulkarni, B. N. Pathak and K. R. Bulusu, *Indian J. Environ. Health* 17, 26-27 (1975).
37. K. R. Bulusu, B. B. Sunderasan, B. N. Pathak, W. G. Nawlakhe, D. N. Kulkarni and V. P. Thergaonkar, *J. Inst. Eng. (India)* 60, 1 (1979).
38. W. G. Nawlakhe and A. V. J. Rao, *J. Indian Water Works Assoc.* 13, 287-290 (1990).
39. C. N. Martyn, D. J. P. Barker, C. Osmond, E. C. Harris, J. A. Edwardson and R. F. Lacey, *Lancet* 333, 61-62 (1989).
40. A. Lhassani, M. Rumeau, D. Benjelloun and M. Pontie, *Water Res.* 35, 3260-3264 (2001).
41. H. Garmes, F. Persin, J. Sadeaur, G. Pourcelly and M. Mountadar, *Desalination* 145, 287-291 (2002).
42. L. Lounici, D. Adour, A. Belhocine, B. Elmidaoni and N. M. Barion, *Chem. Eng. J.* 81, 153-160 (2001).
43. P. Sehn, *Desalination* 223, 73-84 (2008).

44. A. B. Nasr, C. Charcosset, R. B. Amar and K. Walha, *J. Fluorine Chem.* 150, 92-97 (2013).
45. R. W. Schneiter and E. J. Middlebrooks, *Environ. Int.* 9, 289-291 (1983).
46. P. Fu, H. Ruiz, J. Lozier, K. Thompson and C. Spangenberg, *Desalination* 102, 47-56 (1995).
47. M. Arora, R. C. Maheshwari, S. K. Jain and A. Gupta, *Desalination* 170, 105-112 (2004).
48. P. I. Ndiaye, P. Moulin, L. Dominguez, J. C. Millet and F. Charbit, *Desalination* 173, 25-32 (2005).
49. E. Drioli, F. Laganà, A. Criscuoli and G. Barbieri, *Desalination* 122, 141-145 (1999).
50. M. Tahaikt, R. El Habbani, A. Ait Haddou, I. Achary, Z. Amor, M. Taky, A. Alami, A. Boughriba, M. Hafsi and A. Elmidaoui, *Desalination* 212, 46-53 (2007).
51. J. Loeb, *J. Gen. Physiol.* 3, 667-690 (1921).
52. F. Durmaz, H. Kara, Y. Cengeloglu and M. Ersoz, *Desalination* 177, 51-57 (2005).
53. N. Kabay, Ö. Arar, S. Samatya, Ü. Yüksel and M. Yüksel, *J. Hazard. Mater.* 153, 107-113 (2008).
54. S. Annouar, M. Mountadar, A. Soufiane, A. Elmidaoui and M. A. M. Sahli, *Desalination* 165, 437 (2004).
55. S. Lahnid, M. Tahaikt, K. Elaroui, I. Idrissi, M. Hafsi, I. Laaziz, Z. Amor, F. Tiyal and A. Elmidaoui, *Desalination* 230, 213-219 (2008).
56. N. V. R. Mohan Rao and C. S. Bhaskaran, *J. Fluorine Chem.* 41, 17-24 (1988).

57. M. J. Haron, W. M. Z. Wan Yunus and S. A. Wasay, *Int. J. Environ.* 48, 245-255 (1995).
58. C. Castel, M. Schweizer, M. O. Simonnot and M. Sardin, *Chem. Eng. Sci.* 55, 3341-3352 (2000).
59. N. I. Chubar, V. F. Samanidou, V. S. Kouts, G. G. Gallios, V. A. Kanibolotsky, V. V. Strelko and I. Z. Zhuravlev, *J. Colloid Interface Sci.* 291, 67-74 (2005).
60. Y. Zhou, C. Yu and Y. Shan, *Sep. Purif. Technol.* 36, 89-94 (2004).
61. Y. Veressinina, M. Trapido, V. Ahelik and R. Munter, *Proc. Estonian Academy Sci. Chem.* 50, 81-88 (2001).
62. V. K. Gupta, P. J. M. Carrott, M. M. L. Ribeiro Carrott and Suhas, *Crit. Rev. Environ. Sci. Technol.* 39, 783-842 (2009).
63. S.-X. Teng, S.-G. Wang, W.-X. Gong, X.-W. Liu and B.-Y. Gao, *J. Hazard. Mater.* 168, 1004-1011 (2009).
64. F. Helfferich, *Ion Exchange*, Dover Publication Inc., USA (1995).
65. E. R. Weiner, *Applications of Environmental Aquatic Chemistry*, CRC Press, Taylor and Francis Group, Florida (2008).
66. I. B. Solangi, S. Memon and M. I. Bhangar, *J. Hazard. Mater.* 176, 186-192 (2010).
67. S. Meenakshi and N. Viswanathan, *J. Colloid Interface Sci.* 308, 438-450 (2007).
68. A. Sivasamy, K. P. Singh, D. Mohan and M. Maruthamuthu, *J. Chem. Technol. Biotechnol.* 76, 717-722 (2001).
69. S. M. Maliyekkal, A. K. Sharma and L. Philip, *Water Res.* 40, 3497-3506 (2006).



70. S. Tokunaga, M. J. Haron, S. A. Wasay, K. F. Wong, K. Laosangthum and A. Uchiumi, *Int. J. Environ. Stud.* 48, 17-28 (1995).
71. S. Samatya, Ü. Yüksel, M. Yüksel and N. Kabay, *Sep. Sci. Technol.* 42, 2033-2047 (2007).
72. Y. Wang and E. J. Reardon, *Appl. Geochem.* 16, 531-539 (2001).
73. X.-p. Liao and B. Shi, *Environ. Sci. Technol.* 39, 4628-4632 (2005).
74. F. Luo and K. Inoue, *Solvent Extr. Ion Exch.* 22, 305-322 (2004).
75. M. S. Onyango, Y. Kojima, O. Aoyi, E. C. Bernardo and H. Matsuda, *J. Colloid Interface Sci.* 279, 341-350 (2004).
76. M. S. Onyango, Y. Kojima, A. Kumar, D. Kuchar, M. Kubota and H. Matsuda, *Sep. Sci. Technol.* 41, 683-704 (2006).
77. S. A. Wasay, M. J. Haran and S. Tokunaga, *Water Environ. Res.* 68, 295-300 (1996).
78. M. Barathi, A. S. K. Kumar and N. Rajesh, *J. Environ. Chem. Eng.* 1, 1325-1335 (2013).
79. E. Kumar, A. Bhatnagar, M. Ji, W. Jung, S.-H. Lee, S.-J. Kim, G. Lee, H. Song, J.-Y. Choi, J.-S. Yang and B.-H. Jeon, *Water Res.* 43, 490-498 (2009).
80. A. K. Chaturvedi, K. P. Yadava, K. C. Pathak and V. N. Singh, *Water Air Soil Pollut.* 49, 51-61 (1990).
81. S. Ghorai and K. K. Pant, *Sep. Purif. Technol.* 42, 265-271 (2005).
82. M. G. Sujana, R. S. Thakur and S. B. Rao, *J. Colloid Interface Sci.* 206, 94-101 (1998).
83. R. Leyva Ramos, J. Ovalle-Turrubiartes and M. A. Sanchez-Castillo, *Carbon* 37, 609-617 (1999).
84. Y. Ku and H.-M. Chiou, *Water, Air Soil Pollut.* 133, 349-361 (2002).

85. E. Tchomgui-Kamga, V. Alonzo, C. P. Nanseu-Njiki, N. Audebrand, E. Ngameni and A. Darchen, *Carbon* 48, 333-343 (2010).
86. Y. D. Lai and J. C. Liu, *Sep. Sci. Technol.* 31, 2791-2803 (1996).
87. L. Lv, J. He, M. Wei, D. G. Evans and X. Duan, *J. Hazard. Mater.* 133, 119-128 (2006).
88. W.-X. Gong, J.-H. Qu, R.-P. Liu and H.-C. Lan, *Chem. Eng. J.* 189-190, 126-133 (2012).
89. N. Viswanathan and S. Meenakshi, *Appl. Clay Sci.* 48, 607-611 (2010).
90. S. P. Kamble, G. Deshpande, P. P. Barve, S. Rayalu, N. K. Labhsetwar, A. Malyshev and B. D. Kulkarni, *Desalination* 264, 15-23 (2010).
91. S. Jagtap, M. K. N. Yenkie, N. Labhsetwar and S. Rayalu, *Microporous Mesoporous Mater.* 142, 454-463 (2011).
92. A. A. M. Daifullah, S. M. Yakout and S. A. Elreefy, *J. Hazard. Mater.* 147, 633-643 (2007).
93. K. S. Prasad, Y. Amin and K. Selvaraj, *J. Hazard. Mater.* 276, 232-240 (2014).
94. M. G. Sujana, H. K. Pradhan and S. Anand, *J. Hazard. Mater.* 161, 120-125 (2009).
95. S. Lagergren, *Kungliga Svenska Vetenskapsakademiens Handlingar* 24, 1-34 (1898).
96. Y.-S. Ho and G. McKay, *Process Biochem.* 34, 451-465 (1999).
97. S. Ayoob and A. Gupta, *J. Hazard. Mater.* 152, 976-985 (2008).
98. L. M. Camacho, A. Torres, D. Saha and S. Deng, *J. Colloid Interface Sci.* 349, 307-313 (2010).
99. H.M.F.Freundlich, *Z. Phys. Chem. A* 57, 385-470 (1906).
100. I. Langmuir, *J. Am. Chem. Soc.* 38, 2221-2295 (1916).

- 
101. Y. Tang, X. Guan, T. Su, N. Gao and J. Wang, *Colloids Surf. Physicochem. Eng. Aspects* 337, 33-38 (2009).
  102. R. Leyva-Ramos, N. A. Medellin-Castillo, A. Jacobo-Azuara, J. Mendoza-Barron, L. E. Landin-Rodriguez, J. M. Martinez-Rosales and A. Aragon-Piña, *J. Environ. Eng. Manage.* 18, 301-309 (2008).
  103. S. Ghorai and K. K. Pant, *Chem. Eng. J.* 98, 165 (2004).
  104. A. López Valdivieso, J. L. Reyes Bahena, S. Song and R. Herrera Urbina, *J. Colloid Interface Sci.* 298, 1-5 (2006).
  105. P. L. Bishop and G. Sansoucy, *J. Am. Water Works Assoc.* 554-559 (1978).
  106. S. M. Maliyekkal, S. Shukla, L. Philip and M. N. Indumathi, *Chem. Eng. J.* 140, 183 (2008).
  107. A. Bansiwala, P. Pillewan, R. B. Biniwale and S. S. Rayalu, *Microporous Mesoporous Mater.* 129, 54-61 (2010).
  108. A. Teutli-Sequeira, M. Solache-Ríos, V. Martínez-Miranda and I. Linares-Hernández, *J. Colloid Interface Sci.* 418, 254-260 (2014).
  109. S. S. Tripathy and A. M. Raichur, *J. Hazard. Mater.* 153, 1043 (2008).
  110. T. Zhang, Q. Li, Y. Liu, Y. Duan and W. Zhang, *Chem. Eng. J.* 168, 665-671 (2011).
  111. C. Yang, L. Gao, Y. Wang, X. Tian and S. Komarneni, *Microporous Mesoporous Mater.* 197, 156-163 (2014).
  112. G. Lee, C. Chen, S.-T. Yang and W.-S. Ahn, *Microporous Mesoporous Mater.* 127, 152-156 (2010).
  113. W. Li, C.-Y. Cao, L.-Y. Wu, M.-F. Ge and W.-G. Song, *J. Hazard. Mater.* 198, 143-150 (2011).

- 
114. S. S. Tripathy, J.-L. Bersillon and K. Gopal, *Sep. Purif. Technol.* 50, 310-317 (2006).
115. O. J. Hao, A. M. Asce, C. P. Huang and M. Asce, *J. Environ. Eng.* 112, 1054-1069 (1986).
116. S. Ayoob and A. Gupta, *Chem. Eng. J.* 150, 485-491 (2009).
117. A. Goswami and M. K. Purkait, *Chem. Eng. Res. Des.* 90, 2316-2324 (2012).
118. R. Liu, W. Gong, H. Lan, Y. Gao, H. Liu and J. Qu, *Chem. Eng. J.* 175, 144-149 (2011).
119. E. Kumar, A. Bhatnagar, U. Kumar and M. Sillanpää, *J. Hazard. Mater.* 186, 1042-1049 (2011).
120. S.-G. Wang, Y. Ma, Y.-J. Shi and W.-X. Gong, *J. Chem. Technol. Biotechnol.* 84, 1043-1050 (2009).
121. A. Mahapatra, B. G. Mishra and G. Hota, *Ind. Eng. Chem. Res.* 52, 1554-1561 (2013).
122. R. R. Devi, I. M. Umlong, P. K. Raul, B. Das, S. Banerjee and L. Singh, *J. Exp. Nanosci.* 9, 512-524 (2012).
123. S. M. Maliyekkal, n. Anshup, K. R. Antony and T. Pradeep, *Sci. Total Environ.* 408, 2273-2282 (2010).
124. M. Mohapatra, K. Rout, S. Gupta, P. Singh, S. Anand and B. Mishra, *J. Nanopart. Res.* 12, 681-686 (2010).
125. G. Patel, U. Pal and S. Menon, *Sep. Sci. Technol.* 44, 2806-2826 (2009).
126. M. Mohapatra, T. Padhi, S. Anand and B. K. Mishra, *Desalin. Water Treat.* 50, 376-386 (2012).
127. L. Chai, Y. Wang, N. Zhao, W. Yang and X. You, *Water Res.* 47, 4040-4049 (2013).

128. J. He and J. P. Chen, *J. Colloid Interface Sci.* 416, 227-234 (2014).
129. L. H. Velazquez-Jimenez, R. H. Hurt, J. Matos and J. R. Rangel-Mendez, *Environ. Sci. Technol.* 48, 1166-1174 (2014).
130. B. Pan, J. Xu, B. Wu, Z. Li and X. Liu, *Environ. Sci. Technol.* 47, 9347-9354 (2013).
131. L. Chen, S. He, B.-Y. He, T.-J. Wang, C.-L. Su, C. Zhang and Y. Jin, *Ind. Eng. Chem. Res.* 51, 13150-13156 (2012).
132. G. E. J. Poinern, M. K. Ghosh, Y.-J. Ng, T. B. Issa, S. Anand and P. Singh, *J. Hazard. Mater.* 185, 29-37 (2011).
133. V. Sternitzke, R. Kaegi, J.-N. Audinot, E. Lewin, J. G. Hering and C. A. Johnson, *Environ. Sci. Technol.* 46, 802-809 (2012).
134. J. Wang, W. Xu, L. Chen, Y. Jia, L. Wang, X.-J. Huang and J. Liu, *Chem. Eng. J.* 231, 198-205 (2013).
135. M. Mohapatra, D. Hariprasad, L. Mohapatra, S. Anand and B. K. Mishra, *Appl. Surf. Sci.* 258, 4228-4236 (2012).
136. C. Sairam Sundaram, N. Viswanathan and S. Meenakshi, *J. Hazard. Mater.* 172, 147-151 (2009).
137. M. Mohapatra, K. Rout, P. Singh, S. Anand, S. Layek, H. C. Verma and B. K. Mishra, *J. Hazard. Mater.* 186, 1751-1757 (2011).
138. Y. H. Li, S. Wang, X. Zhang, J. Wei, C. Xu, Z. Luan, D. Wu and B. Wei, *Environ. Technol.* 24, 391-398 (2003).
139. C. Jing, J. Cui, Y. Huang and A. Li, *ACS Appl. Mater. Interfaces* 4, 714-720 (2012).
140. D. Mohan, R. Sharma, V. K. Singh, P. Steele and C. U. Pittman, *Ind. Eng. Chem. Res.* 51, 900-914 (2012).

- 
141. N. A. Medellin-Castillo, R. Leyva-Ramos, R. Ocampo-Perez, R. F. Garcia de la Cruz, A. Aragon-Piña, J. M. Martinez-Rosales, R. M. Guerrero-Coronado and L. Fuentes-Rubio, *Ind. Eng. Chem. Res.* 46, 9205-9212 (2007).
142. M. S. Onyango, T. Y. Leswifi, A. Ochieng, D. Kuchar, F. O. Otieno and H. Matsuda, *Ind. Eng. Chem. Res.* 48, 931-937 (2008).
143. P. Cai, H. Zheng, C. Wang, H. Ma, J. Hu, Y. Pu and P. Liang, *J. Hazard. Mater.* 213-214, 100-108 (2012).
144. L. Lv, J. He, M. Wei and X. Duan, *Ind. Eng. Chem. Res.* 45, 8623-8628 (2006).
145. T. Zhang, Q. Li, H. Xiao, H. Lu and Y. Zhou, *Ind. Eng. Chem. Res.* 51, 11490-11498 (2012).
146. S. Mandal, S. Tripathy, T. Padhi, M. K. Sahu and R. K. Patel, *J. Environ. Sci.* 25, 993-1000 (2013).
147. C. Gao, X.-Y. Yu, T. Luo, Y. Jia, B. Sun, J.-H. Liu and X.-J. Huang, *J. Mater. Chem. A* 2, 2119-2128 (2014).
148. A. Vinati, B. Mahanty and S. K. Behera, *Appl. Clay Sci.* 114, 340-348 (2015).
149. S. P. Kamble, P. Dixit, S. S. Rayalu and N. K. Labhsetwar, *Desalination* 249, 687-693 (2009).
150. D. Thakre, S. S. Rayalu, R. Kawade, S. Meshram, J. Subrt and N. Labhsetwar, *J. Hazard. Mater.* 180, 122-130 (2010).
151. M. G. Sujana, G. Soma, N. Vasumathi and S. Anand, *J. Fluorine Chem.* 130, 749-754 (2009).
152. N. Chen, Z. Zhang, C. Feng, D. Zhu, Y. Yang and N. Sugiura, *J. Hazard. Mater.* 186, 863-868 (2011).
153. M. G. Sujana and S. Anand, *Appl. Surf. Sci.* 256, 6956-6962 (2010).

- 
154. R. Liu, W. Gong, H. Lan, T. Yang, H. Liu and J. Qu, *Sep. Purif. Technol.* 92, 100-105 (2012).
155. K. Biswas, S. K. Saha and U. C. Ghosh, *Ind. Eng. Chem. Res.* 46, 5346-5356 (2007).
156. Y. Dong and X. Tian, *J. Non-Cryst. Solids* 356, 1404-1407 (2010).
157. X. Zhao, D. Liu, H. Huang, W. Zhang, Q. Yang and C. Zhong, *Microporous Mesoporous Mater.* 185, 72-78 (2014).
158. N. Chen, Z. Zhang, C. Feng, N. Sugiura, M. Li and R. Chen, *J. Colloid Interface Sci.* 348, 579-584 (2010).
159. N. Chen, Z. Zhang, C. Feng, M. Li, D. Zhu, R. Chen and N. Sugiura, *J. Hazard. Mater.* 183, 460-465 (2010).
160. H. Liu, S. Deng, Z. Li, G. Yu and J. Huang, *J. Hazard. Mater.* 179, 424-430 (2010).
161. N. Sakhare, S. Lunge, S. Rayalu, S. Bakardjiva, J. Subrt, S. Devotta and N. Labhsetwar, *Chem. Eng. J.* 203, 406-414 (2012).
162. B. Zhao, Y. Zhang, X. Dou, X. Wu and M. Yang, *Chem. Eng. J.* 185-186, 211-218 (2012).
163. H.-X. Wu, T.-J. Wang, L. Chen, Y. Jin, Y. Zhang and X.-M. Dou, *Ind. Eng. Chem. Res.* 48, 4530-4534 (2009).
164. X. Wu, Y. Zhang, X. Dou and M. Yang, *Chemosphere* 69, 1758-1764 (2007).
165. K. Biswas, K. Gupta, A. Goswami and U. C. Ghosh, *Desalination* 255, 44-51 (2010).
166. L. Chen, H.-X. Wu, T.-J. Wang, Y. Jin, Y. Zhang and X.-M. Dou, *Powder Technol.* 193, 59-64 (2009).

- 
167. Y. Tang, X. Guan, J. Wang, N. Gao, M. R. McPhail and C. C. Chusuei, *J. Hazard. Mater.* 171, 774-779 (2009).
168. S. Dey, S. Goswami and U. C. Ghosh, *Water Air Soil Pollut.* 158, 311-323 (2004).
169. X. Dou, D. Mohan, C. U. Pittman Jr and S. Yang, *Chem. Eng. J.* 198-199, 236-245 (2012).
170. Z. Qiusheng, L. Xiaoyan, Q. Jin, W. Jing and L. Xuegang, *RSC Adv.* 5, 2100-2112 (2015).
171. P. Miretzky and A. F. Cirelli, *J. Fluorine Chem.* 132, 231-240 (2011).
172. J. Zhang, N. Chen, Z. Tang, Y. Yu, Q. Hu and C. Feng, *Phys. Chem. Chem. Phys.* 17, 12041-12050 (2015).
173. C. S. Sundaram, N. Viswanathan and S. Meenakshi, *J. Hazard. Mater.* 163, 618-624 (2009).
174. J. Nomura, H. Imai and T. Miyake, *Removal of Fluoride Ion from Wastewater by a Hydrous Cerium Oxide Adsorbent*, Emerging Technologies in Hazardous Waste Management, American Chemical Society symposium series, (1990), vol. 422, pp. 157-172.
175. M. G. Sujana and S. Anand, *Desalination* 267, 222-227 (2011).
176. N. Chubar, *J. Colloid Interface Sci.* 357, 198-209 (2011).
177. Z. Hussain, L. Daosheng, L. Xi and K. Jianxiong, *RSC Adv.* 5, 43906-43916 (2015).
178. A. Dhillon and D. Kumar, *J. Mater. Chem. A* 3, 4215-4228 (2015).
179. M. Sarkar, A. Banerjee and P. P. Pramanick, *Ind. Eng. Chem. Res.* 45, 5920-5927 (2006).



- 
180. B. D. Turner, P. Binning and S. Stipp, *Environ. Sci. Technol.* 39, 9561-9568 **(2005)**.
181. S. Chidambaram, S. Manikandan, A. L. Ramanathan, M. V. Prasanna, C. Thivya, U. Karmegam, R. Thilagavathi and K. Rajkumar, *Appl. Water Sci.* 3, 741-751 **(2013)**.
182. M. Barathi, A. Santhana Krishna Kumar and N. Rajesh, *J. Environ. Chem. Eng.* 1, 1325-1335 **(2013)**.
183. R. L. Ramos, J. Ovalle-Turrubiarres and M. A. Sanchez-Castillo, *Carbon* 37, 609 **(1999)**.
184. R. Johnston and H. Heijnen, *Safe Water Technology for Arsenic Removal. Report*, World Health Organization (WHO): Geneva, Switzerland, **(2002)**.
185. H. Farrah, J. Slavek and W. F. Pickering, *Aust. J. Soil Res.* 25, 55-69 **(1987)**.
186. B. Shimelis, F. Zewge and B. S. Chandravanshi, *Bull. Chem. Soc. Ethiopia* 20, 17-34 **(2006)**.
187. J. L. Reyes Bahena, A. Robledo Cabrera, A. López Valdivieso and R. Herrera Urbina, *Sep. Sci. Technol.* 37, 1973-1987 **(2002)**.
188. L. Pietrelli, *Anal. Chim.* 95, 303-312 **(2005)**.
189. W. Zhang, M. Sun and R. Prins, *J. Phys. Chem. B* 106, 11805-11809 **(2002)**.
190. K. Dash, U. Hareesh, R. Johnson and J. Arunachalam, *Water Prac. Technol.* 5, 1-9 **(2010)**.
191. X. S. Zhao, G. Q. Lu and G. J. Millar, *Ind. Eng. Chem. Res.* 35, 2075-2090 **(1996)**.
192. B. Naik and N. N. Ghosh, *Recent Pat. Nanotechnol.* 3, 213-224 **(2009)**.
193. P. Kim, Y. Kim, H. Kim, I. K. Song and J. Yi, *J. Mol. Catal. A: Chem.* 219, 87-95 **(2004)**.

- 
194. R.-H. Zhao, C.-P. Li, F. Guo and J.-F. Chen, *Ind. Eng. Chem. Res.* 46, 3317-3320 (2007).
195. K. Rybakov, A. Ereemeev, S. Egorov, Y. V. Bykov, Z. Pajkic and M. Willert-Porada, *J. Phys. D: Appl. Phys.* 41, 102008 (2008).
196. R. K. Pati, J. C. Ray and P. Pramanik, *J. Am. Ceram. Soc.* 84, 2849-2852 (2001).
197. Z. Ecsedi, I. Lazău and C. Păcurariu, *Process. Appl. Ceram.* 1, 5-9 (2007).
198. W. Zhang, *Chem. Commun.* 1185-1186 (1998).
199. J. Cejka, N. Zilkova, J. Rathousky and A. Zukal, *Phys. Chem. Chem. Phys.* 3, 5076-5081 (2001).
200. S. A. Bagshaw, E. Prouzet and T. J. Pinnavaia, *Science* 269, 1242-1244 (1995).
201. T. F. Baumann, A. E. Gash, S. C. Chinn, A. M. Sawvel, R. S. Maxwell and J. H. Satcher, *Chem. Mater.* 17, 395-401 (2005).
202. Z. Hao, H. Liu, B. Guo, H. Li, J. Zhang, L. Gan, Z. Xu and L. Chen, *Acta Phys. Chim. Sin.* 23, 289-294 (2007).
203. J. C. Ray, K.-S. You, J.-W. Ahn and W.-S. Ahn, *Microporous Mesoporous Mater.* 100, 183-190 (2007).
204. S. Alemu, E. Mulugeta, F. Zewge and B. S. Chandravanshi, *Environ. Technol.* 35, 1893-1903 (2014).
205. Q. Shi, Y. Huang and C. Jing, *J. Mater. Chem. A* 1, 12797-12803 (2013).
206. S. A. Wasay, S. Tokunaga and S.-W. Park, *Sep. Sci. Technol.* 31, 1501-1514 (1996).
207. B. K. Puri and S. Balani, *J. Environ. Sci. Health., Part A* 35, 109-121 (2000).
208. Y. Duan, C. Wang, X. Li and W. Xu, *J. Water Health* 12, 715-721 (2014).
209. J. Cheng, X. Meng, C. Jing and J. Hao, *J. Hazard. Mater.* 278, 343-349 (2014).

- 
210. I. Ali, *Chem. Rev.* 112, 5073-5091 (2012).
211. D. Yang and X. Xu, *Sci. Adv. Mater.* 5, 960-961 (2013).
212. S. Kumar, W. Ahlawat, G. Bhanjana, S. Heydarifard, M. M. Nazhad and N. Dilbaghi, *J. Nanosci. Nanotechnol.* 14, 1838-1858 (2014).
213. T. Bora and J. Dutta, *J. Nanosci. Nanotechnol.* 14, 613-626 (2014).
214. P. Saharan, G. R. Chaudhary, S. K. Mehta and A. Umar, *J. Nanosci. Nanotechnol.* 14, 627-643 (2014).
215. A. Pathak, A. Panda, A. Tarafdar and P. Pramanik, *J. Indian Chem. Soc.* 80, 289-296 (2003).
216. X. Zhao, J. Wang, F. Wu, T. Wang, Y. Cai, Y. Shi and G. Jiang, *J. Hazard. Mater.* 173, 102-109 (2010).
217. C. S. Sundaram, N. Viswanathan and S. Meenakshi, *Bioresour. Technol.* 99, 8226 (2008).
218. C. S. Sundaram, N. Viswanathan and S. Meenakshi, *J. Hazard. Mater.* 155, 206-215 (2008).
219. C.-F. Chang, P.-H. Lin and W. Höll, *Colloids Surf. Physicochem. Eng. Aspects* 280, 194-202 (2006).
220. C.-F. Chang, C.-Y. Chang and T.-L. Hsu, *Desalination* 279, 375-382 (2011).
221. S. K. Swain, T. Patnaik, P. C. Patnaik, U. Jha and R. K. Dey, *Chem. Eng. J.* 215-216, 763-771 (2013).
222. Y.-H. Li, S. Wang, A. Cao, D. Zhao, X. Zhang, C. Xu, Z. Luan, D. Ruan, J. Liang, D. Wu and B. Wei, *Chem. Phys. Lett.* 350, 412-416 (2001).
223. V. Srivastava, C. Weng, V. Singh and Y. Sharma, *J. Chem. Eng. Data* 56, 1414-1422 (2011).
224. M. Farooq, A. Ramli and D. Subbarao, *J. Chem. Eng. Data* 57, 26-32 (2011).

- 
225. S. Rao, R. Singh and S. Chaurasia, Bhabha Atomic Research Centre (BARC) *News Letter*, Mumbai, India, 2002, vol. 219, pp. 6-10.
226. J. Růžička, H. Jakschova and L. Mrklas, *Talanta* 13, 1341-1344 (1966).
227. M. L. Cabello-Tomas and T. West, *Talanta* 16, 781-788 (1969).
228. D. Dayananda, V. R. Sarva, S. V. Prasad, J. Arunachalam and N. N. Ghosh, *Part. Sci. Technol.* 33, 8-16 (2015).
229. K. S. Sing, *Pure Appl. Chem.* 57, 603-619 (1985).
230. D. Dayananda, V. R. Sarva, S. V. Prasad, J. Arunachalam and N. N. Ghosh, *Chem. Eng. J.* 248, 430-439 (2014).
231. T. W. Weber and R. K. Chakravorti, *AIChE J.* 20, 228-238 (1974).
232. D. Dayananda, G. Swapnil, Venkateswara R. Sarva, Sivankutty V. Prasad, Jayaraman Arunachalam and N. N. Ghosh, *Sci. Lett.* 4, 105 (2015).
233. E. Oliveira, S. Montanher, A. Andrade, J. Nobrega and M. Rollemberg, *Process Biochem.* 40, 3485-3490 (2005).
234. D. Dayananda, V. R. Sarva, S. V. Prasad, J. Arunachalam, P. Parameswaran and N. N. Ghosh, *Appl. Surf. Sci.* 329, 1-10 (2015).
235. X. Zhang, K. Qiu, E. Levänen and Z. X. Guo, *Cryst. Eng. Comm.* 16, 8825-8831 (2014).
236. K. Low and C. Lee, *Pertanika* 13, 221-228 (1990).

## List of publications

### Publications related to thesis

1. D. Dayananda and N. N. Ghosh, Applications of nanomaterials for removal of fluoride from water. In *Encyclopedia of Nanoscience and Nanotechnology*, Nalwa, H. S., Ed., American Scientific Publishers, USA, (accepted) (2015).
2. D. Dayananda, V. R. Sarva, S. V. Prasad, J. Arunachalam, N. N. Ghosh. A Simple Aqueous Solution Based Chemical Methodology for Preparation of Mesoporous Alumina: Efficient Adsorbent for Defluoridation of Water. *Part. Sci. Technol.* 33 (2015) 1-9.
3. D. Dayananda, S. Gupta, V. R. Sarva, S. V. Prasad, J. Arunachalam, N. N. Ghosh. Preparation of ZrO<sub>2</sub> nanoparticle loaded mesoporous Al<sub>2</sub>O<sub>3</sub>: A promising adsorbent for defluoridation of water. *Sci. Lett.* 4, 105 (2015).(Citations: 01)
4. D. Dayananda, V. R. Sarva, S. V. Prasad, J. Arunachalam, P. Parameswaran, Narendra N. Ghosh. Synthesis of MgO nanoparticle loaded mesoporous Al<sub>2</sub>O<sub>3</sub> and its defluoridation study. *App. Surf. Sci.* 329 (2015) 1-10. (Citations: 03)
5. D. Dayananda, V. R. Sarva, S. V. Prasad, J. Arunachalam, N. N. Ghosh. Preparation of CaO loaded mesoporous Al<sub>2</sub>O<sub>3</sub>: Efficient adsorbent for fluoride removal from water. *Chem. Eng. J.* 248 (2014) 430-439. (Citations: 12)

### Publications not related to thesis

1. D. Dayananda, V. Desai, B. Naik, M. Kowshik, V. S. Prasad, N. N. Ghosh. A simple method for preparation of Ag nanoparticle loaded mesoporous  $\gamma$ -Al<sub>2</sub>O<sub>3</sub> and their antibacterial property. *J. Nanosci. Lett.* (2014) 4: 15.
2. B. Naik, S. Hazra, D. Dayananda, B. K. Ghosh, M. K Patra, S. R. Vadera and N. N. Ghosh. Preparation of magnetically separable CoFe<sub>2</sub>O<sub>4</sub> supported Ag

nanocatalysts and catalysis reaction towards decolorization of variety of dyes. *RSC Adv.* 5, 40193-40198 (2015).

3. B. Naik, S. Hazra, D. Dayananda, V. S. Prasad, N. N. Ghosh. Preparation of TiO<sub>2</sub> nanoparticle loaded MCM-41 and study of its photo-catalytic activity towards decolorization of Methyl Orange. *J. Nanosci. Nanotechnol.* (2015) (doi:10.1166/jnn.2015.10904).
4. B. Naik, D. Moitra, D. Dayananda, S. Hazra, B. K. Ghosh, S. V. Prasad, N. N. Ghosh. A facile method for preparation of TiO<sub>2</sub> nanoparticle loaded mesoporous  $\gamma$ - Al<sub>2</sub>O<sub>3</sub>: An efficient but cost-effective catalyst for dye degradation. *J. Nanosci. Nanotechnol.* (Accepted 2015).

### Conference Proceedings

1. D. Dayananda, V. R. Sarva, S. V. Prasad, J. Arunachalam, N. N. Ghosh. A Simple Aqueous Solution Based Chemical Methodology for Preparation of Mesoporous Alumina: Efficient Adsorbent for Defluoridation of Water. International Conference & Exhibition of Powder, Granule and Bulk Solids: Innovations and Application (PGBSIA 2013), 27-30 November 2013, Thapar University, India.
2. D. Dayananda, V. R. Sarva, S. V. Prasad, J. Arunachalam, N. N. Ghosh. Preparation of ZrO<sub>2</sub> nanoparticle loaded mesoporous Al<sub>2</sub>O<sub>3</sub>: A promising adsorbent for defluoridation of water. Advanced materials and their applications in nanotechnology (AMAN 2014), May 17-19, 2014, BITS Pilani- K.K. Birla Goa Campus, Goa, India.
3. D. Dayananda, V. R. Sarva, S. V. Prasad, J. Arunachalam, N. N. Ghosh. Defluoridation study of Metal oxide Nanoparticle loaded mesoporous Al<sub>2</sub>O<sub>3</sub>. International Conference on Advances in Materials, Manufacturing and Applications (AMMA – 2015), April 9 -11, 2015, Trichy, India.

## BIO-DATA OF CANDIDATE

### Personal details:

**Name:** Dayananda D  
**Date of Birth:** 02-06-1988  
**Education:** M.Sc. (Organic Chemistry)  
VIT University, Tamilnadu (2010).  
  
B.Sc. (Mathematics, Physics, Chemistry)  
Vijayam Degree College, Chittoor,  
S.V. University, Tirupathi, A.P (2008).  
  
**Email:** dayanandabits@gmail.com

### Scholarships and Awards:

- ❖ Junior Research Fellowship, from “Board of Research in Nuclear Science” (BRNS), India, November 2010-November 2012.
- ❖ Senior Research Fellowship from “Board of Research in Nuclear Science” (BRNS), India, November 2012-March 2014.
- ❖ Senior Research Fellowship, from BITS Pilani, April 2014-till date.

### Publications during Ph.D Programme:

Listed in Appendix I.

**BIO-DATA OF SUPERVISOR**

**Name:** Dr. Narendra Nath Ghosh  
**Current Position:** Associate Professor  
Department of Chemistry  
Birla Institute of Technology and Science-Pilani,  
K. K. Birla, Goa Campus  
City: Zuarinagar, State: Goa-403726, India.  
**Date of Birth:** 01-01-1970  
**Education:** Ph. D. (Chemistry): IIT-Kharagpur (1999).  
M Sc (Chemistry): 1<sup>st</sup> Class-IIT-Kharagpur (1994).  
**Areas of Research:** (i) Nanostructured Magnetic materials  
(ii) Advanced catalysts  
(iii) Polymeric materials.  
(iv) Polymer- ceramic nano-composites.

**No. of Sponsored Research Projects**

<b>(i) As PI:</b>	09 (DST-UKIERI, DRDO, DST, BRNS)
<b>(ii) As Co-PI:</b>	04
<b>No. of International journal Publications</b>	70
<b>No. of International conference proceedings</b>	14
<b>No. of Invited Book Chapter</b>	5
<b>No. of Invited Talks</b>	11

**Honors/Awards/Recognition**

- 1) Research Exchanges with China and India award by The Royal Academy of Engineering (UK) 2010. Collaboration with University of Birmingham, UK.
- 2) Visiting Scientist Fellowship Award by “The Scientific and Technological Research Council of Turkey (TUBITAK)” 2006, 2009.
- 3) Member Expert in Chemistry for selection of candidates for Commonwealth Scholarship., UK Nominated by Ministry of Human Resource Development, Government of India.



- 4) Best Poster paper award “A Simple Chemical Technique For Synthesis of High Surface Area Mesoporous Silica Matrix And Iron-Oxide Incorporated Silicates” International Congress of Environmental Research (ICER 08) 2008.
- 5) Invited as Chairperson (for NANO-O9 and NANO-11 Sessions) in the 16<sup>th</sup> International Conference on Composites or Nano Engineering, ICCE-16, July 20-26, 2008 in Kunming, China.
- 6) Travel Grant Awards received from Indian National Science Academy , New Delhi (Ref No: NBS/ 2008/ 742 (Dated: 10th June-2008).
- 7) Travel Grant Awards received from BITS- Pilani, Rajasthan (Ref No: U/UAG/22-5 (Dated: 08-05-2008).
- 8) Travel Grant Awards received from CSIR, New Delhi (Ref No: 22/ IA/ PFA/180/2008 (Dated: 05-06-2008).
- 9) Travel Grant Awards received from DST, New Delhi, ( SR/ITS/01084/2008-2009).
- 10) Outstanding Scientist of 21<sup>st</sup> Century medal: Cambridge UK 2005.
- 11) Honorary appointment to the Research Board of Advisors of “The American Biographical Institute”, USA.2003.
- 12) Eminent Scientists of Today Medal by International Biographical Center Cambridge, U.K, 2002.
- 13) Aqueous Route to Ceramic Powders- Summary of research work of Dr. N. N. Ghosh was highlighted in High Tech Ceramic News (Published by B.B.C Inc, USA) January 2002.
- 14) Invited as Chairperson for Ceramics and Pre-ceramics Session in National Conference on Materials for the New Millennium. Kochin, India 2001.
- 15) **Reviewer of International Journals:** Thin Solid Films, Materials research Society, USA, Journal of the American Ceramic Society, Macromolecular Symposia, Journal of Surface Coating and Technology, Powder Technology, Journal of Microporous and Mesoporous Materials, International Journal of the Physical Sciences, Journal of Experimental nanoscience, Catalysis Communications, Journal of Magnetism and Magnetic materials, Journal of Electroceramics, Composite Interface, Synthesis and Reactivity in Inorganic, Metal-Organic, and Nano-Metal Chemistry etc.
- 16) Biography has published in several Who’s Who in Science and Engineering from USA, UK.